University of Stavanger

FACULTY OF SCIENCE AND TECHNOLOGY

MASTER'S THESIS

Study programme/specialisation:	Spring semester, 2021
Petroleum Engineering (Natural Gas Technology)	Open

Author: Yasas Bandara

Programme coordinator: Prof. Steinar Evje

Supervisor(s): Prof. Steinar Evje
Dr. Yangyang Qiao

Title of master's thesis:

Mathematical and Numerical Modelling of Lithium Battery

Credits: 30

Keywords:	Number of pages: 146
Lithium-ion battery Mathematical modelling and simulation Pseudo two dimensional model Capacity fading	Stavanger, June 15, 2021

Abstract

Application of lithium-ion batteries have increased in recent years due to their high energy density, low weight and smaller form factor. Machine learning algorithms are used in lithium-ion battery management systems due to the fact that they require less computational power. However, machine learning algorithms are a 'black box' in nature thus, for development and optimization of batteries a physical based model is required which facilitates to understand physical-chemical behaviors that govern the operation of battery. In this thesis, pseudo two dimensional (P2D) electrochemical model was selected and numerical solutions were computed by using MATLAB. Principles of lithium transport in anode, cathode, electrolyte and principles of chemical kinetics are used in this model. The model presents good agreement between simulated results and experimental data which are extracted from the literature. Simulations were conducted in order to investigate initial operation, lithium distribution in electrodes, power delivery, voltage response against current pulses and aging effect. The mathematical model enables to significantly minimize the development and optimization time for batteries because actual testing of batteries demands long time periods.

Acknowledgement

I wish to express my sincere gratitude to my supervisors, Professor Steinar Evje and Dr. Yangyang Qiao, who have provided me with guidance and expertise throughout the process of writing this thesis.

Contents

List of Figures

List of Tables

Abbreviations

Li Lithium.

Li^+ Lithium ion.

e^- Electron.

BMS Battery Management System.

FDM Finite Difference Method.

L.H.S Left Hand Side.

OCV Open Circuit Voltage.

P2D Pseudo Two Dimensional.

PDE Partial Differential Equation.

R.H.S Right Hand Side.

SEI Solid Electrolyte Interface.

SOC State of Charge.

SPM Single Particle Model.

Nomenclature

Greek Letters

α	Transfer coefficient
γ	Bruggeman tortuosity exponent
κ_e	Ionic / electronic conductivity
ϕ_e	Voltage potential in electrolyte
ϕ_s	Voltage potential in solid phase
ρ	Density (Thermal model)
σ	Solid phase conductivity (anode or cathode)
σ_{SB}	Emissivity of surface (Thermal model)
ε	Electrode Porosity
ε_e	Electrolyte Volume Fraction

Parameters

$\tilde{x}$	lithium ratio occupied at surface of negative electrode
$\tilde{y}$	lithium ratio occupied at surface of positive electrode
A_{cell}	Electrode area of battery
a_s	Specific surface area
$c_{e,0}$	Initial Li^+ concentration in electrolyte
c_e	Li^+ concentration in electrolyte
$c_{s,0}$	Initial Li concentration in solid phase
c_s	Li concentration in solid phase (anode or cathode)
CN	Cycle number
D_e	Diffusivity in electrolyte
D_n	Diffusivity in anode
D_p	Diffusivity in cathode
D_s	Diffusivity in solid phase (anode or cathode)
DOD	Depth of discharge
E_{cell}	Battery voltage
F	Faraday constant
$f_\pm$	Activity coefficient for lithium salt
FCC	Full cell capacity
h	Newton's cooling coefficient (Thermal model)
I	Total current density
i_0	Exchange current density
i_e	Electrolyte phase current density
i_n	Local current density

i_s	Solid (electrode) phase current density
K	Thermal conductivity
k_0	Reaction coefficient (anode or cathode)
k_n	Reaction coefficient of anode
k_p	Reaction coefficient of cathode
L	Thickness of battery
L_N	Set of elements in $x-dimension$ for anode
L_n	Thickness of anode
L_P	Set of elements in $x-dimension$ for cathode
L_p	Thickness of cathode
L_S	Set of elements in $x-dimension$ for separator
L_s	Thickness of separator
M	Total number of spacial steps
M_N	Set of elements in $r-dimension$ for anode
M_n	Number of spacial steps of anode
m_n	Number of spacial steps of spheres in anode
M_P	Set of elements in $r-dimension$ for cathode
M_p	Number of spacial steps of cathode
m_p	Number of spacial steps of spheres in cathode
M_s	Number of spacial steps of separator
Q_{cell}	Battery capacity
R	Universal gas constant
r	Radial dimension
r_n	Radii of particles in anode
r_p	Radii of particles in cathode
T	Absolute temperature
t	time
t_+^0	Transference number of lithium ions dissolved in electrolyte
T_{ref}	Reference temperature
U	Equilibrium potential of electrode (anode or cathode)
x	$x-dimension$

Superscripts and Subscripts

a	Anode / Anodic
c	Cathode / Cathodic
eff	Effective
max	Maximum
n	Negative electrode
p	Positive electrode
ref	Reference value
s	Separator/solid phase

Chapter 1

Introduction

1.1 Introduction to Lithium-ion Batteries and Their Applications

Lithium-ion batteries are becoming more popular with the development of renewable energy and energy storage systems. Battery is a simple device that can convert chemical energy to electrical energy.

Primary batteries such as alkaline, Daniel and dry cells, can not be charged after the battery is fully discharged. Thus, they need to be discarded and replace frequently. In contrast, secondary batteries, including lithium-ion batteries, can be discharged and charged many times until the battery become significantly degraded. In secondary batteries, during discharge, chemical energy is converted into electrical energy and during charge, electrical energy is converted into chemical energy. The reusability of secondary batteries make them attractive in commercial applications due to their low life cycle cost.

Recently, lithium-ion batteries have become small in size, with high energy density, light weight and longer life time. These factors make lithium-ion batteries an ideal candidate to be used in mobile applications such as in offshore platforms [3] and in automobiles [4]. Minimum maintenance and favorable on health, safety and environment (HSE) over conventional fuel types are additional advantages of lithium-ion batteries [3].

Decarbonization strategies are greatly dependent on renewable energy and energy management [5, 6]. Depending on demand and supply renewable energy may not be readily available at all times in order to be utilized in energy demanding applications. This creates a requirement for energy storage solution. Recently, hybrid oil & gas rigs and

platforms are entering into service in order to minimize the carbon and energy footprint [3, 6, 7]. A hybrid rig/platform is capable up to 42% reduction in diesel generator utilization using an energy storage system [6].

Lithium-ion batteries are being used in other applications such as autonomous underwater vehicles (AUV), remote operated vehicles (ROV) [8] and plug-in hybrid navel vessels [9] etc. Utilization of lithium-ion batteries in extreme applications such as in well monitoring, christmas trees (XMT), blow-out preventers (BOP) and in bottom hole assemblies (BHA) are gaining momentum with current developments. In order to improve the reliability of batteries in these applications, developments and optimizations are needed to be conducted. However, physical testing and optimization of batteries demands significantly long time thus, computer models and simulations are used for development and optimization.

Development of batteries for a specific application requires an understanding on chemical and physical behavior of batteries. Batteries needed to be optimized based on application that it is being used for, for example electronic applications demands lower power compared to heavy applications such as electric vehicles and hybrid rigs.

The Pseudo Two Dimensional (P2D) model used in this thesis has similarity with 1D reservoir model in petroleum reservoir engineering. The porous reservoir rock is equivalent to porous electrode and interconnected pores as electrolyte. Transport of lithium and lithium ion from electrode matrix through pores is similar to transport of petroleum fluid through solid rock and transport through the porous structure.

1.2 Objectives

The following objectives are met in the thesis:

- Selection of a suitable mathematical model for lithium-ion battery
- Reproduction of the selected model
- Estimation of parameters
- Validation of the model based on data from the literature
- Testing and investigation of the model

In order to physically test the performance of batteries requires more time and expensive equipment. However, utilization of a computer model help to simulate the behavior of

a battery within a short period of time. Thus, resulting fast and efficient development of batteries. Depending on the application (such as high power delivery, longer cycle time, etc.) battery specifications might vary. Thus, it is necessary to determine optimal parameters for batteries for a specific application. The main objective of the thesis is to gain insight into the mechanisms involved in charging and discharging processes within a lithium battery .

1.3 Organization of the Thesis

The model for lithium-ion battery contains three sub-models. The electrochemical model is the core model which governs the process of battery. The capacity fading model is a supporting model to the main electrochemical model which helps to determine the percentage of lithium lost due to aging. A thermal model was also developed (also a supporting model to the main electrochemical model). However, in this thesis analysis of the thermal model is not investigated. The electrochemical model is capable to operate independently without the capacity fading model and/or thermal model.

Selection and review of suitable electrochemical model, capacity fading model and parameters that are required for the model are discussed in chapter 2. Justification for selection of the Pseudo Two Dimensional (P2D) model, model description, details about anode, cathode, separator, and electrolyte are presented in same chapter.

The thermal model was developed based on a cylindrical geometry which is possible to link into main electrochemical model. Theory for the thermal model is presented in appendix C, discretization of the thermal model is presented in appendix D and discretized equations for boundaries are presented in appendix E.

Theory which is required for the construction of the electrochemical model is introduced in chapter 3. Model variables, parameters, constants and all governing equations which are used for construction of the model are presented in the chapter. Capacity fading is based on a semi-empirical model which is also discussed in the same chapter.

Finite Difference Method (FDM) was used to discretize equations which are presented in chapter 3. The process of discretization is presented in chapter 4. Appendix B is an extension to chapter 4 which contains the Newton-Raphson to derive numerical solution for a non-linear system of equations. The discrete version of the model was solved by using MATLAB. A flow diagram for the fundamental program of the electrochemical model is also presented in the same chapter.

Results on estimation of parameters, validation, testing and investigation of the model are discussed in chapter 5. The chapter presents investigation of initial operation of battery, lithium distribution in electrodes, power delivery, voltage response against current pulses and effect of aging.

Chapter 2

Literature Survey

Research on rechargeable lithium batteries were started to develop in 1960s and 1970s [10], however, no major breakthrough was found until early 1990s [10, 11]. In 1991, Sony commercialize first lithium-ion battery [11]. Characteristics such as high specific energy and high power delivery made lithium-ion batteries more popular than other types of secondary batteries [4, 10–12].

2.1 Model Selection

Models which are developed for lithium-ion batteries can be divided into two categories namely, empirical models and electrochemical models [12]. Empirical models utilize machine learning algorithms and are widely used in Battery Management System (BMS) because models are simple and require less computational power [12]. Even though empirical models provide accurate predictions, it is unable to determine and understand physical-chemical behavior inside the battery for development purposes.

Pseudo Two Dimensional (P2D) model is an electrochemical model which was introduced by Doyle et al. [13] in 1993. This model was extensively tested and validated by many authors [12, 14–21] and remains one of the most popular model to date [12]. Single Particle Model (SPM) is also an electrochemical model, but in contrast with the P2D model, SPM model does not consider the effect from the electrolyte [12, 22]. However, SPM model is utilized in P2D model including the electrical potential and mass transfer in electrolyte.

A lithium-ion battery consists of the porous anode (negative electrode) and the porous cathode (positive electrode) separated by an electrically non-conductive porous separator

[20]. Pores are filled with ion-conductive liquid called electrolyte. The separator ensures that no electron is passed between electrodes internally. Thus, electrons pass only through external path (external circuit) while lithium is transported between electrodes internally. P2D model assumes that the electrolyte is a superimposed continuum with anode and cathode [13]. The transport of Li in porous electrodes are considered to occur in a pseudo two dimensional (P2D) space, while transport of Li^+ in electrolyte occurs in general 3 dimensional space [13].

The P2D model is based on porous electrode theory [23] and concentrated solution theory. In this report lithium atoms which exist within two electrodes are denoted by (Li) and lithium-ions exist within the electrolyte is denoted by (Li^+). At the interface between electrode and electrolyte transformation of lithium (Li) to lithium-ion (Li^+), or lithium-ion (Li^+) to lithium (Li) occurs. Diffusion of Li/Li^+ in medium (electrode or electrolyte) is governed by concentration gradient, while intercalation, de-intercalation (lithium transformation) of lithium at electrode-electrolyte interface is governed by current in/out from battery. Reaction rate is a constraint for maximum rate of lithium intercalation and de-intercalation. Direction (sign) of current from battery (known as total current density I) is used to initiate charge/discharge process in P2D model. Subsequent authors have added extensions to P2D model such as capacity fading [24] and moving boundary models for cathodes [21, 25].

Figure 2.1 demonstrates schematic illustration for P2D model. At the top of the image (low opacity) shows the cross section of the battery cell. Anode (negative electrode) at left and cathode (positive electrode) at right are separated by a separator at the middle. Enlarged version of this section (low opacity) is also presented in figure 3.1. According to P2D model [13], porous electrodes are considered to be solid matrices with homogenous spheres where void space is filled with electrolyte. Figure 2.1 illustrates a magnified such particle (sphere) each in anode and cathode.

A fully charged battery has higher lithium concentration in anode spheres compared to cathode [13]. During discharge (fig. 2.1), Li is radially transported towards surface of spheres in anode, loses an electron and enter (de-intercalate) to electrolyte as a Li^+. Then Li^+s are transported though electrolyte towards cathode, receive an electron and enter (intercalate) into cathode spheres as Li [13]. A fully discharged battery has higher Li concentration in cathode compared to anode and reverse of the above mentioned process occurs during the charge of battery [13] (fig. 2.1).

2.1.1 Electrodes

A battery has two electrodes; anode and cathode [26, 27]. In lithium-ion batteries, electrodes act as an inventory for lithium (Li) while providing electrically conductive medium for the moving electrons [28]. Lithium is transported back and forth between two electrodes via electrolyte during charge and discharge processes (fig. 2.1).

Open Circuit Voltage (OCV) is one important characteristic parameter for an electrode. It determines the rate of mass and charge transfer at electrode-electrolyte interface (eq.(3.12)) in P2D model. OCV is the voltage difference between two terminals when the circuit is not connected to a load. For an electrode material, OCV is measured against standard hydrogen electrode [26]. At standard conditions (25^0C, $1\,atm$, $1\,mol/m^3$) OCV of hydrogen electrode is considered to be zero [26]. OCV can be experimentally determined and formulae are developed by authors to determine voltage against other properties such as State of Charge (SOC) of the material (i.e eq.(3.16), eq.(3.15)). If two materials are used as electrodes of a battery, OCV difference between those two materials determine the maximum voltage that can be yielded from battery [26].

State of Charge (SOC) is a parameter which describes the quantity of lithium currently occupied within the electrode material [18, 20, 21, 29]. SOC is expressed as the ratio of lithium currently occupied by electrode material to the maximum lithium that can be occupied by the electrode material. Thus, interval of SOC is $[0, 1]$. The OCV and the SOC are involved in the Butler-Volmer equation which will be discussed in chapter 3.

Anode (Negative Electrode)

Anode is also known as negative electrode because anode is the negative terminal of battery. Negative electrode has lower OCV compared to cathode. Graphite is commercially used as an anode (negative electrode) material in lithium-ion batteries [15, 16, 18, 19, 21, 30–33]. The lithium-ion intercalation in graphite was found in 1979 [33], but until now there is no commercially used anode material which has both stability and energy density as graphite. Silicon is a promising candidate for anode material which has 10 times higher theoretical capacity than graphite but swelling and unstable Solid Electrolyte Interface (SEI) layer create challenges for commercial use [10, 11].

Studies were conducted to improve the performance of graphite anodes [15, 33]. Some optimizations made to graphite electrodes are based on costs and benefits. For example, increase in interfacial surface area of graphite would increase power output of the battery because surface area for lithium intercalation/de-intercalation increases, however, larger

surface area consumes high amount of Li to form the Solid Electrolyte Interface (SEI) layer which reduces the capacity of battery [33].

Cathode (Positive Electrode)

Cathode is also known as positive electrode because cathode is the positive terminal of battery. Positive electrode has higher OCV compared to anode. For cathode, researchers have tested and modeled performance of many materials such as lithium cobalt oxides ($LiCoO_2$), lithium nickel oxides ($LiNiO_2$), lithium manganese oxides ($LiMnO_2$ and $LiMn_2O_4$), lithium iron phosphate ($LiFePO_4$), etc [10, 16, 18, 21, 29, 30, 32]. Each material has its own advantages and disadvantages, for example $LiCoO_2$ and $LiNiO_2$ are classical cathode materials which have better cyclic behavior, high specific charge and high Open Circuit Voltage (OCV), but at high temperatures these can have adverse reactions that could be a threat to safety of operation and challenging ecological, economical impacts during production and disposal [10].

Lithium iron phosphate ($LiFePO_4$) is one of the best suitable material as anode material due its high energy density (about 170 mAh/g), low toxicity, high thermal stability and favorable economic factors [10, 29]. This material was extensively studied by many authors [10, 16–18, 20, 21, 25, 32, 34] in lithium-ion battery context. Even though OCV of $LiFePO_4$ is lower than $LiCoO_2$[10], $LiMn_2O_4$ and some other cathode materials [10, 30, 31], $LiFePO_4$ has comparative high OCV about 3.0-3.5 V [10, 16, 18, 20, 21, 29, 31]. In contrast to other cathode materials, $LiFePO_4$ maintains nearly constant OCV in wide interval of State of Charge (SOC) [16, 18, 29, 31, 34].

2.1.2 Electrolyte

Electrolyte performs a vital role on Li^+ transport across two electrodes [35, 36]. Typically, Lithium salts such as $LiPF_6$, $LiAsF_6$, $LiClO_4$, $LiBF_4$ are dissolved in solvents/gels to use as an electrolyte [36]. Lithium hexafluorophosphate ($LiPF_6$) is widely used in commercial lithium batteries due to high ion conductivity, electrochemical stability and favorable SEI forming ability [36, 37]. Many other electrolyte salts and solvents/gels are under development to minimize the effect of adverse effects while improving electrical and diffusive properties [36].

Valøen and Reimers [35] has conducted study on electrochemical properties of $LiPF_6$ in mixture of propylene carbonate, ethylene carbonate and dimethyl carbonate (PC/ EC/ DMC). Empirical correlations for ionic conductivity (κ_e) and diffusivity (D_e) were

developed which κ_e and D_e depend on Li^+ concentration (c_e) and temperature (T) in electrolyte [35]. Polynomial expansion coefficient function (ν) was also developed by Valøen and Reimers [35] which includes effect from transference number (t_+) and electrolyte salt activity ($f_\pm$). ν is used to substitute concentration potential in ohm's law equation for electrolyte [20]. The results obtained for $LiPF_6$/PC/EC/DMC electrolyte [35] have been used by several subsequent authors to model and simulate P2D models [17, 20, 25].

Electrolyte is filled within the porous space in anode, cathode and in separator [13]. Thus, transport of Li^+ takes place through a porous media. To compensate for additional path length within porous space (tortuosity), effective transport properties needed to be used instead of bulk properties [14, 20, 21, 24]. Bruggeman correlation (ε^γ) is used to calculate tortuosity; where ε is the volume fraction of medium. For electrochemical systems, value of Bruggeman exponent (γ) is 1.5 [13, 38, 39].

2.1.3 Electrode-Electrolyte Interface

At the interface between electrode material (solid phase) and electrolyte (solution phase) an equilibrium of Li/Li^+ intercalation and de-intercalation exists [26, 27, 40],

$$Li \rightleftharpoons Li^+ + e^-$$

This is a dynamic equilibrium which depend on Li concentration at surface of electrode, Li^+ concentration in electrolyte and reactivity (eq.(3.13)). The current that is being exchanged through interface is known as exchange current density ($i_0 > 0$). When two electrodes (anode and cathode) are connected internally (i.e. electrolyte) and externally, this equilibrium become imbalanced due to the Open Circuit Voltage (OCV) difference between two electrodes. This results in a net current flow through interface which is known as the transfer current density (i_n) [26]. The direction of reaction and i_n are dependent on electrode and charge/discharge process. Kinetics of this charge transfer (current density i_n) is governed by the Butler-Volmer kinetics [13, 40, 41].

2.1.4 Separator

This is a porous thin membrane of plastic, glass fiber or ceramic material used to separate anode and cathode, electrically and physically [37, 42]. Materials that are used for separator should be chemically compatible with electrolyte [37, 42]. Francis et al. [37] have done a detail review on separators that used in commercial lithium ions batteries. However, in P2D model only porosity and thickness of the separator are required

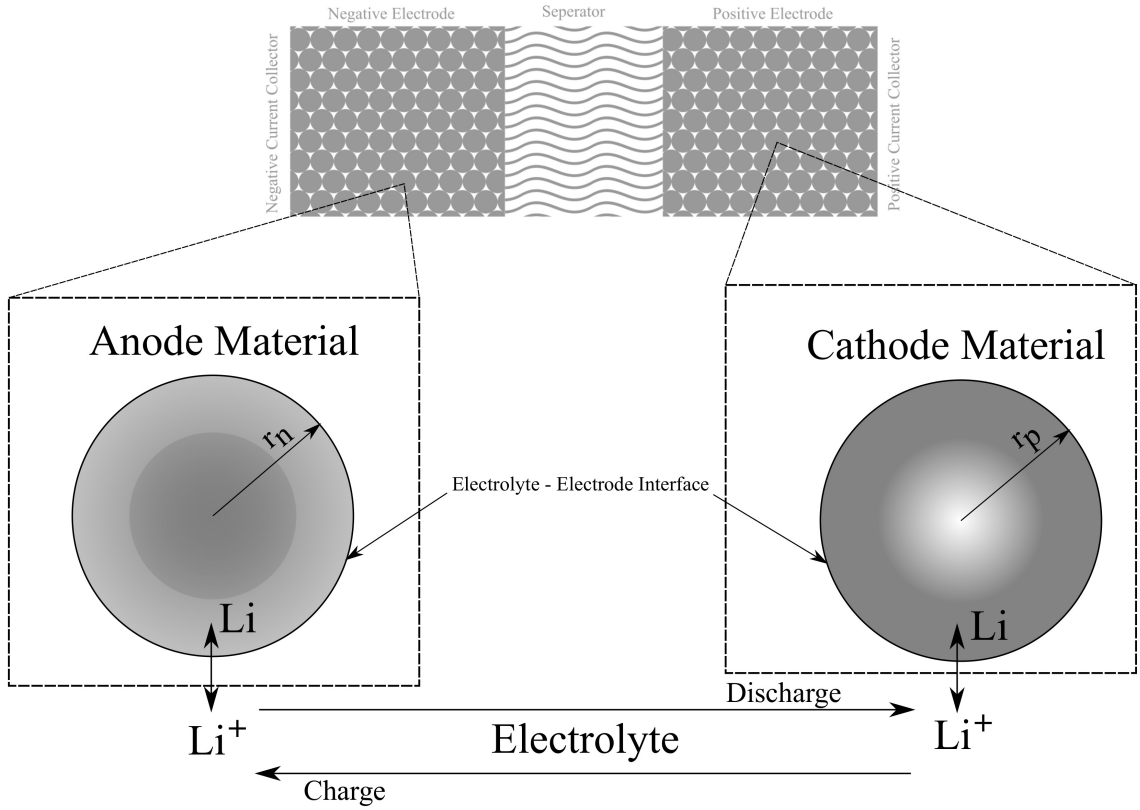

Figure 2.1: Lithium transport between electrode - electrolyte - electrode

Sphere at left indicates a particle at negative electrode. Sphere at right indicates a particle at positive electrode. During discharging, Li radially diffuse outward from left sphere and enter to electrolyte via interface, while at right sphere Li enter via interface and diffuse radially into the core. During charging, reverse of above process occurs. Net Li transfer across interfaces are governed by charge transfer reaction.

[13, 14, 16–18, 20, 21, 30].

2.2 Capacity Fading

Contributing factor for capacity fading in lithium-ion battery is formation and growth of Solid Electrolyte Interface (SEI) layer at anode (negative electrode) [4, 20, 24, 28, 29, 33]. Similar layer also grows in cathode as well, but effect on battery performance is negligible [33]. SEI layer is electrically nonconductive, but has higher selectivity to Li^+ and its diffusion [28, 33]. Since SEI layer is electrically non-conductive, this helps to prevent short-circuit inside battery improving safety of operation. However, about 10% of cyclical lithium is consumed for initial formation of SEI layer [33].

Ning et al. [24] developed an electrochemical model for capacity fading as an extension to P2D model and optimized based on experimental data. Authors have considered electrochemical parasitic reaction which influence capacity fading and increase of anode SEI film resistance [24]. $LiCoO_2$ was the cathode material that was used by Ning et al. [24], which shows considerable voltage reduction and capacity reduction with increase of cycle time. However, Wang et al. [29] have experimented the capacity fading of lithium-ion batteries (with $LiFePO_4$ cathode) and developed a semi-empirical model. Findings show that there are no significant voltage reductions as cycle time increases but battery capacity reduces. Several other authors has validated the semi-empirical model that was developed by Wang et al. [29] in their studies [4, 20].

The advantage of Wang et al. [29] model is that, it can simulate capacity fading, independent of electrochemical model. For example, user can input a desired cycle number and generate required results from electrochemical model. In contrast, principles that are used in Ning et al. [24] model are embedded in electrochemical model itself, thus it makes mandatory to run the complete electrochemical model from cycle 1 onwards to obtain a desired cycle data which could take considerable computational power and time [24].

2.3 Summary

P2D model was developed based on concentrated solution theory and porous electrode theory to evaluate transport of Li/Li^+ within battery [13]. Model is utilized to determine parameters such as battery voltage (E_{cell}), current output/input (I), battery capacity and energy level (SOC) of battery [13, 14, 16, 18, 20, 25, 30]. Both charging and discharging processes can be simulated using this model [29]. Determination of battery heath, variation of output voltage due to aging can be determined by introduction of supplementary models such as capacity fading [24, 29].

The model has flexibility to change properties of anode and cathode materials, battery dimensions and properties of electrolyte. In this thesis, properties of carbon graphite as anode material [18], $LiFePO_4$ as cathode material [18] and $LiPF_6$ in mixture of propylene carbonate, ethylene carbonate and dimethyl carbonate as electrolyte [35] are used to simulate the model.

This model provide flexibility for optimization of battery parameters to improve efficiency, power output, determine battery service frequency and finally determine the useful life time for the battery for specific applications [17, 20, 30]. The main advantage of using a mathematical model is ability to minimize testing and optimization time required because

actual battery testing demands longer time [24, 29].

In this thesis, a suitable electrochemical model (P2D model) was selected based on studies done in literature. The P2D model was reproduced in MATLAB using Finite Difference Method (FDM) approach. The reproduced model was validated against data from literature [18, 20, 29]. Data from literature was used to estimate the parameters of the model and minor tuning was conducted to make proper agreement between simulated results and data from literature. The performance of the model was then investigated for different scenarios such as initial operation of the battery, distribution of lithium in electrodes, power delivery, voltage response & relaxation aginst current pulses and effects due to capacity fading.

Chapter 3

Theory

3.1 Electrochemical Model

In general, negative electrode, separator and positive electrode sheets are sandwiched between two current collectors and spirally wound into cylindrical format [20]. Figure 3.1 indicates a cross section of such sandwiched section of battery. The two electrodes and separator are composed of porous materials. Pore spaces are filled with electrolyte and are continuous in all three sections. Separator allows the pass of Li^+ but prohibits the pass of electrons, thus, electrons pass thorough external circuit while Li^+ ions pass though internally.

The electrochemical model used in this thesis is developed based on Pseudo Two Dimensional (P2D) model [13–21, 28, 30, 31, 35, 41, 43, 44]. Concentrated solution theory, porous electrode theory and kinetic equations are foundation of P2D model [12, 13]. The model assumes that two electrodes are as porous matrices and the behavior of model is interpreted as spheres in electrolyte while lithium intercalation, de-intercalation are occurred at surface area of spheres. [12, 13]. A 1-dimensional approach is used in the formulation of the model (x-axis for electrolyte, r-axis for spheres) because Li/Li^+ transfer processes are predominantly unidirectional [12–14, 16, 18–21]. Governing equations are presented at eq. (3.1), eq. (3.3), eq. (3.7), eq. (3.10), eq. (3.11), eq. (3.12) and eq. (3.17) including valid domains next to the equations.

3.1.1 Description of Constants, Variables and Parameters

Constants that are used in electrochemical model are tabulated in table 3.1. Lengths

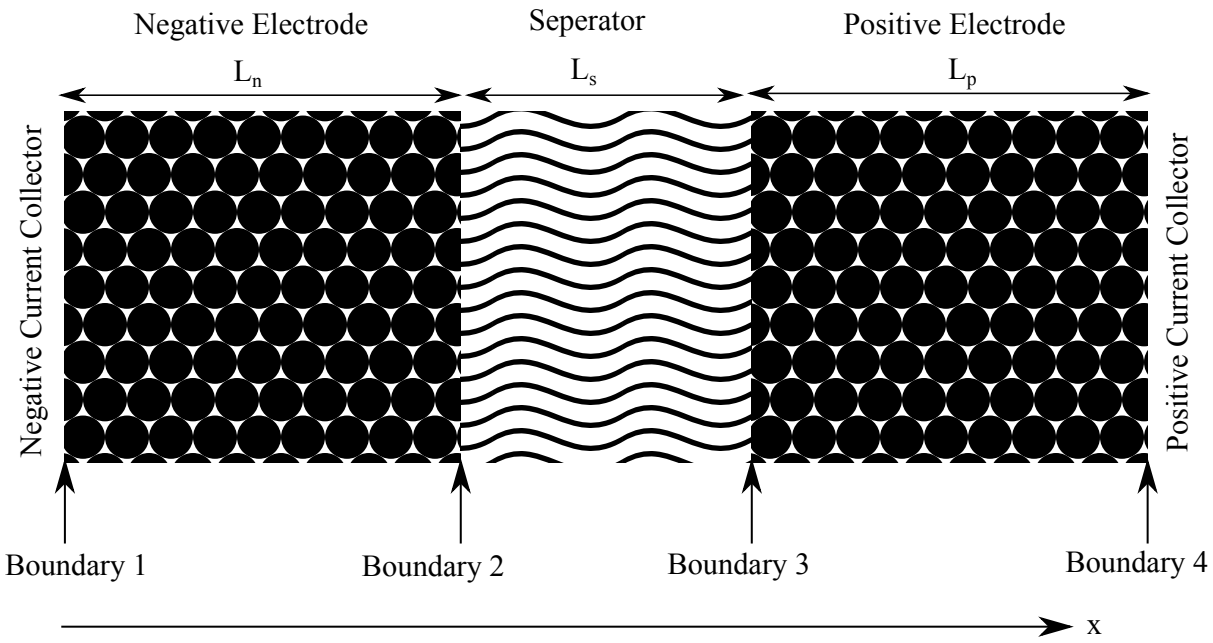

Figure 3.1: Schematic diagram of anode, separator and cathode of battery

Battery consists of negative electrode (anode), separator and positive electrode (cathode). Boundary 1 is negative current collector and boundary 4 is positive current collector. boundary 2 and 3 indicate interfaces between electrodes and separator. Thickness of each section is marked in figure. Direction of x indicates length from left to right where boundary 1 corresponds to $x = 0$.

of three sections in the battery; negative electrode (L_n), separator (L_s) and positive electrode (L_p) are also indicated in figure 3.1. Sum of these three lengths indicated by full length of battery (L). r_p and r_n radii correspond to particle sizes in electrode material at positive and negative electrodes. These radii are indicated at figure 2.1. Effective electrode conductivity (σ^{eff}), specific surface area of electrode material (a_s), volume fraction of electrolyte (ε_e) and porosity of electrode (ε) are considered as constants. Porosity of electrode (ε) reflects the active material within the electrode matrix, therefore $\varepsilon + \varepsilon_e < 1$.

Three main spacial domains were used in this model (do not confuse with x,y,z axes) ; Electrolyte domain, negative electrode domain and positive electrode domain. Electrolyte domain (Defined by set L_B) is defined in x dimension which has three subsets, negative electrode (L_N), separator (L_S) and positive electrode (L_P) (refer fig 3.1). Negative and positive electrode domains are defined based on radial axis (fig 2.1) where domain of negative electrode is defined by $L_N \times R_N$ and domain of positive electrode is defined by $L_P \times R_P$. Sets L_B, R_N and R_P are mutually exclusive sets with each other $\big(n(L_B \cap R_N) = n(L_B \cap R_P) = n(R_P \cap R_N) = 0\big)$. Sets are mathematically defined as follows,

- $L_N = \{x \,|\, 0 \leq x \leq L_n\}$

Table 3.1: Constants - Electrochemical model

Symbol	Description
L_n	Thickness of negative electrode
L_s	Thickness of separator
L_p	Thickness of positive electrode
L	Thickness of battery ($L_n + L_s + L_p$)
r_p	Radius of particles at positive electrode
r_n	Radius of particles at negative electrode
R	Universal gas constant ($8.314\ J\,K^{-1}\,mol^{-1}$)
F	Faraday constant ($96487\ C\,mol^{-1}$)
t_+^0	Transference number of Li^+ ions dissolved in electrolyte
$f_\pm$	Activity coefficient for Li salt
σ^{eff}	Effective conductivity of electrode material
a_s	Specific surface area of electrode material
α_a	Activity coefficient of anodic reaction
α_c	Activity coefficient of cathodic reaction
ε_e	Volume fraction of electrolyte
ε	Porosity of electrode
$c_{n,max}$	Maximum Li concentration in negative electrode material
$c_{p,max}$	Maximum Li concentration in positive electrode material
γ	Bruggeman tortuosity exponent (by default $\gamma = 1.5$)

- $L_S = \{x \,|\, L_n \leq x \leq L_n + L_s\}$
- $L_P = \{x \,|\, L_n + L_s \leq x \leq L\}$
- $L_B = L_N \cup L_S \cup L_P$
- $R_P = \{r \,|\, 0 \leq r \leq r_p\}$
- $R_N = \{r \,|\, 0 \leq r \leq r_n\}$

x-axis (x), radial axis (r) and time (t) act as independent variables to represent a property at specific point in space-time. Total current density (I) and initial temperature (T_{ini}) are user input variables. If thermal model is not used, temperature $\big(T(x,t)\big)$ is $T(x,t) = T_{ini}$. Main dependent variables are Li concentration in electrodes $\big(c_s(r,x,t)\big)$ and Li^+ concentration in electrolyte $\big(c_e(x,t)\big)$. Here Li concentration in electrodes $\big(c_s(r,x,t)\big)$ are defined in a pseudo dimensional space ($R_N \times L_N$ and $R_P \times L_P$) which is explained with the help of porous electrode theory introduced by Newman and Tiedemann [23] in 1975.

Electrode current density $\big(i_s(x,t)\big)$, electrode potential $\big(\phi_s(x,t)\big)$, electrolyte current density $\big(i_e(x,t)\big)$, electrolyte potential $\big(\phi_e(x,t)\big)$ are intermediate variables which are used to determine $c_s(r,x,t)$ and $c_e(x,t)$. However, $\phi_s(x=0,t)$ and $\phi_s(x=L,t)$ are important

variables for the determination of voltage output from the battery (E_{cell}) and calculation of energy input to/output from battery.

Transfer current density $\big(i_n(x,t)\big)$ is an important kinetic parameter which is determined using Butler-Volmer kinetics. This parameter describes the current flux between electrode and electrolyte. $i_n(x,t)$ is appeared as source term in both electrode and electrolyte mass transport equations. According to porous electrode theory by Newman and Tiedemann [23] this parameter is the link between pseudo dimensions (Li in electrodes) and real dimension (Li^+ in electrolyte).

Other parameters such as electrolyte diffusivity $\big(D_e(x,t)\big)$, negative, positive electrodes diffusivity $\big(D_n(x,t)\,,\, D_p(x,t)\big)$, electrolyte conductivity $\big(\kappa_e(x,t)\big)$, negative, positive reaction coefficients $\big(k_n(x,t)\,,\, k_p(x,t)\big)$ and negative, positive OCV $\big(U_n(x,t)\,,\, U_p(x,t)\big)$ depend on Li concentration and/or temperature at respective point in space-time. Table 3.2 tabulates user input, dependent and independent variables which are used in electrochemical model.

It is important to note that in this model, the sign of total current density (I) determines whether the battery is charging or discharging. Total current density (I) is introduced into the model in Eq. (3.8) where, if $I > 0$ initiates discharging process and $I < 0$ initiates charging process.

3.2 Discharging and Charging Process

Figure 3.2 illustrates the schematic diagram of a discharge and charge processes. It is important to note that figure is not presented in scale; electrode matrices (spheres) are enlarged and spaced out in order to demonstrate the mass transfer within spheres and electrolyte. Three dots ($\cdots$) in electrode regions indicate that electrode is shrunken down to save space in figure. Polarity of battery indicated near current collectors in '+' and '−' marks. Continuous line headed arrows ($\rightarrow$) indicate direction of lithium transport within electrode material and dashed line arrows ($\dashrightarrow$) indicate direction of transport of Li^+ ions in electrolyte.

3.2.1 Discharging Process

When battery is connected to load (circuit is closed), electrons start to flow from negative electrode to positive electrode via external circuit (fig. 3.2a). The electromotive force (voltage difference between electrodes) is the driving force of electrons. At electrolyte-

Table 3.2: Variables and parameters - Electrochemical model

Symbol	**Type of Variable**	**Domain**	**Description**
I	User input	$I \in (-\infty, \infty)$	Total current density
T_{ini}	User input	$T_{ini} \in (0, \infty)$	Initial temperature of Battery cell
x	Independent	$x \in L_B$	x dimension of battery cell
r	Independent	$r \in R_N \cup R_P$	Radial dimension of spherical particles
t	Independent	$t \in [0, \infty)$	Time
$T(x,t)$	Dependent	$x \in L_B$	Cell temperature
$c_e(x,t)$	Dependent	$x \in L_B$	Electrolyte concentration of Li^+ ions
$c_s(r,x,t)$	Dependent	$x \in L_N \cup L_P$ $r \in R_N \cup R_P$	Electrode Li concentration
$\phi_e(x,t)$	Dependent	$x \in L_B$	Electrolyte phase potential
$\phi_s(x,t)$	Dependent	$x \in L_N \cup L_P$	Electrode potential
$i_s(x,t)$	Dependent	$x \in L_N \cup L_P$	Electrode local current density
$i_e(x,t)$	Dependent	$x \in L_B$	Electrolyte local current density
$i_n(x,t)$	Dependent	$x \in L_N \cup L_P$	Transfer current density
$D_e(x,t)$	Dependent	$x \in L_B$	Electrolyte diffusivity
$D_n(x,t)$	Dependent	$x \in L_N$	Negative electrode diffusivity
$D_p(x,t)$	Dependent	$x \in L_P$	Positive electrode diffusivity
$\kappa_e(x,t)$	Dependent	$x \in L_B$	Electrolyte conductivity
$k_n(x,t)$	Dependent	$x \in L_N$	Negative electrode reaction coefficient
$k_p(x,t)$	Dependent	$x \in L_P$	Positive electrode reaction coefficient
$U_n(x,t)$	Dependent	$x \in L_N$	Negative electrode OCV
$U_p(x,t)$	Dependent	$x \in L_P$	Positive electrode OCV
$k_0(x,t)$	Dependent	$x \in L_N \cup L_P$	Reactivity ($k_n \ \ OR \ \ k_p$)
$E_{cell}(t)$	Dependent	$t \in [0, \infty)$	Battery voltage
$Q_{cell}(t)$	Dependent	$t \in [0, \infty)$	Battery capacity

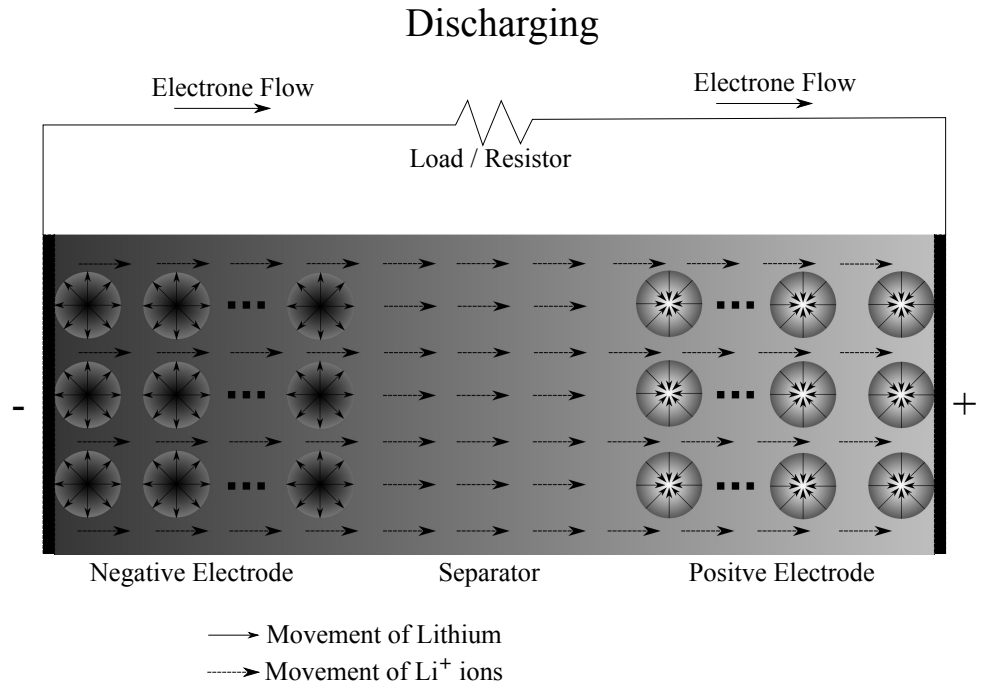

(a) Discharge process

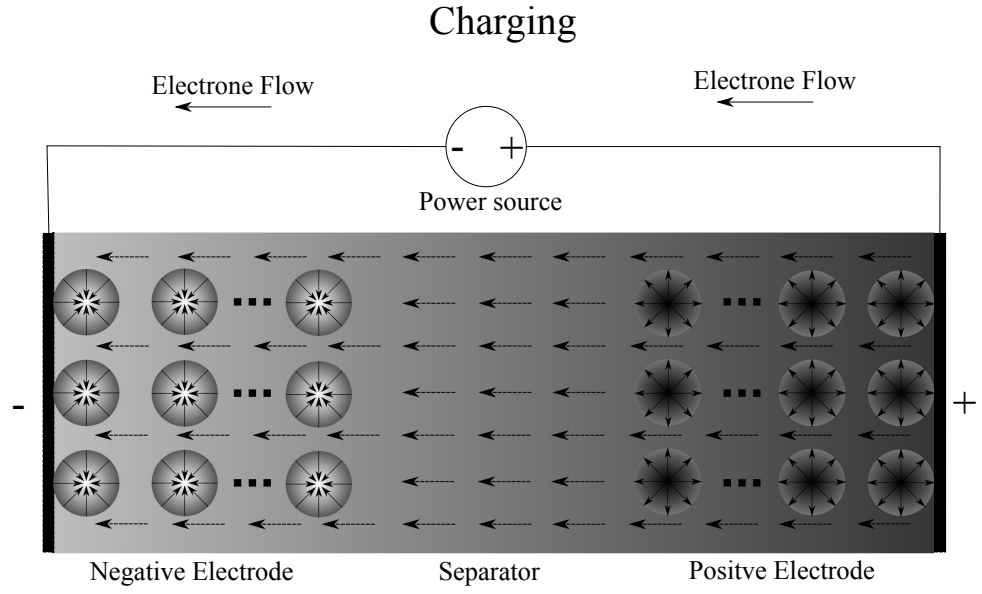

(b) Charge process

Figure 3.2: Schematic diagram of charging and discharging processes

electrode interface of negative electrode, electrons are generated due to following reaction,

$$Li_{(electrode)} \rightarrow Li^{+}_{(electrolyte)} + e^{-}_{(electrode)}$$

where 'e^{-}' denotes an electron. Electrons move through the positive electrode matrix in the direction of the negative current collector and move to external circuit. The reaction creates Li deficit at the surface of negative electrode material (surface of spheres) compared to the core of material (center of spheres) thus, initiating Li diffusive mass transport at negative electrode.

At positive electrode, electrons enter through positive current collector to electrode material. Electrons move through the positive electrode matrix and at electrode-electrolyte interface the following reaction occurs,

$$Li^{+}_{(electrolyte)} + e^{-}_{(electrode)} \rightarrow Li_{(electrode)}$$

The reaction consumes Li^{+} from electrolyte and added to surface of positive electrode material. This creates Li surplus at surface (surface of spheres) as compared to the core of material (center of spheres), initiating mass transport from surface to core.

The above two reaction creates Li^{+} surplus at electrolyte near negative region and Li^{+} deficit at electrolyte near positive region. Thus, concentration gradient is created to initiate mass transport process in electrolyte.

3.2.2 Charging Process

When battery is connected to external power source, the charging process is initiated. The differential voltage is applied by external power source should be higher than voltage difference across the battery to drive electrons from positive electrode to negative electrode via external circuit (fig. 3.2b).

Electrons are removed from positive electrode and enters into external circuit though positive current collector. At the surface of positive electrode material following reaction is initiated to generate electrons,

$$Li_{(electrode)} \rightarrow Li^{+}_{(electrolye)} + e^{-}_{(electrode)}$$

The reaction moves lithium from surface of the positive electrode to electrolyte. Li deficiency at surface compared to core of material initiate mass transport within positive electrode material from core to surface.

Electrons are added to negative electrode through negative current collector. At the surface of negative electrode material, following reaction consumes the electrons that transported into the electrode,

$$Li^{+}_{(electrolyte)} + e^{-}_{(electrode)} \rightarrow Li_{(electrode)}$$

The reaction moves lithium to surface of electrode material from electrolyte. Li surplus is created at surface compared to core of material initiating mass transport from surface to core of negative electrode material.

In the case of charging, Li^{+} at electrode near positive region is higher than the negative region. Thus, Li^{+} concentration gradient is created which initiates mass transport process in electrolyte.

3.3 Governing Equations

Seven governing equations are involved in the electrochemical model. The mechanisms that are involved can be summed up as follows: mass transport in electrolyte $c_e(x,t)$, Ohm's law for electrolyte $i_e(x,t)$, Ohm's law for electrodes $i_s(x,t)$, divergence of current density at electrolyte $\nabla \cdot i_e(x,t)$, divergence of current density at electrodes $\nabla \cdot i_s(x,t)$, transfer current density $i_n(x,t)$ and mass transport in electrodes $c_s(r,x,t)$. These equations are boxed in this section for easy identification.

3.3.1 Conservation of Mass in Electrolyte

Mass transport equation for the electrolyte (c_e) is represented in equation (3.1). Li^{+} concentration $c_e(x,t)$, is described within the electrolyte domain ($x \in L_B$). $i_n(x,t)$ is transfer current density, which present in the source term in the eq. (3.1). $i_n(x,t)$ is determined using Butler-Volmer kinetics (eq. (3.12)). Electrolyte is considered to be superimposed continuum across negative, positive electrodes and separator regions [13, 20, 40]. In eq. (3.1) $c_e = c_e(x,t)$, $D_e^{eff} = D_e^{eff}(x,t)$, $i_n = i_n(x,t)$. Effective diffusivity coefficient (D_e^{eff}) is calculated using electrolyte volume fraction (ε_e) and Bruggeman tortuosity exponent (γ),

$$D_e^{eff}(x,t) = \varepsilon_e^{\gamma} D_e(x,t)$$

$$\frac{\partial(\varepsilon_e c_e)}{\partial t} = \begin{cases} \nabla \cdot (D_e^{eff} \nabla c_e) + \frac{1-t_+^0}{F} a_s i_n \ , & \text{if } x \in L_N \cup L_P \\ \nabla \cdot (D_e^{eff} \nabla c_e) \ , & \text{if } x \in L_S \end{cases} \tag{3.1}$$

At boundary 1 and 4, only current collectors exists and no electrolyte. Thus no change in Li^+ concentration. Therefore boundary conditions for the above equation are given by equation (3.2).

$$\left.\frac{\partial c_e(\cdot,t)}{\partial x}\right|_{x=0} = 0 \qquad and \qquad \left.\frac{\partial c_e(\cdot,t)}{\partial x}\right|_{x=L} = 0 \tag{3.2}$$

3.3.2 Conservation of Current

The modified Ohm's law for the electrolyte which includes variation of activity coefficient of Li salt [13, 21, 35], is given by equation (3.3). Electrolyte current density $\big(i_e(x,t)\big)$ is dependent on electrolyte potential gradient $\big(\nabla\phi_e(x,t)\big)$ and Li^+ concentration gradient within electrolyte $\big(\nabla c_e(x,t)\big)$. In eq. (3.3) $T = T(x,t)$, $\kappa_e^{eff} = \kappa_e^{eff}(x,t)$. κ_e^{eff} is effective ionic conductivity of electrolyte which is calculated using electrolyte volume fraction (ε_e) and Bruggeman tortuosity exponent (γ),

$$\kappa_e^{eff} = \varepsilon^{\gamma} \kappa_e$$

$$i_e = -\kappa_e^{eff} \nabla\phi_e + \underbrace{\frac{2RT\kappa_e^{eff}}{F}(1-t_+^0)\left(1 + \frac{\partial ln\, f_{\pm}}{\partial ln\, c_e}\right)\nabla ln\, c_e}_{K_{junc}} \ , \qquad x \in L_B \tag{3.3}$$

At boundaries 1 and 4, there are only current collectors and no electrolyte. Thus, $(i_e(x,t) = 0 \ , \ x \in \{0, L\})$ which results derivative of electric potential $(\nabla\phi_e)$ to be zero at two boundaries. Boundary conditions for above equation (eq. (3.3)) are indicated at equation (3.4)

$$\left.\frac{\partial \phi_e(\cdot,t)}{\partial x}\right|_{x=0} = 0 \qquad and \qquad \left.\frac{\partial \phi_e(\cdot,t)}{\partial x}\right|_{x=L} = 0 \tag{3.4}$$

Liquid junction potential term (K_{junc}) [20] in eq. (3.3) is replaced by equation (3.5). $\nu(c_{el}, T)$ (eq (3.6)) is a thermodynamic factor which depends on electrolyte activity [20, 35]. Eq. (3.6) was determined by Valøen and Reimers [35] using experimental methods. The units of c_e in this equation is in $mol\ m^{-3}$ and T is in Kelvin (K).

$$K_{junc}(x,t) = \frac{2RT(x,t)}{F}(1-t_+^0)\left(1+\frac{\partial ln\, f_\pm}{\partial ln\, c_e(x,t)}\right) = \frac{2RT(x,t)}{F}\,\nu(x,t) \tag{3.5}$$

$$\nu(x,t) = 0.601 - 0.24\sqrt{10^{-3}c_e(x,t)} + 0.982\left(1 - 0.0052(T(x,t)-294)\sqrt{10^{-9}c_e^3(x,t)}\right) \tag{3.6}$$

Ohm's law for solid electrodes are presented in equation (3.7) [13, 20, 21]. This equation is applied for negative and positive electrodes separately. σ^{eff} is the effective conductivity of the electrode material which is calculated using electrode porosity (ε) and Bruggeman tortuosity exponent (γ),

$$\sigma^{eff} = \varepsilon^{\gamma}\sigma$$

$$i_s(x,t) = -\sigma^{eff}\nabla\phi_s(x,t)\ , \qquad x \in L_N \cup L_P \tag{3.7}$$

Negative current collector (at $x = 0$) of the battery is considered to be grounded, thus potential at boundary 1 is zero ($\phi_s(\cdot,t)|_{x=0} = 0$). This value does not affect final results, but act as a datum value for electric potentials. The total current density (I) which is drawn out/in from battery goes through negative and positive current collectors (boundary 1 and 4). Therefore $i_s(x,t) = I$ where $x \in \{0, L\}$. Based on this, boundary conditions for boundary 1 and 4 are defined as $-\sigma^{eff}\frac{\partial\phi_s}{\partial x} = -I$. Boundaries 2 and 3 (interface between separator and electrodes) have zero current ($i_s(x,t) = 0$ where $x \in \{L_n, L_n + L_s\}$), resulting electric potential gradients to be zero. These boundary conditions can be summarized as in equation (3.8).

$$\begin{aligned} -\sigma^{eff}\nabla\phi_s(\cdot,t)|_{x=0} &= -I & -\sigma^{eff}\nabla\phi_s(\cdot,t)|_{x=L} &= -I \\ -\sigma^{eff}\nabla\phi_s(\cdot,t)|_{x=L_n} &= 0 & -\sigma^{eff}\nabla\phi_s(\cdot,t)|_{x=L_n+L_s} &= 0 \end{aligned} \tag{3.8}$$

Conservation of current imposes that at any given point of the battery, sum of local current density through electrolyte (i_e) and local current density though solid phase (i_s) should be same as total current density (I). However, at separator region ($x \in L_S$) since

there is no existence of local current density of electrode (i_s), local current density of electrolyte (i_e) is same as total current density (I). This also means that at any point at the battery, the current flowing through it is constant. Thus, equation (3.9) represents the current conservation inside the battery cell.

$$I = \begin{cases} i_s(x,t) + i_e(x,t)\ , & \text{if } x \in L_N \cup L_P \\ i_e(x,t)\ , & \text{if } x \in L_S \end{cases} \tag{3.9}$$

Divergence of local current densities ($\nabla \cdot i_e\ ,\ \nabla \cdot i_s$) are proportional to transfer current density (i_n). The magnitude of divergence also depends on specific surface area of electrode material (a_s). $\nabla \cdot i_e$ and $\nabla \cdot i_s$ have opposite signs because current leaves from one phase and enter into another phase (e.g. when electrode losses Li, electrolyte gain that Li^+). Divergence for local current density at electrolyte ($\nabla \cdot i_e$) is represented by eq. (3.10) and divergence for electrodes' local current densities ($\nabla \cdot i_s$) represented by eq. (3.11) [13, 25, 40].

$$\nabla \cdot i_e(x,t) = \begin{cases} a_s i_n(x,t)\ , & \text{if } x \in L_N \cup L_P \\ 0\ , & \text{if } x \in L_S \end{cases} \tag{3.10}$$

$$\nabla \cdot i_s(x,t) = -a_s i_n(x,t)\ , \qquad x \in L_N \cup L_P \tag{3.11}$$

According to Doyle et al. [13], at the interface between electrode and electrolyte (refer fig. 2.1), mass transfer $\big(c_s(r,x,t),\ c_e(x,t)\ \textit{where}\ r \in \{r_n, r_p\},\ x \in L_N \cup L_P\big)$ which is also known as lithium intercalation/de-intercalation, is assumed to be governed by Butler Volmer kinetics. The same approach was used by many authors who used this model to determine charge transfer at interface [20, 21, 26, 40]. Calculation of transfer current by Butler-Volmer equation is represented by equation (3.12). In eq. (3.12) $i_n = i_n(x,t)$, $i_0 = i_0(x,t)$, $T = T(x,t)$, $\phi_s = \phi_s(x,t)$, $\phi_e = \phi_e(x,t)$ and $U = U(x,t)$. Here U represents OCV which is replaced by $U = U_n$ at negative electrode and $U = U_p$ at positive electrode. The shape of eq.(3.12) is presented in figure 3.3.

$$i_n = i_0 \left(\exp\!\left(\frac{\alpha_a F}{RT}(\phi_s - \phi_e - U) \right) - \exp\!\left(-\frac{\alpha_c F}{RT}(\phi_s - \phi_e - U) \right) \right)\ , \qquad x \in L_N \cup L_P \tag{3.12}$$

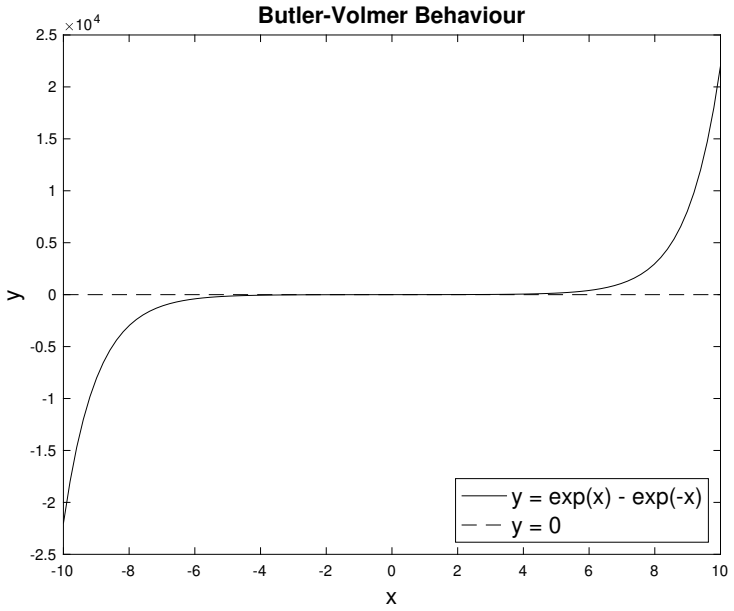

Figure 3.3: Butler-Volmer kinetic behaviour

Graph illustrates the behaviour of Butler-Volmer kinetics which is presented in equation (3.12). *Here the equation is presented in* $y = e^{x} - e^{-x}$ *format. From the graph it is apparent that sign of* y *depends on sign of* x.

Exchange current density (i_0) is dependent on reactivity of electrode material (k_0), Li^+ concentration in electrolyte (c_e) and surface Li concentration in electrodes ($c_s(r, x, t),\ r \in \{r_n, r_p\}$). Exchange current density can be determined by equation (3.13) and it requires to solve for negative and positive electrodes separately. F represents Faraday constant, α_a and α_c represent anodic and cathodic activity coefficients respectively.

$$i_0(x,t) = F\, k_0\, c_s^{\alpha_c}(r = r_i, x, t)\Big(c_{s,max} - c_s(r = r_i, x, t)\Big)^{\alpha_a} c_e^{\alpha_a}(x,t)\ , \qquad (3.13)$$
$$x \in L_N \cup L_P \qquad r_i \in \{r_p, r_n\}$$

Open Circuit Voltage (OCV) (U) for anode and cathode are dependent on concentration of Li at surface of electrodes ($c_s(r \in \{r_n, r_p\}, x, t)$) [16, 21, 30] and battery temperature (T) [17, 20]. The dependance of OCV (U) with temperature can be expressed as in equation (3.14) [17, 20]. U_{ref} is the reference OCV at reference temperature (25^oC) and $\frac{dU}{dt}$ is the entropy for anode/cathode material.

$$U(x,t) = U_{ref}(x,t) + (T - T_{ref})\frac{dU(x,t)}{dT}\ , \qquad x \in L_N \cup L_P \qquad (3.14)$$

Reference OCV for natural graphite ($U_{n,ref}$) which is commonly used in negative electrode is presented in equation (3.15) at 25^oC [18, 20]. $\tilde{x}$ represents the ratio between surface

concentration of Li in negative electrode ($c_s(r = r_n, x, t)$) to maximum Li concentration that can hold up in the material ($c_{n,max}$). Units of U_n is in volts (V).

$$\begin{aligned} U_{n,ref}(x,t) = {} & 0.6379 + 0.5416\exp(-305.5309\tilde{x}) + 0.044\tanh\left(-\frac{\tilde{x} - 0.1958}{0.1088}\right) \\ & - 0.1978\tanh\left(\frac{\tilde{x} - 1.0571}{0.0854}\right) - 0.6875\tanh\left(\frac{\tilde{x} + 0.0117}{0.0529}\right) \\ & - 0.0175\tanh\left(\frac{\tilde{x} - 0.5692}{0.0875}\right), \end{aligned} \tag{3.15}$$

$$\tilde{x}(x,t) = \frac{c_s(r = r_n, x, t)}{c_{n,max}}, \qquad x \in L_N$$

$LiFePO_4$ is a popular cathode material which is used in positive electrodes in commercial applications [10]. Equation (3.16) represents reference OCV for $LiFePO_4$ ($U_{p,ref}$) at 25^oC [18, 20]. $\tilde{y}$ represents the ratio between surface concentration of Li in positive electrode ($c_s(r = r_p, x, t)$) to maximum Li concentration that can hold up in the material ($c_{p,max}$). Units of U_p is in volts (V).

$$\begin{aligned} U_{p,ref}(x,t) = {} & 3.4323 - 0.8428\exp\big(-80.2493(1-\tilde{y})^{1.3198}\big) \\ & - 3.2474 \times 10^{-6}\exp\big(20.2645(1-\tilde{y})^{3.8003}\big) \\ & + 3.2482 \times 10^{-6}\exp\big(20.2646(1-\tilde{y})^{3.7995}\big), \end{aligned} \tag{3.16}$$

$$\tilde{y}(x,t) = \frac{c_s(r = r_p, x, t)}{c_{p,max}}, \qquad x \in L_P$$

Eq. (3.15) [18] and Eq. (3.16) [18] were developed based on experimental data . Both equations valid in the interval of $[0, 1]$ for $\tilde{x}$ and $\tilde{y}$; where 0 indicates no lithium and 1 indicates maximum lithium concentration in electrode material. Behavior of these two equations are represented at fig. 3.4.

OCV entropy values for negative and positive electrodes ($\frac{dU_n}{dT}$ and $\frac{dU_p}{dT}$) are also extracted from experimental data which are published in literature [17, 45]. These equations are presented in appendix A. Entropy for negative electrode ($\frac{dU_n}{dT}$) is represented in eq.(A.2), and entropy for positive electrode ($\frac{dU_p}{dT}$) is represented in eq.(A.1).

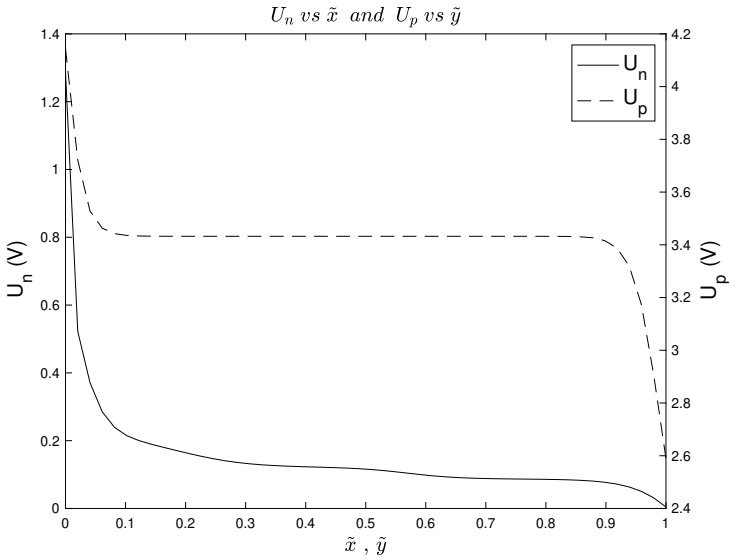

Figure 3.4: Open circuit voltages of electrodes

Graph represents OCV of negative and positive electrodes at 25^oC*, which are indicated in eq.* (3.15) *and eq.* (3.16)*. x axis is shared by both* $\tilde{x}$ *and* $\tilde{y}$ *variables.*

3.3.3 Conservation of Mass in Electrodes

Porous electrodes are considered to be made by micro size homogeneous spherical particle matrix [13, 20, 21]. Figure 2.1 illustrates interaction between micro-size electrode particle and electrolyte. Mass transport within electrodes (c_s) can be determined by Fick's law which is represented in equation (3.17) [20]. Equation determines distribution of Li in spheres (c_s) at each x position in electrodes. Therefore, distribution of Li in an electrode is calculated within a Pseudo Two Dimensional (P2D) space (r-axis and x-axis) and time.

$$\frac{\partial c_s(r,x,t)}{\partial t} = \frac{1}{r^2}\frac{\partial}{\partial r}\left(D_s r^2 \frac{\partial c_s(r,x,t)}{\partial r}\right), \quad \left(x \in L_N \;\; AND \;\; r \in R_N\right) \; OR \; \left(x \in L_P \;\; AND \;\; r \in R_P\right) \tag{3.17}$$

At center of sphere ($r = 0$) there is no Li mass, thus, derivative of Li concentration (c_s) with respect to radius (r) is zero. At surface of sphere charge transfer reaction occurs. Therefore, mass transfer at surface ($r \in \{r_n, r_p\}$) is proportional to transfer current density (i_n). Equation (3.18) represents boundary conditions which described above.

$$-D_s \frac{\partial c_s(\cdot,x,t)}{\partial r}\bigg|_{r=0} = 0 \qquad -D_s \frac{\partial c_s(\cdot,x,t)}{\partial r}\bigg|_{r=r_i} = \frac{i_n}{F}\ , \tag{3.18}$$
$$\left(x \in L_N \ \ AND \ \ r_i = r_n\right) \ OR \ \left(x \in L_P \ \ AND \ \ r_i = r_p\right)$$

3.3.4 Calculation of Diffusion Coefficients for Electrodes

According to Ye et al. [20] diffusion coefficients for electrodes are considered to be following Arrhenius equation. Diffusion coefficient for negative (natural graphite) and positive ($LiFePO_4$) electrodes are calculated using equations (3.19) and (3.20) respectively [20, 25]. D_n and D_p values substitute D_s in equation (3.17) depending on which electrode, the mass transport is calculated for. Units of D_n, D_p are in $m^2\ s^{-1}$ and T is in Kelvin (K).

$$D_n(x,t) = 3.9 \times 10^{-14} \exp\left(\frac{35000}{R}\left(\frac{1}{298.15} - \frac{1}{T(x,t)}\right)\right)\ , \qquad x \in L_N \tag{3.19}$$

$$D_p(x,t) = 1.18 \times 10^{-18} \exp\left(\frac{35000}{R}\left(\frac{1}{298.15} - \frac{1}{T(x,t)}\right)\right)\ , \qquad x \in L_P \tag{3.20}$$

3.3.5 Calculation of Electrolyte Diffusivity and Ionic Conductivity

Electrolyte diffusivity (D_e) and ionic conductivity (κ_e) depend on concentration of Li^+ ions in electrolyte and temperature [20, 25, 35]. Respective formulae are obtained from experimental data which was investigated by Valøen and Reimers [35]. Diffusion coefficient (D_e) is used in electrolyte mass transport equation (eq.(3.1)) and ionic conductivity (κ_e) is used in electrolyte Ohm's law (eq.3.3). Diffusion coefficient (D_e) and conductivity of electrolyte (κ_e) are represented as in Eq. (3.21) and (3.22) respectively. Unit of D_e is $m^2\ s^{-1}$, unit of c_e is $mol\ m^{-3}$, unit of κ_e is $S\ m^{-1}$ and T is in kelvin (K). In Eq. (3.22) $\kappa_e = \kappa_e(x,t)$, $c_e = c_e(x,t)$ and $T = T(x,t)$ where $x \in L_B$. Eq.(3.21) and eq.(3.22) are plotted in figure 3.5.

$$D_e(x,t) = 1 \times 10^{-4} \times 10^{-4.43 - \frac{54}{T(x,t)-229-0.005c_e(x,t)} - 2.2\times10^{-4}c_e(x,t)}\ , \qquad x \in L_B \tag{3.21}$$

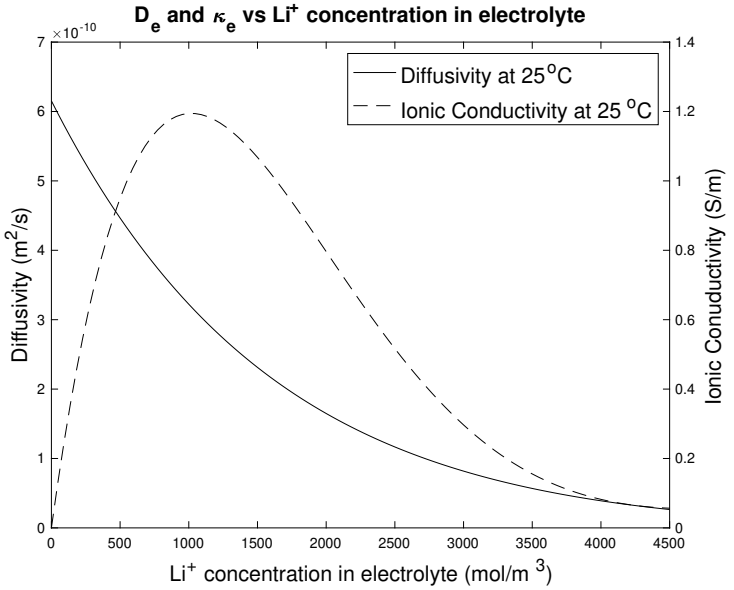

Figure 3.5: Diffusivity and ionic conductivity of electrolyte

Graph illustrates the behaviour of diffusivity (D_e) and ionic conductivity (κ_e) of electrolyte. D_e and κ_e are presented against lithium-ion concentration in electrolyte (c_e) at $T = 298.15\,K$.

$$\begin{aligned}\kappa_e =& 1 \times 10^{-4} c_e(-10.5 + 0.074T - 6.69 \times 10^{-5}T^2 + 6.68 \times 10^{-4}c_e \\ & - 1.78 \times 10^{-5}c_eT + 2.8 \times 10^{-8}c_eT^2 + 4.94 \times 10^{-7}c_e^2 - 8.86 \times 10^{-10}c_e^2T)^2\end{aligned} \tag{3.22}$$

3.3.6 Calculation of Reaction Rates

Reactivity of lithium transformation (intercalation/de-intercalation) at electrode-electrolyte interface follows Arrhenius formula [20]. Reactivity for negative (natural graphite) and positive ($LiFePO_4$) electrodes are shown in equation (3.23) and equation (3.24) respectively. k_n and k_p values substitute k_0 in equation (3.13) depending on which electrode the equation is applied for.

$$k_n(x,t) = 3 \times 10^{-11} \exp\left(\frac{20000}{R}\left(\frac{1}{298.15} - \frac{1}{T(x,t)}\right)\right), \qquad x \in L_N \tag{3.23}$$

$$k_p(x,t) = 1.4 \times 10^{-12} \exp\left(\frac{30000}{R}\left(\frac{1}{298.15} - \frac{1}{T(x,t)}\right)\right), \qquad x \in L_P \tag{3.24}$$

3.3.7 Calculation of Specific Surface Area of Electrodes

Specific surface area (a_s) is used in mass transport (eq.(3.1),(3.17)) and charge conservation equations (eq.(3.10),(3.11)). Specific surface area a_s represented in equation (3.25) [40]. Normally radii of particles (r) and electrode porosity (ε) for negative and positive electrodes are distinct values, thus, for negative and positive electrodes, a_s should be determined separately.

$$a_s = \frac{3\varepsilon}{r} \tag{3.25}$$

3.3.8 Battery Capacity and Voltage Calculation

Battery capacity (Q_{cell}) is defined as aggregate of current which is drawn out/in from the battery. This quantity is calculated using total current density (I) and time (t). Calculation of Battery capacity (Q_{cell}) is presented by eq.(3.26). The total current density (I) can vary over time (t). Units of Q_{cell} is Ampere hours ($A\,h$), total current density (I) in $A\,m^2$ and time (t) is in seconds.

$$Q_{cell}(t) = \int_0^t \frac{I(t)}{3600}\,dt \tag{3.26}$$

E_{cell} is the voltage difference between the negative and positive terminals of the battery which is calculated using eq.(3.27).

$$E_{cell}(t) = \phi_s(x = L, t) - \phi_s(x = 0, t) \tag{3.27}$$

Generally, E_{cell} depends on SOC and total current density (I). A high quality battery provides constant E_{cell} regardless of SOC and the drop of E_{cell} with increasing discharge current (I) is minor.

3.3.9 Summary

Principles of conservation of mass and conservation of current (charges) are used to develop the electrochemical model. Mass and charge transport due to Li and charge transport due to electrons are considered. The mass transport of electrons are excluded because mass of electrons are negligible compared to Li. The model depends on three

spacial domains namely, electrolyte, negative electrode and positive electrode domains.

Conservation of Li in electrodes (eq. (3.17)) are solved within P2D space and time (i.e. (r, x, t)). Source term for electrodes are only applied at interface between electrode and electrolyte (embedded in boundary condition, eq. (3.18)). Magnitude and direction of source term is governed by charge transfer reaction (Eq. (3.12)).

Conservation of Li^+ in electrolyte (eq. (3.1)) is solved within x-dimension and time. (i.e. (x, t)). Source term for electrolyte applied within negative and positive electrode regions. At the separator region there exists no source term. The magnitude and direction of source term is depend on charge transfer reaction (Eq. (3.12)).

Conservation of current (eq. (3.3), (3.7), (3.10), (3.11) and (3.12)) is solved within x-dimension and time (i.e. (x, t)). The kinetics are based on Ohm's law and Butler-Volmer kinetics. Solution for system of equations mainly depend on total current density (I) that is drawn in/out from battery. Solution obtained from charge transfer system of equations then used to determine Li mass transfer between electrode-electrolyte interfaces.

When battery is not connected to an external circuit (circuit is open), There is no flow of current. When battery is connected to an external circuit electrons start to flow through the external circuit due to electric potential difference. Thus, charge transfer reaction initiates. The potential difference across battery (E_{cell}) is determined by eq.(3.27),

$$E_{cell}(t) = \phi_s(x = L, t) - \phi_s(x = 0, t)$$

If material or chemistry of negative electrode is changed, formulae for OCV (eq. (3.15)), Diffusivity (eq. (3.19)) and for reactivity (eq. (3.23)) need to be replaced with new equations or values correspond to material. Similarly, if material in positive electrode is changed, formulae for OCV (eq. (3.16)), Diffusivity (eq. (3.20)) and for reactivity (eq. (3.24)) need to be replaced. Ionic conductivity (eq. (3.22)), and ionic diffusivity (eq. (3.21)) need to be replaced if different electrolyte is used other than $LiPF_6$ in propylene carbonate, ethylene carbonate and dimethyl carbonate.

3.4 Capacity Fading

The construction of battery initially consumes about 10% of active lithium to form the Solid Electrolyte Interface (SEI) layer [28, 33]. This effect should be accounted when defining initial Li concentration for negative electrode.

The capacity fading due to aging is determined using semi empirical model developed by Wang et al. [29]. This model has been used by several other authors, which indicate good approximations with experimental data [4, 20]. The semi-empirical model was developed for lithium battery with graphite anode and $LiFePO_4$ cathode [29]. This model can be used independent of output data by P2D model [20].

Equation (3.28) is used for the calculation of capacity reduction [29]. C_{loss} is the percentage of active lithium lost compared to initial lithium at electrode. C_Rate is a parameter to indicate the discharge rate of battery; for example 1C means the current that is required to discharge/charge the full battery capacity in 1hour, 2C means the current that is required to discharge/charge the full battery capacity in 0.5 hours, 0.5C means the current that is required to discharge/charge the full battery capacity in 2 hours, etc.

Pre-exponent factor (B) is dependent on C_Rate. These values were calculated by Wang et al. [29] and are presented in table 3.3. FCC is the full cell capacity in Ampere hour units. DOD is depth of discharge which represents the percentage of capacity that is discharged from battery compared to initial capacity. DOD does not have significant effect on capacity reduction at low discharge rates (i.e. 0.5C) [29]. CN indicates the cycle number which the battery has encountered. Discharge and subsequent charge of battery is defined as one cycle.

$$C_{loss}(\%) = B \times \exp\left(\frac{-31700 + 370.3 \times C\_Rate}{RT}\right) \times A_h^{0.55} \tag{3.28}$$

Where,

$$A_h = FCC \times DOD \times CN$$

$C_{loss}(\%)$	- Percentage of average lost lithium to averaged initial lithium
B	- Pre exponent factor
C_Rate	- Discharge rate
R	- Universal gas constant ($J\,K^{-1}\,mol^{-1}$)
T	- Absolute temperature (K)
FCC	- Full cell capacity (A h)
DOD	- Depth of Discharge
CN	- Cycle number

Table 3.3: Pre-exponent (B) values for capacity fade equation

C_Rate	0.5C	2C	6C	10C
B	31630	21681	12934	15512

Figure 3.6 demonstrates the effect of capacity loss described by equation (3.28) for 2 Ah battery with 100% depth of discharge at 298.15 K Temperature.

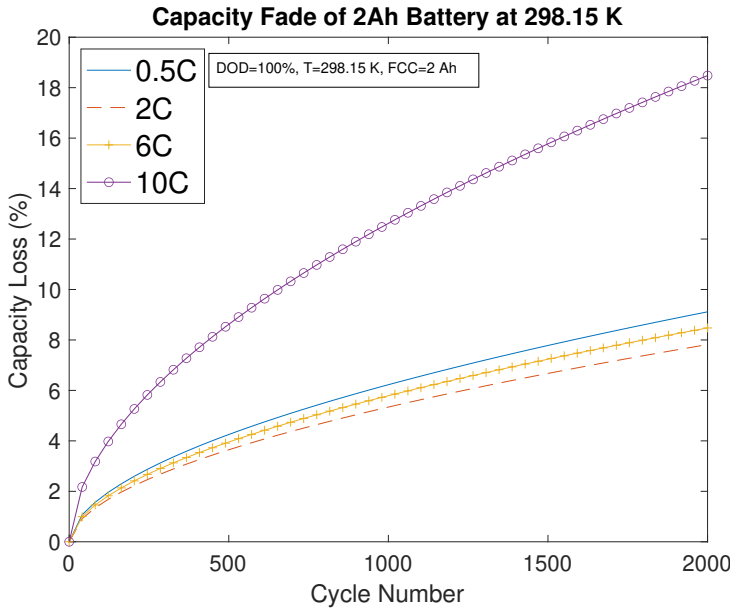

Figure 3.6: Capacity fade of 2 Ah battery at 298.15 K

Chapter 4

Methodology

The electrochemical model and thermal model are designed such that, if necessary, the electrochemical model can operate without an input from the thermal model (isothermal operation). The thermal model is documented in appendices C, D and E. Two different independent environments were used to design electrochemical and thermal models. When both models are operating together, the electrochemical model depends on temperature (T) input from the thermal model, and the thermal model depends on electric potentials of electrodes (ϕ_s), electrolyte (ϕ_e), Open Circuit Voltage (U), transfer current density (i_n), electrolyte concentration (c_e) and time (t) from the electrochemical model.

MATLAB is used to solve numerically the system of PDEs that are involved in the mathematical model describing discharging/charging of a lithium battery. Finite Difference Method (FDM) is used to numerically solve governing equations [41]. The Matlab code and the input data file are presented in appendix F.

4.1 Solution Strategy

4.1.1 Definition and Organization of Variables and Parameters

Input parameters for the battery and discretization parameters were tabulated in an Excel sheet. This ensured that proper organization of variables, convenient data entry and import data into Matlab easily. Input parameters which were used in this model are tabulated in table 4.1 and discretization parameters are presented in table 4.2. The electrochemical model presented in this section contains time, $x - dimension$ and quasi $r - dimension$ as dimensions and the thermal model presented in appendices C, D and

Table 4.1: Input parameters

Symbol	Description
L_n	Thickness of negative electrode
L_s	Thickness of separator
L_p	Thickness of positive electrode
ε	Porosity of electrodes
ε_e	Electrolyte volume fractions
σ_s	Electric conductivity of Electrodes
c_{max}	Maximum Li concentration at electrode materials
c_0	Initial concentration of Li at electrodes and separator
ρ	Densities
C_p	Specific heat capacities
K	Thermal conductivities
r_p	Radii of electrode particles
α	Anodic and cathodic activity coefficients for two electrodes
R	Universal gas constant
$T_{initial}$	Initial temperature
F	Faraday constant
t_+^0	Transference number of Li^+

E contains time, r_c and z as dimensions.

4.1.2 Defining Initial Conditions

After the import of data into Matlab, initial conditions were defined based on input and discretization parameters. Variable vectors and matrices were defined with respect to their number of spacial domains. Figure 4.1 illustrates three main spacial domains used for the battery model; negative electrode, positive electrode domains and electrolyte domain. For example, a variable which incorporates two spacial domains is Li concentration in negative electrode ($c_{s,n}$). This is defined such that for each grid cell in electrolyte domain (L_N), m_n number of grid cells are defined. Thus, negative electrode Li concentration ($c_{s,n}$) becomes ($M_n \times m_n$) matrix. Similarly, other vectors and matrices are also defined and tabulated in table 4.3. The table describes sizes of vectors/matrices and their descriptions.

It is impossible to correctly determine the initial value for electric potentials in electrodes and electrolyte ($\phi_s(x, t = 0)$, $\phi_e(x, t = 0)$). However, four assumptions have been made to determine an initial condition for electric potentials ϕ_s and ϕ_e:

1. Negative terminal of battery is grounded (Already mentioned in chapter 3)

Table 4.2: Discretization parameters

Symbol	Description
t	Length of time that battery operate
t_n	Number of time steps
dt	Time step size
M_n	Number of spacial steps at negative electrode
M_s	Number of spacial steps at separator
M_p	Number of spacial steps at positive electrode
M	Total number of spacial steps ($M_n + M_s + M_p$)
m_n	Number of special steps at spheres of negative electrode
dr_n	Length of spacial step at spheres of negative electrode
m_p	Number of special steps at spheres of positive electrode
dr_p	Length of spacial step at spheres of positive electrode

2. Initial total current density (I) is zero

3. Initial electrolyte potential (ϕ_e) is constant throughout the electrolyte domain (L_B)

4. Initial Li distribution in electrodes are homogenous

Thus, $I = 0$ and at the boundary 1 $\phi_s(x = 0, t) = 0$ (Eq. (3.8)). Based on these assumptions, the initial electric potential (ϕ_s, ϕ_e) at each grid cell is defined such that the transfer current density (i_n) is zero ($i_n = 0$, which implies that total current density (I) is zero). Since no current flows through the electrode (eq. (3.11)), the electrode potential (ϕ_s) becomes zero from boundary 1 to boundary 2 (Fig. 3.1),

$$\phi_s(x, t = 0) = 0\,, \qquad x \in L_N$$

Therefore, from equation (3.12), initial electrolyte potential becomes,

$$\phi_e(x, t = 0) = U_n\,, \qquad x \in L_B$$

and, electrode potential (ϕ_s) from boundary 3 to boundary 4 becomes,

$$\phi_s(x, t = 0) = U_p + U_n\,, \qquad x \in L_P$$

It is important to note that, governing equations are based only on potential differences, thus determination of absolute electric potential inside battery is not strictly necessary.

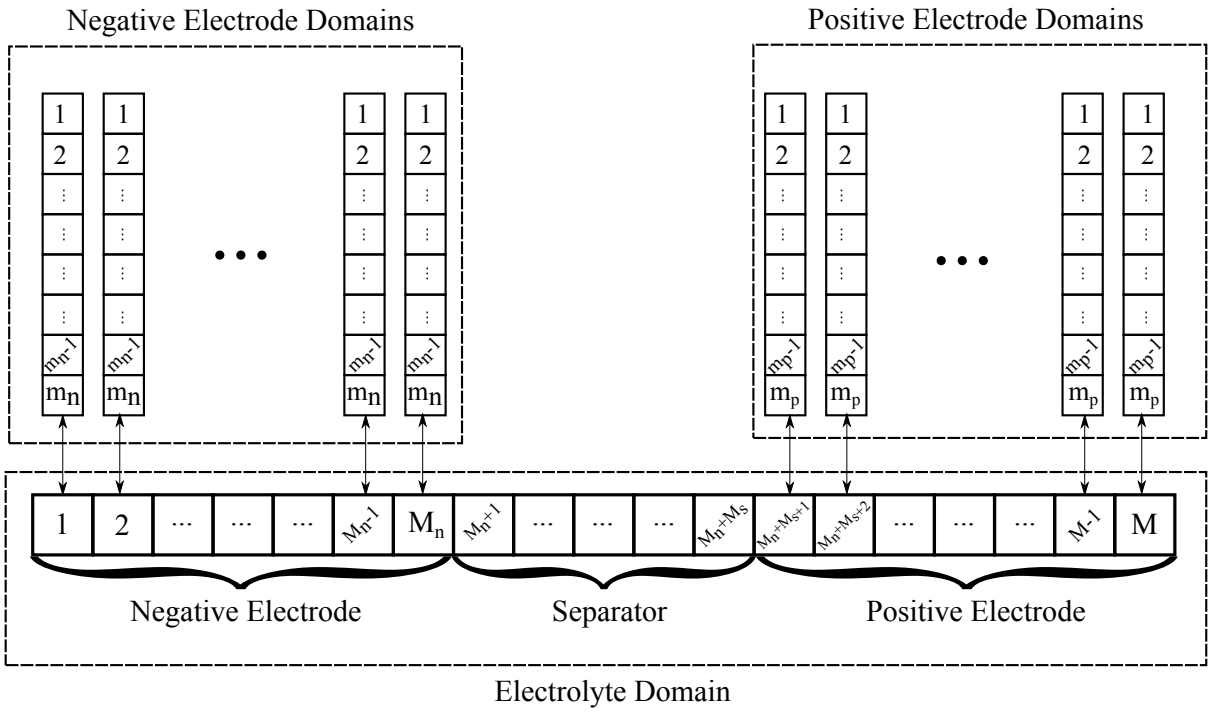

Figure 4.1: Spacial domains in battery model

Three main spacial domains; Negative electrode, Positive Electrode and Electrolyte domains are marked in the image. Double headed arrows illustrate charge transfer interface between electrode and electrolyte. Charge transfer occurs between electrolyte cell and last cells of electrode domains which represent the surface of the spheres (particles) which constitute the electrode. Continuous electrolyte domain divided into three parts, negative, positive electrode sections and separator section.

Table 4.3: Variable vectors and matrices

Symbol	Vector/Matrix Size	Description
$c_{s,n}$	$(M_n \times m_n)$	Li concentration at negative electrode
$c_{s,p}$	$(M_p \times m_p)$	Li concentration at positive electrode
D_n	$(1 \times M_n)$	Diffusivity at negative electrode
D_p	$(1 \times M_p)$	Diffusivity at positive electrode
ϕ_s	$(1 \times M)$	Electric potential at electrodes*
ϕ_e	$(1 \times M)$	Electric potential at electrolyte
c_e	$(1 \times M)$	Li^+ concentration at electrolyte
$c_{s,s}$	$(1 \times M)$	Surface Li concentration at electrodes*
i_n	$(1 \times M)$	Transfer current density*
i_s	$(1 \times M)$	Local current density in electrodes*
i_e	$(1 \times M)$	Local current density in electrolyte
U	$(1 \times M)$	OCV*
T	$(1 \times M)$	Absolute temperature
D_e	$(1 \times M)$	Diffusivity at electrolyte
κ_e	$(1 \times M)$	Ionic conductivity at electrolyte
k_0	$(1 \times M)$	Reactivity at electrodes*

**From cell (index) $M_n + 1$ to $M_n + M_s$ values are replaced with zero because these values are not defined/null at separator region.*

4.1.3 Looping the Algorithm with Evolving Time

After defining the initial conditions, a loop is necessary to compute solutions with advancing time. The main condition of the loop is to complete the number of time steps until a designated time is approached. Within the loop, calculations are divided into six functions. The following six functions are run in order, to compute a solution as it evolves over one time step:

1. Update parameters
2. Ohm's law and Butler-Volmer equations
3. Electrolyte mass balance equation
4. Mass balance equations for two electrodes
5. Thermal model equations
6. Battery voltage and capacity calculation

Update Parameters

The objective of 'Update parameters' is to calculate parameters for new time step based on the values from previous time step. These parameters are D_n, D_p, U, D_e, κ_e and k_0. Bruggeman tortuosity effect is also included in the formulae during the calculation of D_e and κ_e in order to convert them into effective values.

Ohm's Law and Butler-Volmer Equations

The objective of solving 'Ohm's law and Butler-Volmer equation' is to determine electrode potential (ϕ_s), Electrolyte potential (ϕ_e) and transfer current density (i_n). Governing equations (3.3), (3.7), (3.9), (3.10), (3.11), (3.12) and boundary conditions from equations (3.4), (3.8) are utilized for the derivation of solution.

Since, only $x - dimension$ is considered in this case, Ohm and Butler-Volmer equations which are related to electrodes (eq.(3.7), eq.(3.11) and eq.(3.12)) can be simplified into eq. (4.1) by substitutions.

$$\frac{\partial}{\partial x}\left(\sigma\frac{\partial \phi_s}{\partial x}\right) = a_s \underbrace{i_0\left(\exp\left(\frac{\alpha_a F}{RT}(\phi_s - \phi_e - U)\right) - \exp\left(-\frac{\alpha_c F}{RT}(\phi_s - \phi_e - U)\right)\right)}_{i_n} \tag{4.1}$$

Similarly, Ohm and Butler-Volmer equations which are related to electrolyte (eq.(3.3), eq.(3.5), eq.(3.10) and eq.(3.12)) can be simplified into eq. (4.2) by substitutions.

$$\begin{aligned}\frac{\partial}{\partial x}\left(\kappa_e\frac{\partial \phi_e}{\partial x} - \frac{2RT}{F}\nu\frac{\partial \ln c_e}{\partial x}\right) = \\ - a_s \underbrace{i_0\left(\exp\left(\frac{\alpha_a F}{RT}(\phi_s - \phi_e - U)\right) - \exp\left(-\frac{\alpha_c F}{RT}(\phi_s - \phi_e - U)\right)\right)}_{i_n}\end{aligned} \tag{4.2}$$

In equations (4.1) and (4.2), the sections related to transfer current density (i_n) are marked with i_n using under-braces. This is because in later stages in this chapter, i_n is used to represent the large section of these equations to save space and make equations more concise.

In order to compute a solution for this function, equations (4.1) and (4.2) are solved by

using FDM and Newton-Raphson method which is discussed later in this chapter [17].

Electrolyte Mass Balance Equation

Since a value for transfer current density (i_n) was determined in previous step (Ohm's Law and Butler-Volmer Equations), Equation (3.1) with boundary conditions in equation (3.2) are used to determine the transport of Li^+ within the electrolyte.

Mass Balance Equations for Two Electrodes

In 'Mass balance equations for two electrodes', equation (3.17) and boundary conditions in equation (3.18) are used to determine the transport of Li in electrodes. The equation (3.17) should be solved for both negative and positive electrodes separately.

Thermal Model Equations

The objective of 'Thermal model equations' is to determine battery temperature based on internal heat generation and heat loss from surfaces. The thermal model depends on electric potentials of electrodes (ϕ_s), electrolyte (ϕ_e), Open Circuit Voltage (U), transfer current density (i_n), electrolyte concentration (c_e) from electrochemical model. The thermal model outputs the volume average temperature of the battery into the electrochemical model. In addition, thermal model can produce a graph which demonstrates the heat distribution in cylindrical geometry. The theory for the thermal model is presented in appendix C and discretization is presented in appendices D and E. However, simulations conducted in this thesis only considers iso-thermal condition of a battery. Thus, thermal model is not utilized.

Battery Voltage and Capacity Calculation

This is a simple function which calculates battery voltage (E_{cell}) and battery capacity (Q_{cell}). These are two main output variables of the simulation.

4.1.4 Algorithm

The solution strategy which was discussed above can be summarized into following al-

gorithm. Comments in blue italic text indicate the respective functions which were discussed above and additional comments are indicated in red italic text. The keywords are mentioned in capital text.

1. START
2. IMPORT input data into the simulator
3. DEFINE t = 0 ← *define time step*
4. DEFINE initial conditions
   for $c_{s,n}$, $c_{s,p}$, c_e, ϕ_s, ϕ_e, D_n, D_p, i_n, U, T, D_e, κ_e, k_0 ← *Defining Initial Conditions*
5. t = t+1 ← *Update time step*
6. CALCULATE parameters D_n, D_p, U, D_e, κ_e, k_0 ← *Update Parameters*
7. SOLVE for ϕ_s, ϕ_e, i_n ← *Ohm's Law and Butler-Volmer Equations*
8. SOLVE for c_e ← *Electrolyte Mass Balance Equation*
9. SOLVE for $c_{s,n}$, $c_{s,p}$ ← *Mass Balance Equations for Two Electrodes*
10. SOLVE for T ← *Thermal Model Equations*
11. CALCULATE E_{cell}, Q_{cell} ← *Battery Voltage and Capacity Calculation*
12. IF $t < t_{end}$ == TRUE, go to step 5 ← *Condition for loop*
13. PRINT, PLOT, SAVE solutions
14. END

4.2 Discretization

4.2.1 Discretization and Notations Used

Variables and coefficients that are used in discretization of equations are presented in following notations,

$$\left[V_{\beta}^{\eta}\right]_{z}^{\tau}$$

V - Variable/Coefficient.
η - Superscript of variable.
β - Subscript of variable.
τ - Time step value.
z - Spacial step value.

To improve the conciseness of presented discretized equations, variable coefficients which depend on spacial variables are presented as,

$$\Omega_{+} = [\Omega]_{z+\frac{1}{2}} = \frac{[\Omega]_{z+1} + [\Omega]_{z}}{2}$$
$$\Omega_{-} = [\Omega]_{z-\frac{1}{2}} = \frac{[\Omega]_{z} + [\Omega]_{z-1}}{2}$$

Note that Ω is a symbol which represents a discretizable variable.

Following finite discretization used for time derivatives (generalized version),

$$\frac{\partial V}{\partial t} = \frac{[V]_{z}^{t+1} - [V]_{z}^{t}}{\Delta t}$$

Forward difference method is used for discretization of 1^{st} order spacial derivative [41]. Generalized discretization as follows,

$$\frac{\partial V}{\partial x} = \frac{[V]_{z+1} - [V]_{z}}{\Delta x}$$

Central difference method is used for discretization of 2^{nd} order spacial derivative[41] including a coefficient. Generalized discretization as follows,

$$\frac{\partial}{\partial x}\left(\Omega\frac{\partial V}{\partial x}\right) = \frac{1}{\Delta x}\left[\Omega_{+}\left(\frac{[V]_{z+1} - [V]_{z}}{\Delta x}\right) - \Omega_{-}\left(\frac{[V]_{z} - [V]_{z-1}}{\Delta x}\right)\right]$$

by re-arranging,

$$\frac{\partial}{\partial x}\left(\Omega\frac{\partial V}{\partial x}\right) = \frac{1}{\Delta x^{2}}\left(\Omega_{+}[V]_{z+1} - (\Omega_{+} + \Omega_{-})[V]_{z} + \Omega_{-}[V]_{z-1}\right)$$

4.2.2 Ohm's Law and the Butler-Volmer Equation

This is the most complex and longest function in the electrochemical model. Thus, it is important to note that several additional subsections and equations related to this section are presented in appendix B.

In this function, solutions for electrode potential (ϕ_s), electrolyte potential (ϕ_e) and transfer current (i_n) are derived for a single time step. The Ohm's law equation and Butler-Volmer equation do not contain time derivative (i.e. eq.(4.1) and eq.(4.2)). These two equations are non-linear PDEs which needed to be solved for electrode potential (ϕ_s) and electrolyte potential (ϕ_e) simultaneously. Therefore, discretized equations are solved using Newton-Raphson method to approximate the solution [17].

Eq.(4.1) and eq.(4.2) are solved only in spacial domain (i.e. electrolyte domain), and no time domain is involved. However, to derive at a solution using Newton-Raphson method, iterations are used. In this section the number of iterations are denoted by symbol 'n'.

Concise Equations Using $[i_n]_z$

In order to ensure that equations are concise and short, transfer current density (i_n) was used in Eq.(4.1) and eq.(4.2). It is important to derive the discretization of expression denoted by i_n because discretized formulae presented in appendix B and discretized formulae presented later in this section contains i_n. Thus, discretization of i_n is presented by eq.(4.3).

$$[i_n]_z = i_0 \left(\exp\left(\frac{\alpha_a F}{RT}([\phi_s]_z - [\phi_e]_z - [U]_z)\right) - \exp\left(-\frac{\alpha_c F}{RT}([\phi_s]_z - [\phi_e]_z - [U]_z)\right)\right) \tag{4.3}$$

Eq.(4.1) and eq.(4.2) are solved for electrode potential (ϕ_s), electrolyte potential (ϕ_e). In order to derive a solution, the Newton-Raphson method demands derivatives of discretized eq.(4.1) and eq.(4.2) with respect to discretized electrode potential ($[\phi_s]_z$) and discretized electrolyte potential ($[\phi_e]_z$). Therefore, it is important to determine derivative of $[i_n]_z$ with respect to $[\phi_s]_z$ and $[\phi_e]_z$. Thus, derivative of $[i_n]_z$ with respect to $[\phi_s]_z$ is presented by eq.(4.4).

$$\frac{\partial [i_n]_z}{\partial [\phi_s]_z} = i_0 \left(\frac{\alpha_a F}{RT} \exp\left(\frac{\alpha_a F}{RT} ([\phi_s]_z - [\phi_e]_z - [U]_z) \right) + \frac{\alpha_c F}{RT} \exp\left(-\frac{\alpha_c F}{RT} ([\phi_s]_z - [\phi_e]_z - [U]_z) \right) \right) \tag{4.4}$$

Similarly, the derivative of $[i_n]_z$ with respect to $[\phi_e]_z$ is presented by eq.(4.5).

$$\frac{\partial [i_n]_z}{\partial [\phi_e]_z} = -i_0 \left(\frac{\alpha_a F}{RT} \exp\left(\frac{\alpha_a F}{RT} ([\phi_s]_z - [\phi_e]_z - [U]_z) \right) + \frac{\alpha_c F}{RT} \exp\left(-\frac{\alpha_c F}{RT} ([\phi_s]_z - [\phi_e]_z - [U]_z) \right) \right) \tag{4.5}$$

Subjects of eq.(4.3), eq.(4.4) and eq.(4.5) (term in L.H.S) are used in latter formulae and formulae in appendix B in order to concise the equations. Whenever a latter equation uses $[i_n]_z$, it refers to eq.(4.3). Similarly, $\frac{\partial [i_n]_z}{\partial [\phi_s]_z}$ refers to eq.(4.4) and $\frac{\partial [i_n]_z}{\partial [\phi_e]_z}$ refers to eq.(4.5).

Newton-Raphson Formula

Discretization of eq.(4.1) and eq.(4.2) result $M + (M_n + M_p)$ number of variables to be solved: M number of variables due to electrolyte potential (ϕ_e) and $(M_n + M_p)$ number of variables due to electrode potential (ϕ_s). Thus, these two equations need to be solved in matrix format. Equation (4.6) shows the matrix format of Newton-Raphson formula. The Newton-Raphson formula (eq.(4.6)) needs to be solved for each iteration. It is important to note that the iterations executed in Newton-Raphson method do not evolve in time.

$$[J][\Delta\phi] = [-f] \tag{4.6}$$

$[J]$ is known as the Jacobian matrix which houses all derivatives of eq.(4.1) and eq.(4.2). Jacobian matrix ($[J]$) is a $(M + (M_n + M_p)) \times (M + (M_n + M_p))$ square matrix. The format of this matrix is presented in appendix B.2.2 and will be discussed later in this section.

The Eq. (4.6) is solved for $[\Delta\phi]$. $[\Delta\phi]$ houses differential values that are added to the previous step ϕ values as iteration advances. This is a $(M + (M_n + M_p)) \times 1$ column

matrix and the format is presented in appendix B.2.1. As the iteration advances, new ϕ values are calculated by using following equation,

$$\phi_{n+1} = \phi_n + \Delta\phi_n$$

Here, ϕ represents either the electrode potential (ϕ_s) or the electrolyte potential (ϕ_e). n is the iteration number.

$[-f]$ matrix in eq.(4.6) is a $(M + (M_n + M_p)) \times 1$ column matrix. The format of this matrix is presented in appendix B.2.1. In order to solve eq.(4.1) and eq.(4.2) they need to be converted into functions. Let functions derived from eq.(4.1) (electrode) as f_1 and functions derived from eq.(4.2) (Electrolyte) as f_2 such that $f = f_1 \cup f_2$. Therefore, $[-f]$ matrix houses all the f functions which needs to be solved for $f = 0$ or $f \approx 0$.

Define and Discretization of f_1 Function (Electrodes)

The function f_1 presented in eq. (4.7) is derived from eq.(4.1). This equation is valid only for negative and positive electrodes in electrolyte domain ($L_N \cup L_P$).

$$f_1 = \frac{\partial}{\partial x}\left(\sigma \frac{\partial \phi_s}{\partial x}\right) - a_s\, i_n \tag{4.7}$$

Due to the similar characteristics in negative and positive electrodes, the discretized f_1 function for center grid cells is common for both electrodes. However, the boundary conditions are different to each other. Thus, individual discretization should be made for the four different boundaries.

For center grid cells, discretization of eq.(4.7) results in eq.(4.8). The expression for $[i_n]_z$ can be found in eq. (4.3). The function represented in Eq. (4.8) is denoted as $f_1(z)$ where z expresses the index of grid cell ($1 < z < M_n \quad or \quad M_n + M_s + 1 < z < M$).

$$f_1(z) = \frac{1}{\Delta x^2}\Big(\sigma_+[\phi_s]_{z+1} - (\sigma_+ + \sigma_-)[\phi_s]_z + \sigma_-[\phi_s]_{z-1}\Big) - a_s[i_n]_z \tag{4.8}$$

Discretized functions for the two boundaries in negative electrode are presented in eq.(4.9) and eq.(4.10). These equations are derived by substitution of boundary conditions from eq.(3.8) to eq.(4.7) during discretization. The eq.(4.9) is used for the boundary 1 and the eq. (4.10) is used for the boundary 2 (fig. 3.1).

Boundary 1 - Negative Electrode

$$f_1(1) = \frac{1}{\Delta x}\left(\sigma_+ \frac{[\phi_s]_2 - [\phi_s]_1}{\Delta x} + I\right) - a_s[i_n]_1 \tag{4.9}$$

Boundary 2 - Negative Electrode

$$f_1(M_n) = -\sigma_- \frac{[\phi_s]_{M_n} - [\phi_s]_{M_n-1}}{\Delta x^2} - a_s[i_n]_{M_n} \tag{4.10}$$

Discretized functions for the two boundaries in positive electrode are presented in eq.(4.11) and eq.(4.12). These equations are derived by substitution of boundary conditions from eq.(3.8)) to eq.(4.7) during discretization. The eq.(4.11) is used for the boundary 3 and the eq.(4.12) is used for the boundary 4 (fig. 3.1).

Boundary 3 - Positive Electrode

$$f_1(M_n + M_s + 1) = \sigma_+ \frac{[\phi_s]_{(M_n+M_s+2)} - [\phi_s]_{(M_n+M_s+1)}}{\Delta x^2} - a_s[i_n]_{(M_n+M_s+1)} \tag{4.11}$$

Boundary 4 - Positive Electrode

$$f_1(M) = \frac{1}{\Delta x}\left(-I - \sigma_- \frac{[\phi_s]_M - [\phi_s]_{M-1}}{\Delta x}\right) - a_s[i_n]_M \tag{4.12}$$

The sign of total current density (I) is important in substitution to eq.(4.7) during discretization. The total current density (I) has been substituted to eq.(4.9) and eq.(4.12) such that, a negative I value represents the discharge process and a positive I value represents the charge process.

Define and Discretization of f_2 Function (Electrolyte)

The function f_2 presented in eq.(4.13) is derived from eq.(4.2). This function is valid in the electrolyte domain (L_B).

$$f_2 = \frac{\partial}{\partial x}\left(\kappa_e \frac{\partial \phi_e}{\partial x}\right) - \frac{\partial}{\partial x}\left(\frac{2RT\kappa_e}{F}\nu \frac{\partial \ln c_e}{\partial x}\right) + a_s\, i_n \tag{4.13}$$

The eq.(4.13) is discretized for center grid cells. The resulting function is presented in eq.(4.14). The expression for $[i_n]_z$ can be found in eq.(4.3). $f_2(z)$ is used to denote the

function in eq.(4.13) where, z expresses the index of grid cell ($1 < z < M$).

$$\begin{aligned} f_2(z) =& \frac{1}{\Delta x^2}\Bigg(\Big(\kappa_{e,+}[\phi_e]_{z+1} - (\kappa_{e,+} + \kappa_{e,-})[\phi_e]_z + \kappa_{e,-}[\phi_e]_{z-1}\Big) \\ & - \frac{2R}{F}\Big(T_+\kappa_{e,+}\nu_+(\ln[c_e]_{z+1} - \ln[c_e]_z) - T_-\kappa_{e,-}\nu_-(\ln[c_e]_z - \ln[c_e]_{z-1})\Big)\Bigg) \\ & + a_s[i_n]_z \end{aligned} \tag{4.14}$$

Unlike the function f_1, boundary conditions for the function f_2 only applies at boundary 1 and boundary 4. This is because electrolyte is continuous through the boundary 2 and boundary 3. Eq.(4.15) and eq.(4.16) show the boundary equations. These functions are derived by using substitution of the boundary conditions from eq.(3.4) to eq.(4.13) during discretization. The eq.(4.15) represents the function for the boundary 1 and the eq.(4.16) represents the function for the boundary 4 (fig. 3.1).

Boundary 1 - Electrolyte

$$f_2(1) = \frac{\kappa_{e,+}}{\Delta x^2}\Bigg(\Big([\phi_e]_2 - [\phi_e]_1\Big) - \frac{2R}{F}\Big(T_+\nu_+(\ln[c_e]_2 - \ln[c_e]_1)\Big)\Bigg) + a_s[i_n]_1 \tag{4.15}$$

Boundary 4 - Electrolyte

$$f_2(M) = -\frac{\kappa_-}{\Delta x^2}\Bigg(\Big([\phi_e]_M - [\phi_e]_{M-1}\Big) - \frac{2R}{F}\Big(-T_-\nu_-(\ln[c_e]_M - \ln[c_e]_{M-1})\Big)\Bigg) + a_s[i_n]_M \tag{4.16}$$

Jacobian Matrix $[J]$ and Derivatives

The approximation of solution using Newton-Raphson method requires to determine derivatives of functions f_1 and f_2 with respect to electrode potential (ϕ_s) and electrolyte potential (ϕ_e). The values for these derivates are organized in the Jacobian matrix ($[J]$) (see appendix B.2.2). Table 4.4 shows the functions that need to be evaluated for its derivatives. Third column of the table shows the discretized variables that are used for differentiation of respective function. The discretization of these functions are presented in appendix B.

Since discretized functions f_1 and f_2 depend on neighboring electrode ($[\phi_s]$) and electrolyte ($[\phi_e]$) potentials in the grid, it is necessary to consider only the derivatives which are mentioned in appendix B (also in table 4.4). The other derivatives become zero.

Table 4.4: Derivates for Jacobian matrix

Eq.	Function	Derivatives with respect to
(4.8)	$f_1(z)$	$[\phi_s]_{z-1}$, $[\phi_s]_z$, $[\phi_s]_{z+1}$, $[\phi_e]_z$
(4.9)	$f_1(1)$	$[\phi_s]_1$, $[\phi_s]_2$, $[\phi_e]_1$
(4.10)	$f_1(M_n)$	$[\phi_s]_{M_n-1}$, $[\phi_s]_{M_n}$, $[\phi_e]_{M_n}$
(4.11)	$f_1(M_n + M_s + 1)$	$[\phi_s]_{M_n+M_s+1}$, $[\phi_s]_{M_n+M_s+2}$, $[\phi_e]_{M_n+M_s+1}$
(4.12)	$f_1(M)$	$[\phi_s]_{M-1}$, $[\phi_s]_M$, $[\phi_e]_M$
(4.14)	$f_2(z)$	$[\phi_e]_{z-1}$, $[\phi_e]_z$, $[\phi_e]_{z+1}$, $[\phi_s]_z$
(4.15)	$f_2(1)$	$[\phi_e]_1$, $[\phi_e]_2$, $[\phi_s]_1$
(4.16)	$f_2(M)$	$[\phi_e]_{M-1}$, $[\phi_e]_M$, $[\phi_s]_M$

Other derivates - for example:

$$\frac{\partial f_1(z)}{\partial [\phi_s]_{z\pm i}} = 0\,,\ \frac{\partial f_2(z)}{\partial [\phi_e]_{z\pm i}} = 0\,,\ \text{where } i \neq 0,\ i \neq 1,\ i \in \mathbb{Z}$$
$$\frac{\partial f_1(z)}{\partial [\phi_e]_{z\pm j}} = 0\,,\ \frac{\partial f_2(z)}{\partial [\phi_s]_{z\pm j}} = 0\,,\ \text{where } j \neq 0,\ j \in \mathbb{Z}$$

Deriving at a Solution

After organization of $[J]$ and $[-f]$ matrices as stated in appendix B, iterations are used to arrive at a solution (eq.(4.6)). For each iteration, values in $[J]$ and $[-f]$ matrices are needed to be updated for new potentials (ϕ_s and ϕ_e). The iterations are carried out until errors becomes reasonably small. In this thesis, error tolerance for $[\phi]$ matrix was selected as $max\left(\frac{[\Delta\phi]_n}{[\phi]_n}\right) < 0.001$. Since Newton-Raphson method converges into a solution quadratically, comparatively less number of iterations are required.

After deriving the solution for the electrode (ϕ_s) and electrolyte (ϕ_e) potentials, transfer current density (i_n) is calculated for each grid cell using eq.(4.3). The transfer current density (i_n) is a critical variable for determination of mass transport in electrolyte and in electrodes.

4.2.3 Electrolyte Mass Balance Equation

The mass transport in electrolyte is presented by eq.(3.1). The discretized version of this equation is presented by eq.(4.17). The discretization was done based on x, t dimensions and using implicit scheme. $[i_n]_z^t$ has been already determined by eq.(4.3) from the previous function.

$$-\frac{\Delta t\, D_{e,+}}{\Delta x^2\, \varepsilon_e}[c_e]_{z+1}^{t+1} + \left(1 + \frac{\Delta t\, (D_{e,+} + D_{e,-})}{\Delta x^2\, \varepsilon_e}\right)[c_e]_z^{t+1} - \frac{\Delta t\, D_{e,-}}{\Delta x^2\, \varepsilon_e}[c_e]_{z-1}^{t+1} = [c_e]_z^t + \frac{\Delta t}{\varepsilon_e}\left(\frac{1 - t_+^0}{F}\right) a_s\, [i_n]_z^t \tag{4.17}$$

Substitution of boundary conditions from eq.(3.2) to eq.(3.1) during discretization results in eq.(4.18) for left boundary and eq.(4.19) for right boundary of electrolyte.

Boundary 1

$$-\frac{\Delta t\, D_{e,+}}{\Delta x^2\, \varepsilon_e}[c_e]_{z+1}^{t+1} + \left(1 + \frac{\Delta t\, D_{e,+}}{\Delta x^2\, \varepsilon_e}\right)[c_e]_z^{t+1} = [c_e]_z^t + \frac{\Delta t}{\varepsilon_e}\left(\frac{1 - t_+^0}{F}\right) a_s\, [i_n]_z^t \tag{4.18}$$

Boundary 4

$$\left(1 + \frac{\Delta t\, D_{e,-}}{\Delta x^2\, \varepsilon_e}\right)[c_e]_z^{t+1} - \frac{\Delta t\, D_{e,-}}{\Delta x^2\, \varepsilon_e}[c_e]_{z-1}^{t+1} + = [c_e]_z^t + \frac{\Delta t}{\varepsilon_e}\left(\frac{1 - t_+^0}{F}\right) a_s\, [i_n]_z^t \tag{4.19}$$

Since implicit method is used to derive at a solution, L.H.S of eq.(4.17), eq.(4.18) and eq.(4.19) are organized into a matrix A and a matrix x. x is a column matrix which contains all Li^+ concentrations at subsequent time step ($[c_e]_z^{t+1}$, $[c_e]_{z+1}^{t+1}$, $[c_e]_{z-1}^{t+1}$). A is a square matrix which houses coefficients of ($[c_e]_z^{t+1}$, $[c_e]_{z+1}^{t+1}$ and $[c_e]_{z-1}^{t+1}$). R.H.S of these equations are organized in to a column matrix b. Therefore, the solution for Li^+ concentration in electrolyte (c_e) at a certain time step is obtained by solving the x matrix using $x = A^{-1}b$.

4.2.4 Mass Balance Equation for the Two Electrodes

Mass balance for the two electrodes (eq.(3.17)) are applied within negative ($R_N \times L_N$) and positive ($R_P \times L_P$) electrode domains. Discretization of the eq.(3.17) in r and t dimensions result in eq.(4.20) for center grid cells. It is important to note that 'z' in eq.(4.20), eq.(4.21) and eq.(4.22) represent the index of grid cell in $r - dimension$. Some parameters in eq(4.20) are represented with new parameter called λ in order to maintain the equation concise and short. Parameter λ, is also used in defining discretized boundary conditions in eq.(4.21) and eq.(4.22).

$$-\lambda\left(2 + \frac{r}{\Delta r}\right)[c_s]_{z+1}^{t+1} + \left(1 + 2\lambda + \frac{2\lambda r}{\Delta r}\right)[c_s]_z^{t+1} - \frac{\lambda r}{\Delta r}[c_s]_{z-1}^{t+1} = [c_s]_z^t \tag{4.20}$$

$$\lambda = \frac{D_s\,\Delta t}{r\,\Delta r}$$

The core and surface are two boundaries of a sphere. Substitution of boundary conditions from eq.(3.18) in eq.(3.17) during discretization gives eq.(4.21) for core and eq. (4.22) for surface of sphere. D is the diffusion coefficient.

Core of sphere

$$-\left(2\lambda + \frac{\lambda r}{\Delta r}\right)[c_s]_{z+1}^{t+1} + \left(1 + 2\lambda + \frac{\lambda r}{\Delta r}\right)[c_s]_z^{t+1} = [c_s]_z^t \tag{4.21}$$

Surface of sphere (interface between electrode and electrolyte)

$$\left(1 + \frac{\lambda r}{\Delta r}\right)[c_s]_z^{t+1} - \frac{\lambda r}{\Delta r}[c_s]_{z-1}^{t+1} = [c_s]_z^t - \frac{\lambda[i_n]_z^t(2\Delta r + r)}{D\,F} \tag{4.22}$$

The implicit method is used to derive the solution for this system of equations. Typically, L.H.S of eq.(4.20), eq.(4.21) and eq.(4.22)) are organized into a materix A and x. x is a column matrix which contains all Li concentrations at subsequent time step ($[c_s]_z^{t+1}$, $[c_s]_{z+1}^{t+1}$, $[c_s]_{z-1}^{t+1}$). A is a square matrix which houses coefficients of ($[c_s]_z^{t+1}$, $[c_s]_{z+1}^{t+1}$ and $[c_s]_{z-1}^{t+1}$). R.H.S of these equations are organized in to a column matrix b. Then, Li concentration values (c_s) in the electrode for subsequent time step are obtained from $x = A^{-1}b$. The two domains which this system of equations are solved for, can be mentioned as follows,

Negative Electrode: - The eq.(4.20), eq.(4.21) and eq.(4.22) system needs to be solved in R_N domain for each index from 1 to M_n in electrolyte domain L_N.

Positive Electrode: - The eq.(4.20), eq.(4.21) and eq.(4.22) system needs to be solved in R_P domain for each index from $M_n + M_s + 1$ to M in electrolyte domain L_P.

Figure 4.1 can be used as an aid to construct the matrices for Li concentrations in negative and positive electrodes.

4.2.5 Battery Voltage and Battery Capacity

Battery capacity (Q_{cell}) is determined in time domain. Equation(3.26) is discretized which results in eq.(4.23). Here, n represents the number of time step and t represents time step at the required time.

$$[Q_{cell}]^t = \frac{1}{3600} \sum_{n=0}^{t} I \, \Delta t \, n \tag{4.23}$$

$$[E_{cell}]^t = [\phi_s]^t_{z=M} - [\phi_s]^t_{z=1} \tag{4.24}$$

Battery voltage (E_{cell}) is also determined in time domain. Discretization of equation(3.27) is presented by eq.(4.24).

4.3 Matlab Program Structure

The electrochemical model was developed in Matlab (Version: R2020b) software. Figure 4.2 illustrates the flow diagram for fundamental Matlab program structure which is developed for electrochemical model. Matlab functions are defined for each main operations and each main functions/operations are numbered in fig. 4.2 and described below.

(1) ⇒ This function import battery parameters, initial conditions and discretization parameters, constants and current density (I) from a spreadsheet (i.e INPUT.xlsx) file. If capacity fading model is used, the output result from capacity fading model should be written to spreadsheet (i.e INPUT.xlsx) file before executing the electrochemical model.

(2) ⇒ This function creates vectors and matrices that are required to execute the simulation. Initial values (at $t = 0$) are then input into the vectors/matrices. Individual vectors/matrices are defined for each variables which are presented in table 4.3 for their respective spacial domains (grid cells).

(3) ⇒ This is a logical condition to terminate the program when desired time limit is achieved.

(4) ⇒ This function updates parameters that are required to execute the next time step operations. These parameters include cell temperature (T), diffusivity in electrodes (D_n), OCVs (U), diffusivity in electrolyte (D_e), ionic conductivity in electrolyte (κ_e), conductivity in electrodes (σ) and reaction coefficients (k_0). Some parameters depend on variables such as temperature (T) and lithium concentration (c_s, c_e). These values are taken from the previous time step. Function for thermal model can be introduced in this section to determine cell temperature (T) if user decides to include a thermal model into the simulation.

(5) ⇒ This function solves the Ohm's equations and Butler-Volmer equation using Newtons-Raphson method. Output from this function includes electrode and electrolyte potential distribution (ϕ_s and ϕ_e) for grid cells in electrolyte domain. The function utilizes equations presented in section 4.2.2 and appendix B.

(6) ⇒ This function calculates transfer current density (i_n) for grid cells in electrolyte domain. Input to this function includes electrode and electrolyte potentials (ϕ_s and ϕ_e) which were determined in (5) function. The function utilizes eq.(4.3).

(7) ⇒ Based on the transfer current density (i_n) which was calculated in (6), mass transport of Li^+ in electrolyte (c_e) is determined. The function utilizes equations presented in section 4.2.3.

(8) ⇒ Based on the transfer current density (i_n) which was calculated in (6), mass transport of Li in electrodes (c_s) are determined. The function utilizes equations presented in section 4.2.4.

(9) ⇒ This function calculate battery voltage (E_{cell}) and battery capacity (Q_{cell}). The function utilizes equations presented in section 4.2.5.

(10) ⇒ This is a logical condition to ensure that simulation is run between desired battery voltage interval (V_{high}- upper boundary, V_{low}- lower boundary). Decision box terminates the program if calculated battery voltage (E_{cell}) is out of the interval. This function also ensures that no complex number solution is generated at function (5) due to inversion (change of sign) of voltage.

(11) ⇒ Required data is saved as a Matlab (.mat) file and plots are generated to visualize the results. Generated plots are E_{cell} vs. Q_{cell} and E_{cell} vs. and time (t).

Functions (4), (5), (6), (7), (8) and (9) are the core of simulation. Equations that are used in these functions are tabulated in table 4.5. It is strictly necessary to run functions (4), (5) and (6) sequentially. However, if the computer is capable of parallel processing, since functions (7), (8) and (9) are independent from each other, these three functions can be run in parallel in order to reduce the simulation time.

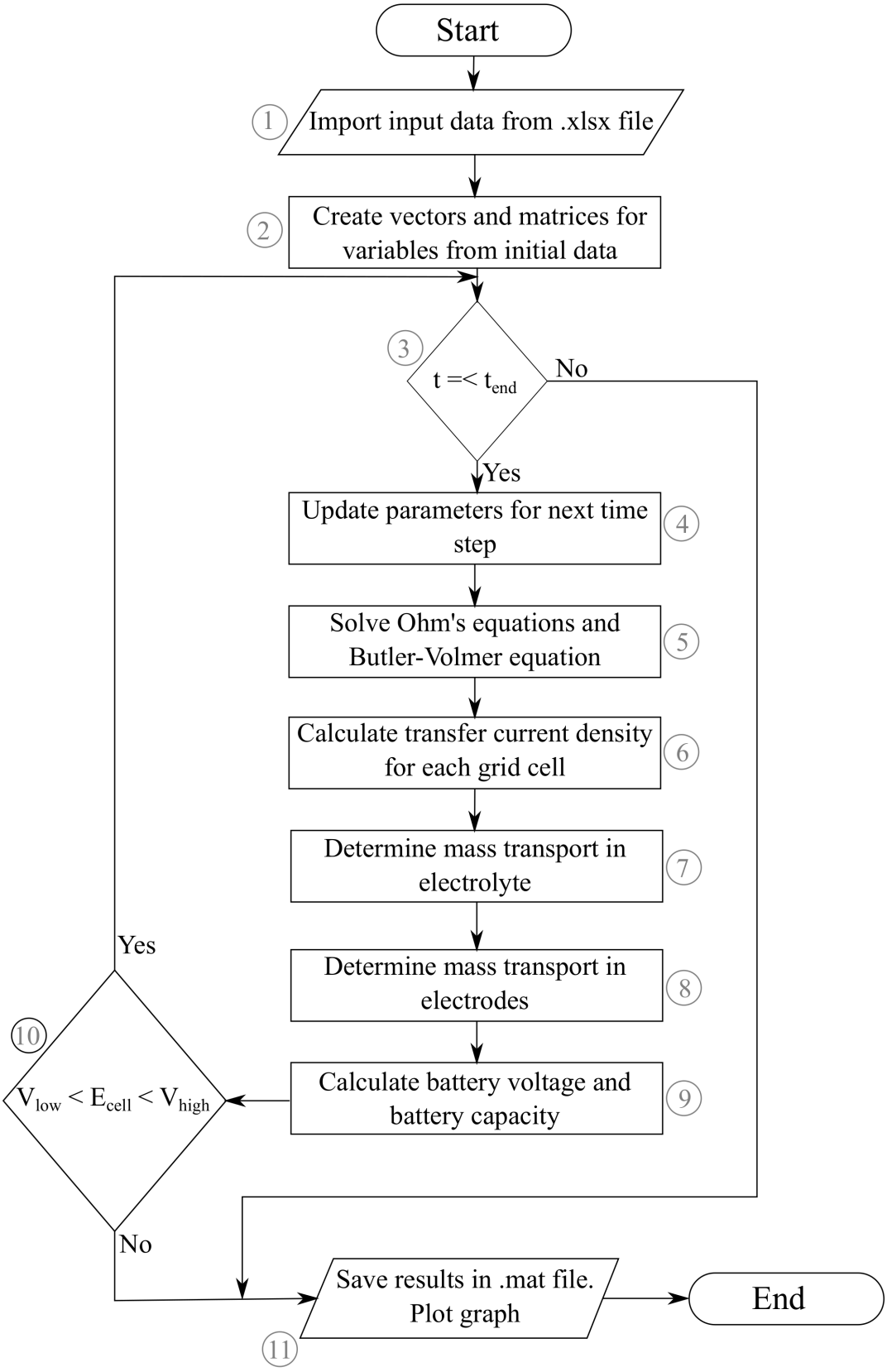

Figure 4.2: Matlab program structure - flow diagram

Table 4.5: Respective equations for functions

Function number	**Equations**
④	Eq.(3.13), Eq.(3.14), Eq.(3.15), Eq.(3.16), Eq.(3.19), Eq.(3.20), Eq.(3.21), Eq.(3.22), Eq.(3.23), Eq.(3.24).
⑤	Eq.(4.3), Eq.(4.4), Eq.(4.5), Eq.(4.6), All equations listed in appendix B.
⑥	Eq.(4.3)
⑦	Eq.(4.17), Eq.(4.18), Eq.(4.19)
⑧	Eq.(4.20), Eq.(4.21), Eq.(4.22)
⑨	Eq.(4.23), Eq.(4.24)

Chapter 5

Simulation Results and Discussion

The first section in this chapter presents validation of the electrochemical model with experimental data which are extracted from literature. The validation includes different discharge, charge and temperature cases. Factors which affects for the performance of the battery are discussed in the second section of this chapter with the help of simulations. All simulations were conducted for C26650 battery type which has $LiFePO_4$ cathode and natural graphite anode.

The total current density (I), temperature (T) and initial Li concentration in electrodes (c_s), are main input variables of the electrochemical model. The process of discharge implies that $I < 0$ and the process of charge implies that $I > 0$.

Ideally, a fully discharge battery means $c_s(r, x, t) = 0,\ r \in R_N,\ x \in L_N$ and a fully charge battery means $c_s(r, x, t) = 0,\ r \in R_P,\ x \in L_P$. However, in practical situations these conditions are impossible to satisfy. Therefore, It is assumed that a fully discharge battery has a battery voltage (E_{cell}) less than $2.5\,V$ and a fully charged battery has a battery voltage (E_{cell}) higher than $3.5\,V$. However, these values are only applicable for C26650 battery type which has $LiFePO_4$ cathode and natural graphite anode. Other lithium battery types might have different values.

Generally, battery management systems (BMS) utilize battery voltage (E_{cell}), total current density (I) and temperature (T) to determine state of charge (SOC) [40]. Since in these simulations, the total current density (I) and temperature (T) are held constant, above assumption is justified.

The keywords which were introduced above are tabulated in Table 5.1. The table describes keywords and their respective mathematical expressions.

Table 5.1: Keywords and mathematical expressions

Keyword	Mathematical expression
Charging	$I > 0$
Discharging	$I < 0$
Fully charged	$E_{cell} \geq 3.5\,V$
Fully discharged	$E_{cell} \leq 2.5\,V$

5.1 Model Validation

In section 5.1.1, validation of the electrochemical model (from eq.(3.1) to eq.(3.27)) is presented. Input parameters, initial conditions and boundary conditions for different cases were extracted from literature sources [18, 20, 29]. Discretization parameters which were used in the electrochemical model are tabulated in Table 5.4.

The Input parameters, initial conditions, boundary conditions and discretization parameters are fed into the algorithm which was presented in chapter 4. The algorithm computes solutions for the variables as the time evolves. Since many literature sources presents their experimental results in battery voltage (E_{cell}) vs battery capacity (Q_{cell}) format, battery voltage (E_{cell}) and battery capacity (Q_{cell}) were selected as main output variables. Thus, simulated results can be compared with the experimental data.

The battery operation time depends on the discharge ($I < 0$) and charge ($I > 0$) rates. C-rate is a parameter which is used to describe the discharge ($I < 0$) or charge ($I > 0$) rate based on the rated battery capacity. $1C$ is the value of current rate which can fully discharge (or charge) a battery within 1 hour. This is an important unit because many authors have used C-rate to express the battery charge and discharge rates in their studies [17, 18, 20, 21, 29, 46, 47]. The relationship between total current density (I) and C-rate for $2.3\,Ah$ C26650 battery (which is used in simulations) are presented in Table 5.2.

In section 5.1.2, validation of the electrochemical model including eq.(3.28) is presented. Here, capacity fading (eq.(3.28)) was introduced into the algorithm (which is presented in chapter 4) such that eq.(3.28) was only used for determination of initial lithium concentration in anode ($c_s(r, x, t = 0),\ r \in R_N,\ x \in L_N$).

5.1.1 Electrochemical Model Validation

The electrochemical model (from eq.(3.1) to eq.(3.27)) is validated against experimental data. The experimental data were extracted from Safari and Delacourt [18] and Wang

Table 5.2: Relationship between total current density (I) and C rate for 2.3 Ah C26650 battery

Discharge / Charge	C-rate	I (A/m^2)	Time* (hrs)
Discharge	$3C$	$I = -39$	0.33
	$1C$	$I = -13$	1
	$0.5C$	$I = -6.5$	2
	$0.1C$	$I = -1.3$	10
Charge	$3C$	$I = 39$	0.33
	$1C$	$I = 13$	1
	$0.5C$	$I = 6.5$	2
	$0.1C$	$I = 1.3$	10

* ***Time*** *- Approximate time taken to fully discharge a fully charged battery or fully charge a fully discharged battery with constant total current density* (I).

et al. [29]. Figures 5.1, 5.2, 5.3, 5.4 and figure 5.5 represent charge ($I > 0$) and discharge ($I < 0$) scenarios for C26650 lithium-ion battery type [18]. $y - axes$ in figures indicate the voltage output of the battery (E_{cell}); the voltage is the potential difference between positive and negative electrodes (eq.(3.27)). $x - axes$ in figures indicate the battery capacity (Q_{cell}; eq.(3.26)) which is delivered ($I < 0$) or absorbed ($I > 0$) by battery in Ampere hours (Ah). The area of the battery (A_{cell})[1] is considered to be $0.1694\,m^2$ [20]. Discharge ($I < 0$) and charge ($I > 0$) rates are presented in 'C-rate' unit (refer Table 5.2).

Common note about fig.5.1 - fig.5.7

Simulation results and experimental data represent a 2.3 Ah C26650 lithium-ion battery. $Y - axes$ of these graphs represent the battery voltage (E_{cell}) in Volts (V) and $X - axes$ represent actual battery capacity ($Q_{cell} \times A_{cell}$) in Ampere hours ($A\,h$). Lines represent simulated results and markers represent experimental data from literature. The discharge (or charge) rates are presented in C-rate instead of total current density (I) (refer Table 5.2).

Figure 5.1 illustrates discharge ($I < 0$) scenarios at 25^oC. Markers represent experimental data which are extracted from Safari and Delacourt [18]. Lines represent simulation results from the model. $0.1C$ ($I = -1.3\ A/m^2$), $0.5C$ ($I = -6.5\ A/m^2$), $1C$ ($I = -13\ A/m^2$) and $3C$ ($I = -39\ A/m^2$) discharge rates are validated against experimental data. The figure verifies that the model is able to predict actual voltage (E_{cell}) variation against battery capacity (Q_{cell}) for $0.1C$, $0.5C$ and $1C$ discharge rates. However, at

[1] A_{cell} - This is the electrode area of the battery. Do not confuse with specific surface area of the electrode (a_s). The battery capacity (Q_{cell}; eq.(3.26)) was defined as the capacity of battery per $1\,m^2$ electrode area. However, $x - axes$ in fig.5.1 - fig.5.7 are presented in actual battery capacity. Thus, the actual battery capacity can be calculated using $Q_{cell} \times A_{cell}$.

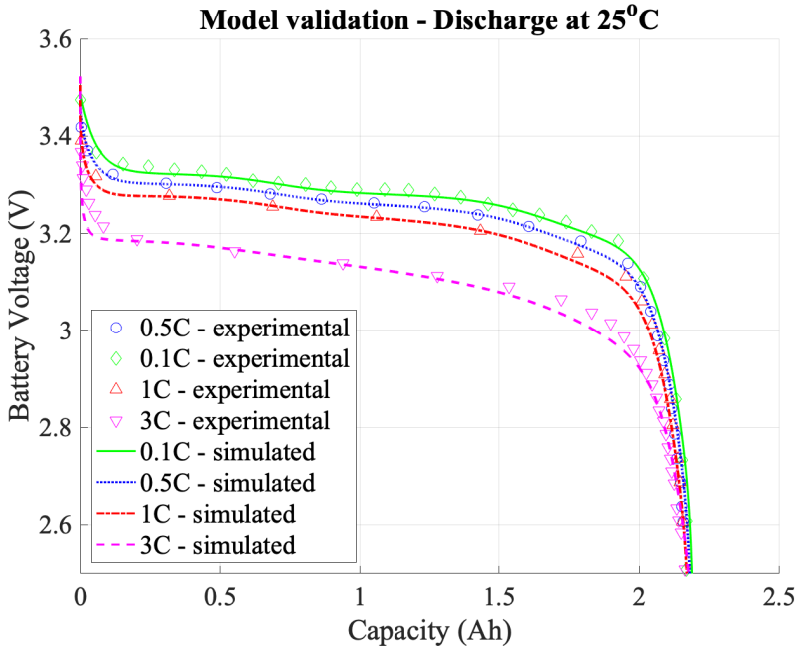

Figure 5.1: Electrochemical model validation for discharge process at 25^oC

Figure represents validation of the electrochemical model for discharging at 25^oC. Experimental data (markers) are extracted from Safari and Delacourt [18]. Refer "Common note about fig.5.1 - fig.5.7" on page 56.

higher discharge rate ($3C$; $I = -39\,A/m^2$), the model slightly under-estimates E_{cell} at the beginning of discharge and end of discharge.

Figure 5.2 illustrates charge ($I > 0$) scenarios at 25^oC. Markers represent experimental data with charge rates $0.1C$ ($I = 1.3\,A/m^2$), $0.5C$ ($I = 6.5\,A/m^2$) and $1C$ ($I = 13\,A/m^2$), which are extracted from Safari and Delacourt [18]. Lines represent simulation results from the model. The figure indicates a good agreement between experimental data and simulated results for E_{cell} vs Q_{cell}.

Similarly, figure 5.3 and figure 5.4 were constructed to compare the simulation results and experimental data for discharge ($I > 0$) and charge ($I > 0$) at 45^oC. The experimental data for both graphs were extracted from Safari and Delacourt [18]. The figure 5.3 represents $0.1C$ ($I = -1.3\,A/m^2$), $0.5C$ ($I = -6.5\,A/m^2$) and $1C$ ($I = -13\,A/m^2$) discharge rates and the figure 5.4 represents $0.1C$ ($I = 1.3\,A/m^2$), $0.5C$ ($I = 6.5\,A/m^2$) and $1C$ ($I = 13\,A/m^2$) charge rates. Both figures indicate a good agreement between experimental data and simulated results for E_{cell} vs Q_{cell}.

Figure 5.5 demonstrates discharge ($I < 0$) scenarios at 0^oC and 60^oC temperatures. Markers represent data which are extracted from Wang et al. [29]. The discharge rate is $0.5C$ ($I = -6.5\,A/m^2$) for both cases. Discharge scenario simulated at 60^oC temperature

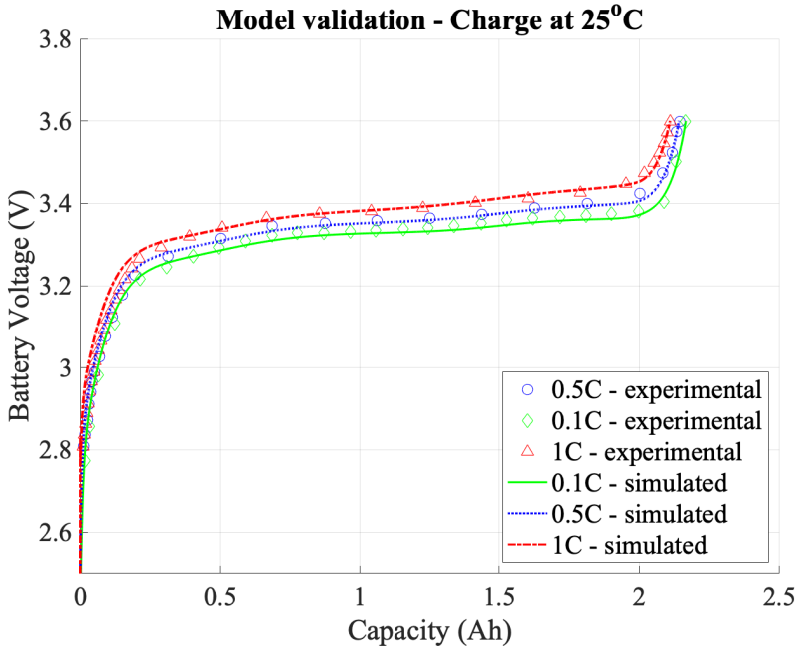

Figure 5.2: Electrochemical model validation for charge process at 25^oC

Figure represents validation of the electrochemical model for charging at 25^oC. Experimental data (markers) are extracted from Safari and Delacourt [18]. Refer "Common note about fig.5.1 - fig.5.7" on page 56.

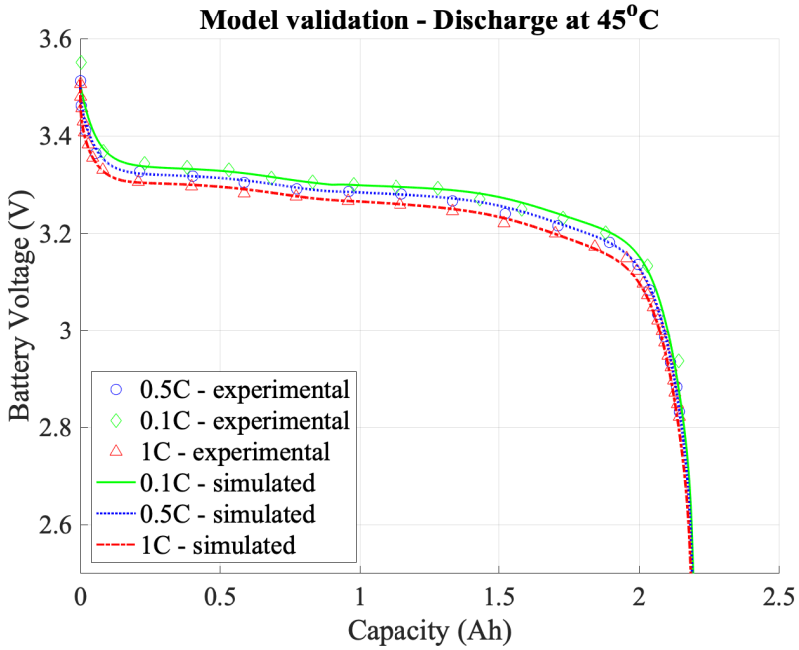

Figure 5.3: Electrochemical model validation for discharge process at 45^oC

Figure represents validation of the electrochemical model for discharging at 45^oC. Experimental data (markers) are extracted from Safari and Delacourt [18]. Refer "Common note about fig.5.1 - fig.5.7" on page 56.

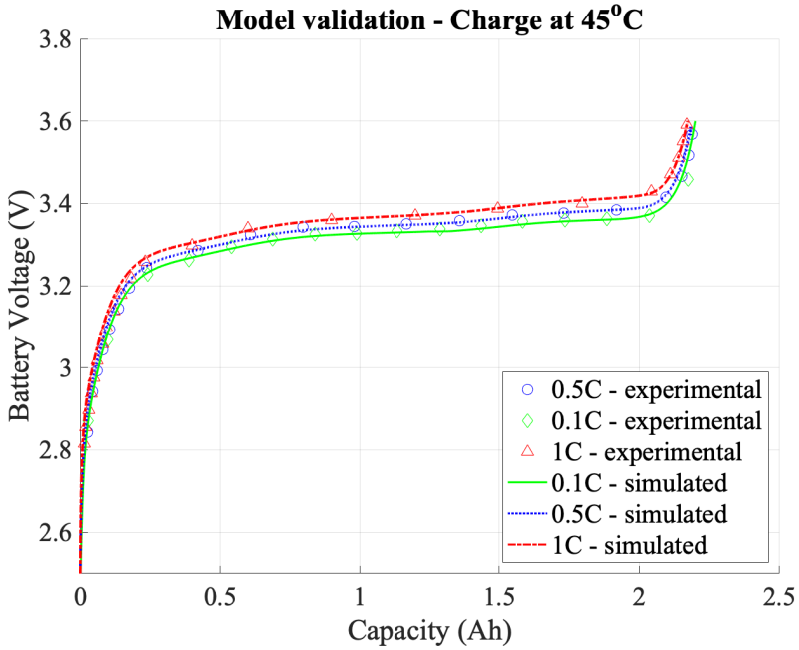

Figure 5.4: Electrochemical model validation for charge process at 45^oC

Figure represents validation of the electrochemical model for charging at 45^oC. Experimental data (markers) are extracted from Safari and Delacourt [18]. Refer "Common note about fig.5.1 - fig.5.7" on page 56.

indicates a good approximation. However, minor deviations can be observed between simulated and experimental data at 0^oC temperature, but simulation results are within an acceptable range.

From figure 5.1 to figure 5.5, it is possible to observe that, battery voltage (E_{cell}) is highly varied in low battery capacity ($< 0.3\,Ah$) and high battery capacity ($> 2\,Ah$). This is because, the battery voltage (E_{cell}) is mainly dependent on the Open Circuit Voltage (OCV) of electrode materials. A fully charged battery has high lithium concentration (c_s) in anode and low lithium concentration in cathode. Since $LiFePO_4$ (cathode) has high OCV in low lithium concentration (fig. 3.4), the battery voltage (E_{cell}) is steeply increased when the battery is fully charged. Similarly, a fully discharged battery has low lithium concentration (c_s) in anode. The OCV of graphite (anode) material is increased rapidly in low lithium concentration (fig. 3.4). This creates a steep decrease in battery voltage (E_{cell}) when the battery is in low capacity.

Generally, the curves presented in fig.5.1 - fig.5.5 have a similar shape. However, the values are different. This occurs mainly due to the internal resistance of the battery [2]. The internal resistance of the battery depends on temperature (T) and materials that are used to construct it. Typically, Diffusion coefficients (D_n, D_p, D_e), conductivity (κ_e), reactivity (k_0) and OCV depend on temperature (T). As discharge rate (or charge

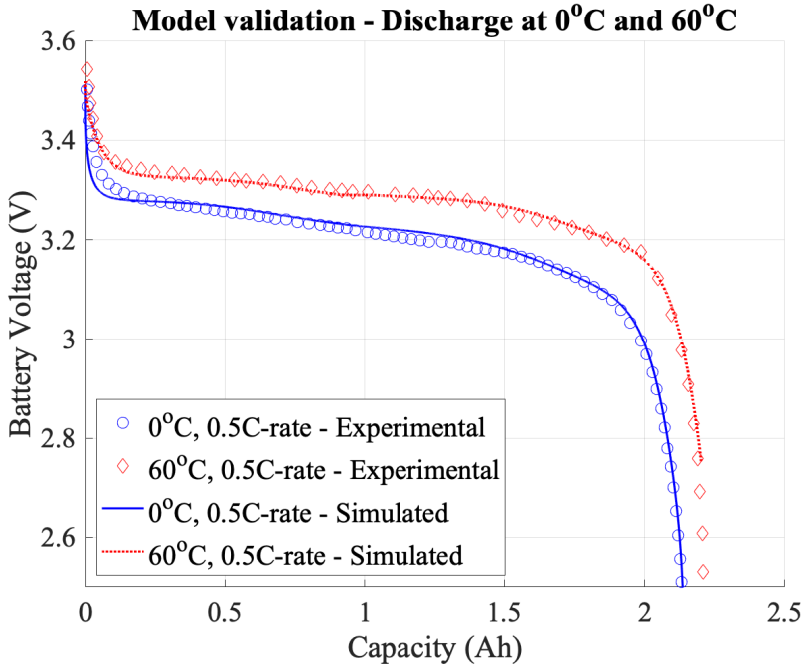

Figure 5.5: Electrochemical model validation for discharge process at 0^oC and 60^oC

Figure represents validation of the electrochemical model for discharging at 0^oC and 60^oC. The rate of discharge is 0.5C ($I = -6.5\ A/m^2$). Experimental data (markers) are extracted from Wang et al. [29]. Refer "Common note about fig.5.1 - fig.5.7" on page 56.

rate) increases, additional energy is required to overcome the internal resistance. This additional energy loss is reflected as a decrease in battery voltage (E_{cell}) during discharge ($I < 0$), and increase in battery voltage (E_{cell}) during charge ($I > 0$).

During the validation of the electrochemical model minor offset was observed between simulation results and experimental data for battery voltage (E_{cell}) vs battery capacity (Q_{cell}). This is partly due to the existence of two paths of OCV curve for graphite between charge and discharge processes [48]. Allart et al. [48] have presented significance of this phenomena using experimental data which indicates existence of two OCV curves for de-lithiation (discharge) and lithiation (charge) process for graphite. Thus, a correction factor ($CF_{n,OCV}$) was introduced into the electrochemical model which resulted multiplication of equation (3.15) with eq.(5.1).

$$CF_{n,OCV} = \begin{cases} 1.1, & I < 0 \text{ (Discharging)} \\ 1, & I = 0 \\ 0.9, & I > 0 \text{ (Charging)} \end{cases} \tag{5.1}$$

Similarly, instead of single entropy path for graphite ($\frac{dU_n}{dT}$; eq.(A.2)), two paths exist for graphite de-lithiation (discharge) and lithiation (charge) [48]. However, existence of two

entropy paths were not introduced into the electrochemical model because the simulated results indicated a good agreement with experimental data even without this adjustment (i.e. fig.5.3, fig.5.4, fig.5.5).

5.1.2 Capacity Fading Validation

Capacity fading (aging) is determined using equation (3.28). The eq.(3.28) calculates the percentage loss of lithium concentration ($C_{loss}(\%)$) in a battery based on the number of cycles (CN); Discharge and subsequent charge of a battery is defined as one cycle. The concentration of lithium in anode[2] ($c_{s,n,initial}$) when battery is in fully charged state at 0^{th} cycle (new battery) is used as the initial lithium concentration for capacity fading calculation. Loss of lithium[3] (c_{loss}) is then calculated for a specific cycle (CN) and value of the remaining lithium concentration in anode ($c_{s,n,initial} - c_{loss}$) is input into the electrochemical model as the initial lithium concentration in anode ($c_s(r, x, t = 0),\ r \in R_N,\ x \in L_N$).

Generally, aging of batteries are experimented with constant total current densities (I) and temperatures (T) [4, 24, 29]. Therefore, Li concentration in an anode can be easily calculated for a specific cycle (CN) using a semi-empirical equation (i.e. eq.(3.28)).

However, It is also possible to program the algorithm (which is presented in chapter 4) in order to calculate lithium loss (c_{loss}) based on complex and varying total current densities ($I(t)$) and temperatures ($T(t)$). This requires simulation to be run from 0^{th} cycle ($CN = 0$) because the lithium loss (c_{loss}) is a function of total current density ($I(t)$) and temperature ($T(t)$) [4, 24, 29]. However, this method is not investigated in this thesis because there was no sufficient data for validation.

Figure 5.6 and figure 5.7 represent discharge ($I < 0$) scenarios for different cycles (CN) of the battery. $Y - axes$ and $x - axes$ of figures represent battery voltage (E_{cell}) and battery capacity (Q_{cell}) respectively. Experimental data are presented in markers, which are extracted from Wang et al. [29]. The simulations were conducted such that for each cycle (CN), the initial lithium concentration (c_s) in anode was calculated with the help of the eq.(3.28). The calculated initial lithium concentration (c_s) in anode was then introduced into the electrochemical model as an initial condition of lithium concentration in anode ($c_s(r, x, t = 0),\ r \in R_N,\ x \in L_N$). Therefore, for each cycle (CN) presented in the figures, the simulation was conducted individually.

[2] $c_{s,n,initial} = c_s(r, x, t = 0),\ r \in R_N,\ x \in L_N$ when $CN = 0$

[3] $c_{loss} = c_{s,n,initial} \times C_{loss}(\%)$

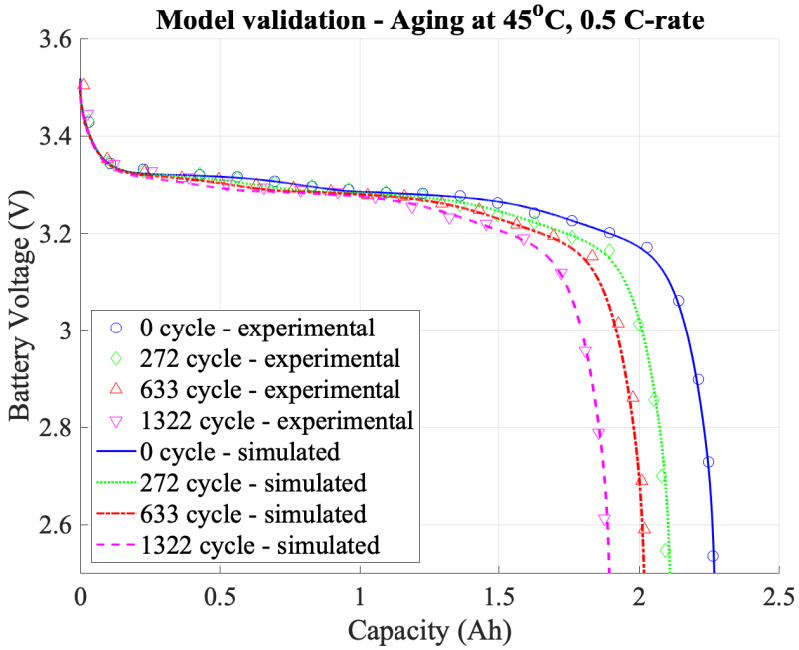

Figure 5.6: Model validation - Aging at 45^oC

Figure represents validation of capacity fading with the electrochemical model. The battery aging temperature is 45^oC which is operated at 0.5C ($I = -6.5\ A/m^2$). Each curve represents a cycle (CN) of the battery. Experimental data (markers) are extracted from Wang et al. [29]. Refer "Common note about fig.5.1 - fig.5.7" on page 56.

Figure 5.6 illustrates aging of battery at 45^oC with a $0.5C$ discharge rate. 0^{th}, 272^{nd}, 633^{rd} and 1322^{nd} cycles (CN) are simulated and compared against experimental data. It shows that the simulation results obtained from the electrochemical model with capacity fading, indicate a good agreement against experimental values.

Figure 5.7 illustrates aging of battery at 60^oC for $0.5C$ discharge rate. 0^{th}, 185^{th} and 754^{th} cycles (CN) are simulated and compared against experimental data. Simulated data sightly over-estimates aging of battery. However, the variations are in an acceptable range.

5.2 Investigation of Battery Characteristics Using Simulations

Simulations were conducted for C26650 lithium-ion battery with $LiFePO_4$ cathode and natural graphite anode. Same configuration of model was maintained which was used for validation, however Li^+ in electrolyte was changed from 1000 mol/m^3 to 1200 mol/m^3. This is because, approximately at 1200 mol/m^3 electrolyte has the highest ionic conduc-

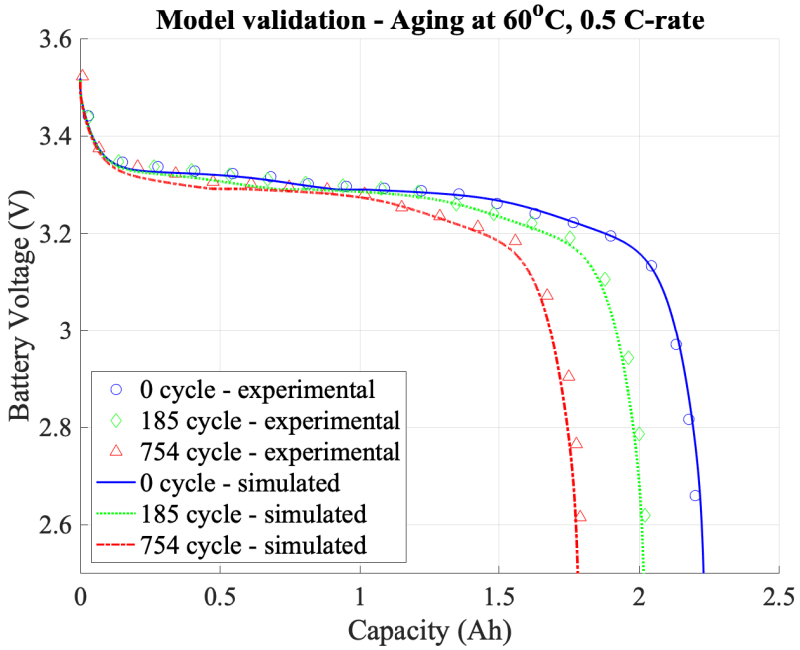

Figure 5.7: Model validation - Aging at 60^oC

Figure represents validation of capacity fading with the electrochemical model. The battery aging temperature is 60^oC which is operated at 0.5C ($I = -6.5\ A/m^2$). Each curve represents a cycle (CN) of the battery. Experimental data (markers) are extracted from Wang et al. [29]. Refer "Common note about fig.5.1 - fig.5.7" on page 56.

tivity (fig. 3.5) which is favorable to maintain low internal resistance during operation. Battery parameters that were used in simulations are tabulated in Table 5.3.

Parameters that are used for Finite Difference Method (FDM) are tabulated in Table 5.4. The length of spacial step is equal for anode, separator and cathode sections ($\frac{L_n}{M_n} = \frac{L_s}{M_s} = \frac{L_p}{M_p}$). The number of grid cells for $x - dimension$ (M_n, M_s, M_p) are selected by program itself such that interface between an electrode and separator lie exactly on the boundary between two grid cells. Values that are presented in Table 5.4 is applicable for all simulations unless otherwise explicitly mentioned. Specially size of the time step (dt) was varied in some simulations such as pulse response analysis and depending on the resolution required.

Simulations were mainly conducted for $0.5C$ ($6.5\,A/m^2$) and $1C$ ($13\,A/m^2$) charge and discharge rates. Operating voltage window of the battery was kept at $V_{low} = 2.5\,V$ and $V_{high} = 3.6\,V$. Operating temperature of the battery was kept between 0^oC and 60^0C in simulations.

Table 5.3: Battery parameters

Description	Parameter	Anode	Separator	Cathode	Unit
Thickness	L_n, L_s, L_p	34^a	30^a	70^a	μm
Particle radii	r_n, r_p	3.5^a	-	0.0365^b	μm
Electrode porosity	ε	0.55^a	-	0.43^a	
Electrolyte volume frac.[1]	ε_e	0.33^a	0.54^a	0.332^a	
Max.[2] Li con.[3] - electrode	$c_{s,max}$	31370^a	-	22806^a	mol/m^3
Init.[4] Li con.[3] - electrode	$c_{s,0}$	26194^c	-	685^b	mol/m^3
Anodic transfer coeff.[5]	α_a	0.5^b	-	0.5^b	
Cathodic transfer coeff.[5]	α_c	0.5^b	-	0.5^b	
Bruggeman exponent	γ	1.5^b	1.5^b	1.5^b	
Electrode conductivity	σ	100^a	-	0.5^a	S/m
OCV	U	Eq.(3.15)	-	Eq.(3.16)	V
Electrode diffusivity	D_s	Eq.(3.19)	-	Eq.(3.20)	m^2/s
Reactivity	k_0	Eq.(3.23)	-	Eq.(3.24)	$\frac{m^{4.5}}{mol^{0.5}\,s}$

Description	Parameter	Values	Unit
Init.[4] Li^+ con.[3] - electrolyte	$c_{e,0}$	1200^b	mol/m^3
Electrolyte diffusivity	D_e	Eq.(3.21)	m^2/s
Electrolyte conductivity	κ_e	Eq.(3.22)	S/m
Transference number of Li	t_+^0	0.363^a	
Reference temperature	T_{ref}	298.15	K
Active surface area	A_{cell}	0.1694^b	m^2

[1]Fraction, [2]Maximum, [3]Concentration, [4]Initial, [5]Coefficient.
[a]Khandelwal et al. [25], [b]Ye et al. [20], [c]Safari and Delacourt [18].

Table 5.4: Finite Difference Method (FDM) parameters

Description	Symbol	Value
Time step size	dt	$0.25\,s$
Number of spacial grid - Negative electrode	M_n	25
Number of spacial grid - Separator	M_s	22
Number of spacial grid - Positive electrode	M_p	52
Number of spacial grid - Total	M	99
Number of spacial grid in spheres - Positive electrode	m_p	50
Number of spacial grid in spheres - Negative electrode	m_n	50

5.2.1 Initial Operation of Battery

Initial conditions for the model assumes that battery had sufficient relaxation time (rest time) before its operation. This is because Li concentration in electrodes and Li concentration in electrolyte are assumed to be homogeneous throughout space domain when initial conditions are input into the simulation. However, if sufficient relaxation time is not available between cycles (This is the case in real world operations), non-homogeneous distribution of Li in electrodes and Li^+ electrolyte affect the voltage response (E_{cell}) from the battery.

In this section, the effect on battery voltage (E_{cell}) is investigated for different discharge ($I < 0$) and charge ($I > 0$) rates and temperatures (T) due to non-homogeneous distribution of lithium. E_{cell} is analyzed against discharge time of the battery since this reflects the effect on battery operation time as well.

Figure 5.8 demonstrates initial $1\frac{1}{2}$ cycle[4] operation of battery for different scenarios. In all graphs, $x-axes$ demonstrate battery operation time in hours and $y-axes$ demonstrate battery voltage (E_{cell}) in Volts. Time for each charge ($I > 0$) and discharge ($I < 0$) are counted from $t = 0$ such that each charge/discharge scenario can be compared with each other.

Discharge → charge → discharge

Fig. 5.8a, fig. 5.8b, fig. 5.8c and fig. 5.8d demonstrate initial (1^{st}) discharge ($-$), then immediate (1^{st}) charge ($--$) and then immediate (2^{nd}) discharge ($-\cdot$) of the battery. The 1^{st} discharge represents the discharge of the battery after long relaxation (rest) time. Between 1^{st} discharge and 1^{st} charge there is no relaxation time. Similarly, between 1^{st} charge and 2^{nd} discharge there is no relaxation time.

Fig. 5.8a illustrates discharge and charge rate with 1C ($I = \pm 13 A/m^2$) at 25^oC. A clear difference can be observed between 1^{st} discharge and 2^{nd} discharge in terms of both battery voltage (E_{cell}) and battery operation time. The initial reduction of E_{cell} is more shaper in 2^{nd} discharge than 1^{st} discharge. At end of the battery capacity, E_{cell} of 2^{nd} discharge has lower value than the 1^{st} discharge. It is also possible to identify that battery operation time in 2^{nd} discharge has been reduced by $68.8\,s$ compared to 1^{st} discharge.

[4] $1\frac{1}{2}$ **cycle** - This represents the process of a fully charged battery is being fully discharged ($I < 0$) → subsequent fully charge ($I > 0$) → subsequent fully discharge ($I < 0$) or the process of a fully discharge battery is being fully charged ($I > 0$) → subsequent fully discharge ($I < 0$) → subsequent fully charge ($I > 0$), which depend on the case. There is no time gap between a charge-discharge or discharge-charge process.

However, the adverse effects on battery voltage (E_{cell}) and battery operation time (1^{st} and 2^{nd} discharges) are possible to minimize by increasing temperature (T) for the same C-rate (fig.5.8b). It is also possible to operate the battery with lower C-rates (fig.5.8c) at the same temperature in order to minimize these adverse effects.

Operation of battery at high C-rates such as $3C$ (fig. 5.8d) causes inability to yield full energy stored in the battery. These effect arise due to the limitation of lithium diffusion and lithium distribution in electrodes. The distribution of lithium in electrodes will be discussed in subsequent section "Distribution of lithium in electrodes".

Charge → discharge → charge

Fig. 5.8e and fig. 5.8f demonstrate initial (1^{st}) charge ($-$), then immediate (1^{st}) discharge ($--$) and then immediate (2^{nd}) charge ($-\cdot$) of the battery. The 1^{st} charge represents the charge of the battery after long relaxation (rest) time. Between 1^{st} charge and 1^{st} discharge there is no relaxation time. Similarly, between 1^{st} discharge and 2^{nd} charge there is no relaxation time.

Similar behavior was observed in this section as in discharge → charge → discharge case. Low charge and discharge rate allow battery to charge to maximum level. Increase of battery temperature improves the utilization of maximum possible energy capacity of the battery. Figure 5.8e shows operation at 25^oC and figure 5.8f shows operation at 45^oC. Two figures are used to compare the effect on battery voltage (E_{cell}) and charging time. Even though in figure 5.8e shows a shorter charging time, the battery is not charged to its maximum possible capacity.

A main cause for above phenomena is the lithium distribution in electrodes. Farkhondeh et al. [1] have discussed the dynamics of lithium distribution in $LiFePO_4$ cathode using pulse analysis method. Therefore, a better understanding can be obtained by investigation of lithium distribution at an end of a charge or a discharge.

Distribution of lithium in electrodes

The purpose of this section is to further explain the results which were seen in the figure 5.8. The explanation is based on the distribution of lithium in anode and cathode.

Internal resistance of the battery has mainly two parts; Ohmic resistance and resistance due to SOC [2]. The resistance due to SOC is significantly dependent on diffusion and distribution of lithium in electrode. In general, OCV is governed by the amount of lithium

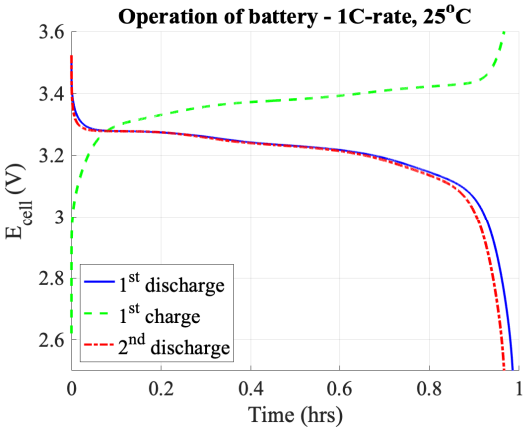

(a) Dicharge-charge-discharge, 1C, 25^oC

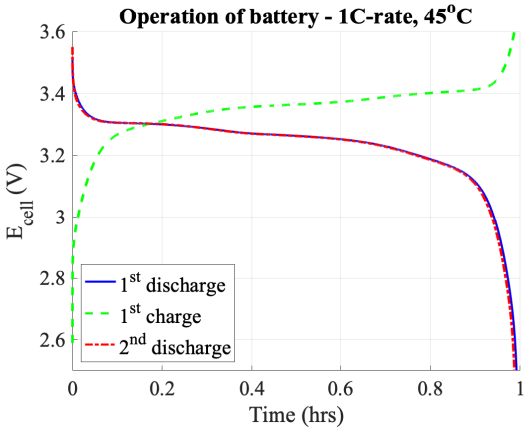

(b) Dicharge-charge-discharge, 1C, 45^oC

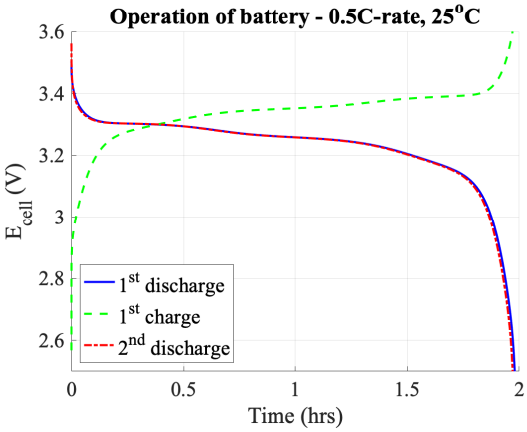

(c) Dicharge-charge-discharge, 0.5C, 25^oC

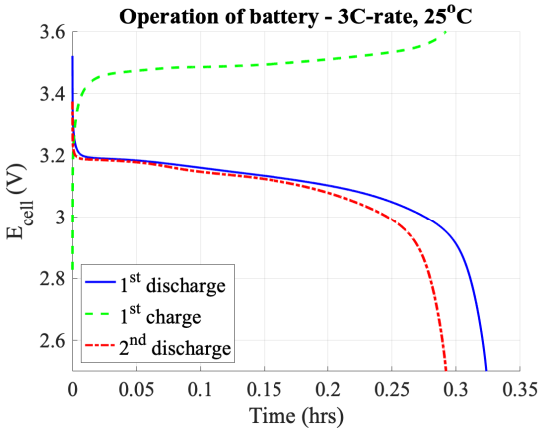

(d) Dicharge-charge-discharge, 3C, 25^oC

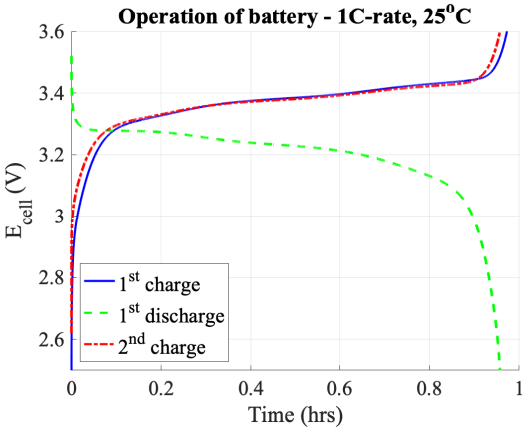

(e) Charge-discharge-charge, 1C, 25^oC

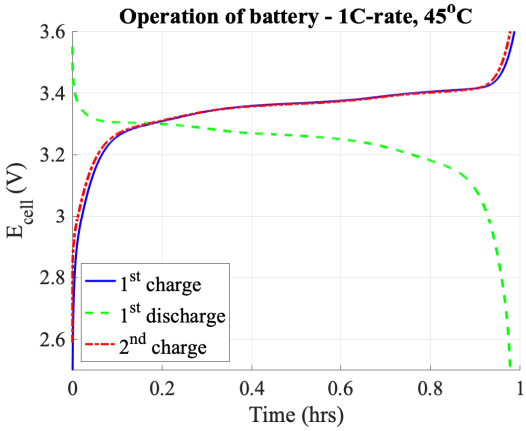

(f) Charge-discharge-charge, 1C, 45^oC

Figure 5.8: Initial operation of battery

Figures illustrate initial $1\frac{1}{2}$ cycle of battery. All figures represent E_{cell} (V) vs time (hours). For each charge/discharge operation, time is counted from 0 hrs so that curves can be compared with each other.

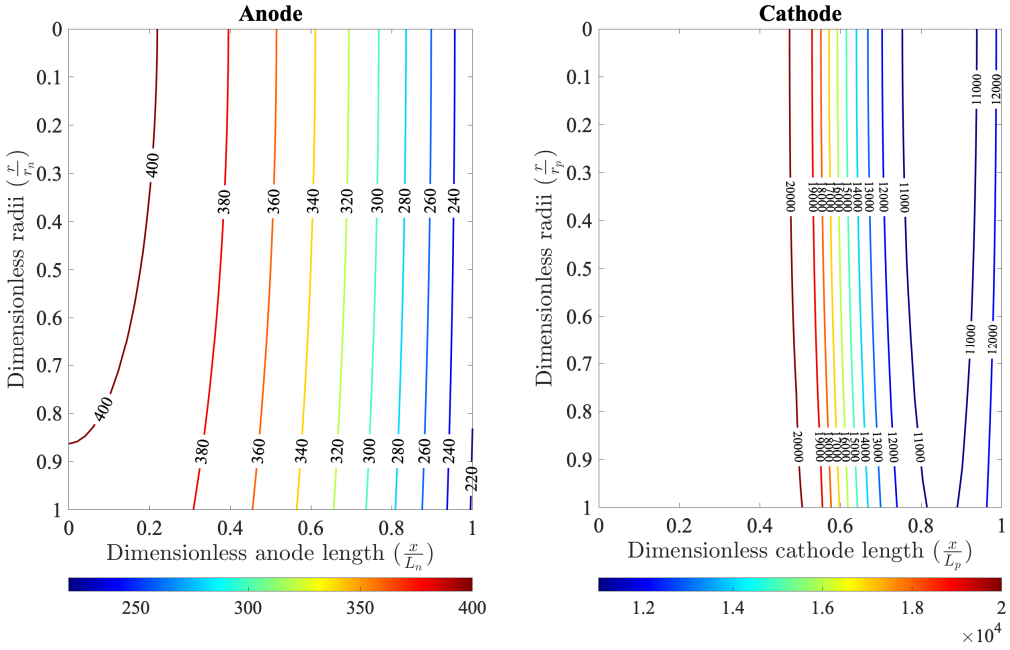

Figure 5.9: Distribution of Li in electrodes - discharged at 0.5C, 25^oC

Please refer to "Common note about fig.5.9 - fig.5.12" on page 71.

occupied at the interface between electrode and electrolyte (eq.(3.15) and eq.(3.16)).

Figure 5.9 and figure 5.10 represent distribution of lithium concentration in anode and cathode just after the $1\frac{1}{2}$ cycles. Lithium concentrations are presented in mol/m^3 units and indicated by contour lines. Figures represent a fully discharged battery where figure 5.9 corresponds to the case presented in figure 5.8c and figure 5.10 corresponds to the case presented in figure 5.8d.

Operating the battery at low discharge rate (e.g. $I = -6.5\,A/m^2$) indicates that lithium intercalation and de-intercalation occurs in more organized order. Figure 5.9 illustrates intercalation of lithium into cathode gradually fill from left to right. Spheres in cathode which are near to the separator are saturated initially. However, discharge of the battery at high $C-rates$ result intercalation of lithium into the cathode irregular (fig. 5.10). Spheres in the cathode which are near the separator are not fully saturated according to figure 5.10. It is important that movement of lithium should be kept close to separator area because this provides shortest length between anode and cathode. Increase in lithium transport length increases the internal resistance of the battery.

In contrast to cathode, lithium distribution in anode (graphite) has little effect from discharge rate. However, lithium concentration retained in anode for high discharge rate case is significantly higher than low discharge case.

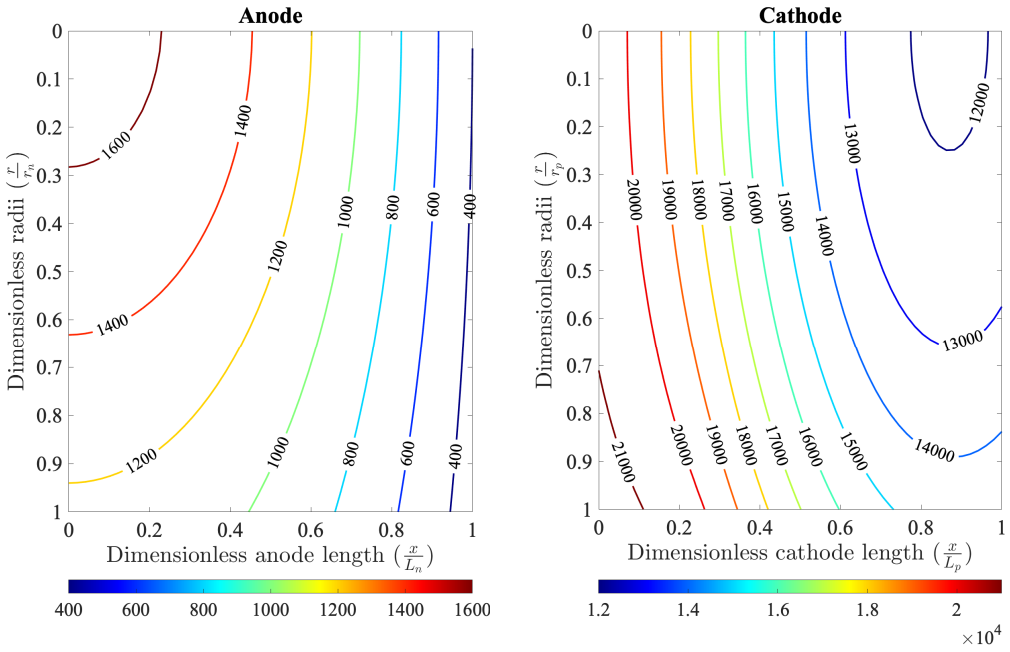

Figure 5.10: Distribution of Li in electrodes - discharged at 3C, 25^oC

Please refer to "Common note about fig.5.9 - fig.5.12" on page 71.

Figure 5.11 and figure 5.12 represents lithium distribution in anode and cathode just after the $1\frac{1}{2}$ cycles. Lithium concentrations are presented in mol/m^3 units and indicated by contour lines. Figures represent a fully charge battery at a rate of $1C$ where Figure 5.11 corresponds to the case presented in figure 5.8e and figure 5.12 corresponds to the case presented in figure 5.8f.

High temperature (fig. 5.12) provides suitable conditions to de-intercalate lithium from cathode and intercalate into anode more orderly. However, with same battery operation $c-rate$ but low temperature (fig. 5.11) does not provide suitable conditions to de-intercalate lithium from cathode. As shown in figure 5.11, retained lithium in cathode is higher compared to the high temperature case and more lithium is concentrated towards the core of the spheres in mid region.

In contrast, anode has no significant effect due to change in temperature or change in $c-rate$. This implies that majority of limiting factors for lithium-ion batteries arise due to the cathode material. Specially, low conductivity (σ) and diffusivity (D_p) are key parameters that limit the performance of the battery. New cathode materials and composite cathode materials are tested and developed by many authors [4, 10, 30, 34] to overcome the limitations of cathode materials.

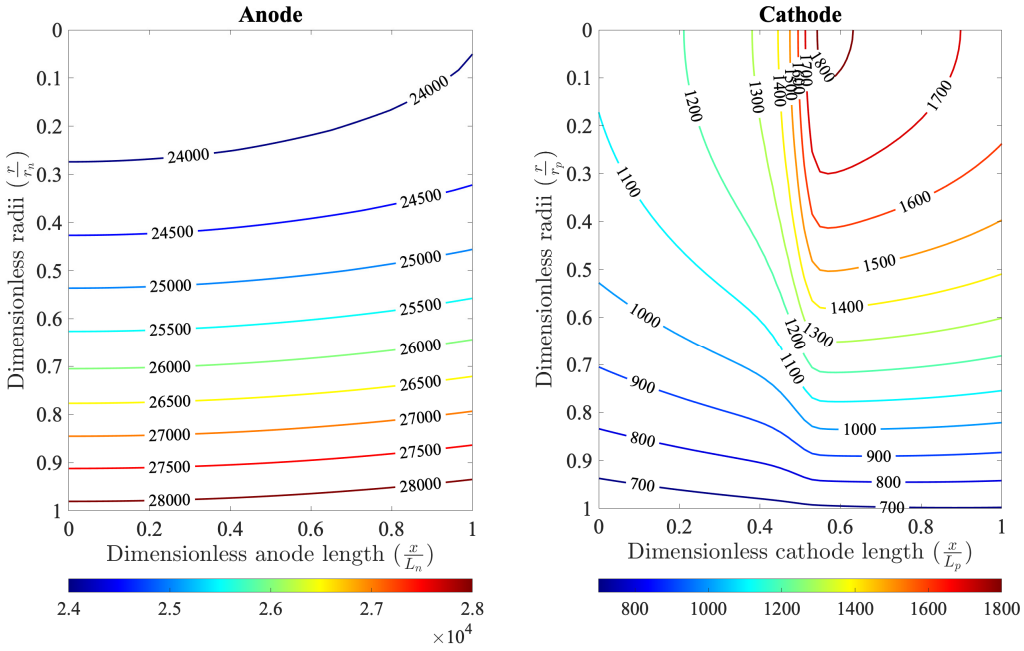

Figure 5.11: Distribution of Li in electrodes - charged at 1C, 25^oC

Please refer to "Common note about fig.5.9 - fig.5.12" on page 71.

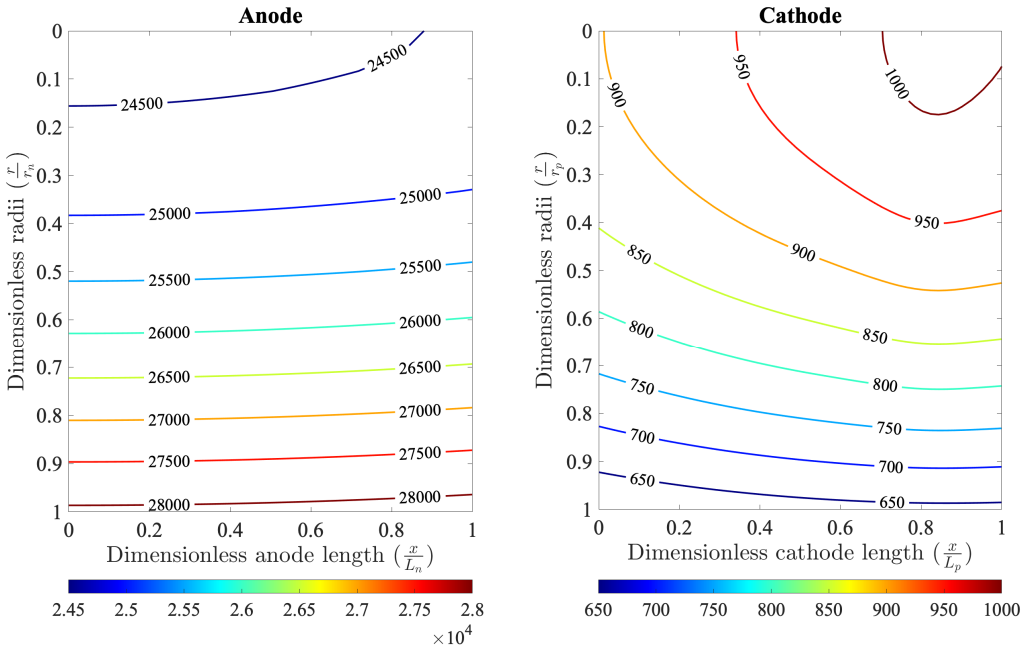

Figure 5.12: Distribution of Li in electrodes - charged at 1C, 45^oC

Please refer to "Common note about fig.5.9 - fig.5.12" on page 71.

Common note about fig.5.9 - fig.5.12

The pair of graphs illustrate Li distribution in electrodes just after $1\frac{1}{2}$ *cycles. Left graph indicates the anode and right graph indicates the cathode. Note that* $y-axes$ *of graphs increase from top to bottom. Li concentrations are marked on the contour lines in* mol/m^3*. In both anode and cathode,* $\frac{r}{r_n} = \frac{r}{r_p} = 1$ *represents surface of spheres and* $\frac{r}{r_n} = \frac{r}{r_p} = 0$ *represents core of the spheres.* $(\frac{x}{L_n} = 1, \frac{r}{r_n} = 1)$ *in anode graph and* $(\frac{x}{L_p} = 0, \frac{r}{r_p} = 1)$ *in cathode graph represent the interface with separator.*

5.2.2 Constant-Current Power Delivery

Power delivery is an important parameter for a battery. Delivery of power depends on many factors, such as SOC, internal resistance, temperature and battery discharge rate. In this section the effect of temperature and SOC are investigated. Power (P) delivery is the product of voltage of the battery (E_{cell}) and current (I) which can be denoted by following equation,

$$P = E_{cell} \times I$$

Figure 5.13 illustrates power delivery at constant current $1C$ ($13\ A/m^2$) discharge rate. $Y - axis$ of the figure indicates power delivery in Watts (W) and $x - axis$ represents State of Charge (SOC) of the battery. Note that power presented in figure is specific to C26650 battery type which has an electrode surface area of $0.1694\,m^2$ (A_{cell} in Table 5.3). Figure represents power delivery for three distinct temperatures; 25^oC, 45^oC and 60^oC. From the graph it is apparent that with increasing temperature the rate of increase in power delivery reduces.

Operation of battery at elevated temperatures provide additional power. In this case ($1C$ - discharge) the average increase in value is about $0.5\,W$. This effect is more significant at high discharge rates. At elevated temperatures the internal resistance of the battery is reduced due to increase in diffusivities and conductivity [20, 35]. This results reduction in Joule heating[5] inside the battery [49]. Thus, this wasted power can be yielded as productive power.

After the initial reduction in power between 100% - 95% (fig. 5.13), power delivery is nearly constant with SOC. However, SOC between 30% - 10% power starts to gradually decrease and when SOC becomes lower than 10%, power sharply reduces. This is an important aspect to be considered for high power applications. This is because at if the power demand remains constant, but due to reduction of voltage battery it is unable

[5]**Joule heating** - Heat generated due to the internal resistance of a battery.

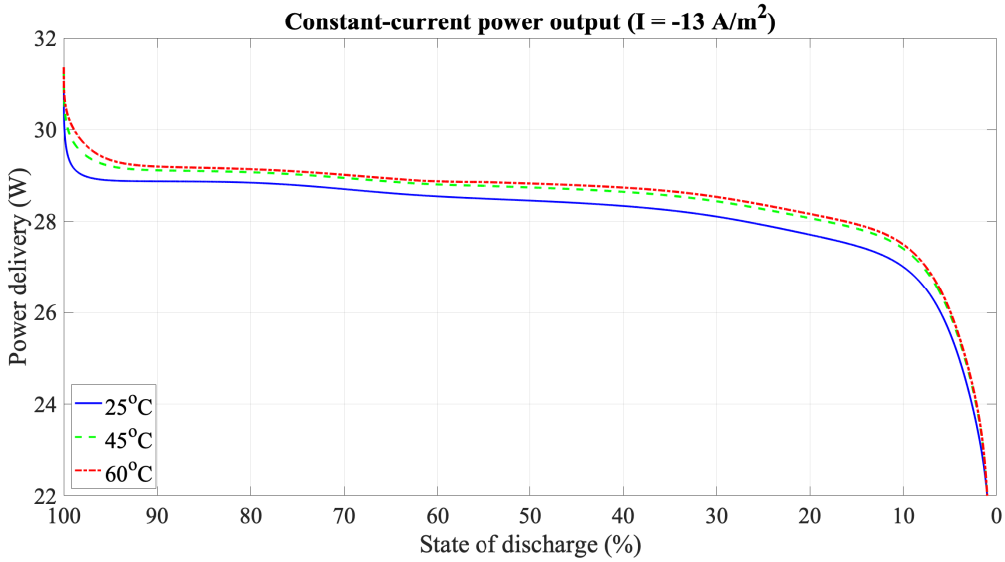

Figure 5.13: Constant-current ($I = -13\ A/m^2$) power delivery

Figure illustrates power delivery from the battery with $I = -13\,A/m^2$ constant current for 3 distinct temperatures (T). $x-axis$ represents state of discharge of the battery where 100% *represent fully charged battery and* 0% *represent fully discharged battery.*

to supply the required power, this requires high current to be drawn out of the battery resulting increase in power wasted as Joule heat inside the battery. Thus, battery which are used for high power applications should be used in high SOC range (preferably over 30% according to this case) and operate at elevated temperatures over room temperature.

5.2.3 Battery Response to Current Pulses

In real world scenarios current that is drawn out/in from battery is not constant with time. The change in current results voltage fluctuation in battery. Thus, application of current pulses to battery facilitates to understand and interpret battery behavior such as relaxation time and change in internal resistance against State of Charge (SOC) [49].

Investigation of voltage response against current pulses

Figure 5.14 demonstrates variation of battery voltage (E_{cell}) against current pulses. Inset illustrates the total current density (I) which was drawn out of the battery in square-wave form; 6 minutes $1C$ ($I = -13\ A/m^2$) discharge and 6 minutes relaxation period ($I = 0$). Pulses were continued to apply until the battery reaches lower voltage limit ($V_{low} = 2.5V$). Since this case investigates the reaction of the battery on impulses, the time step was lowered to $dt = 0.1s$.

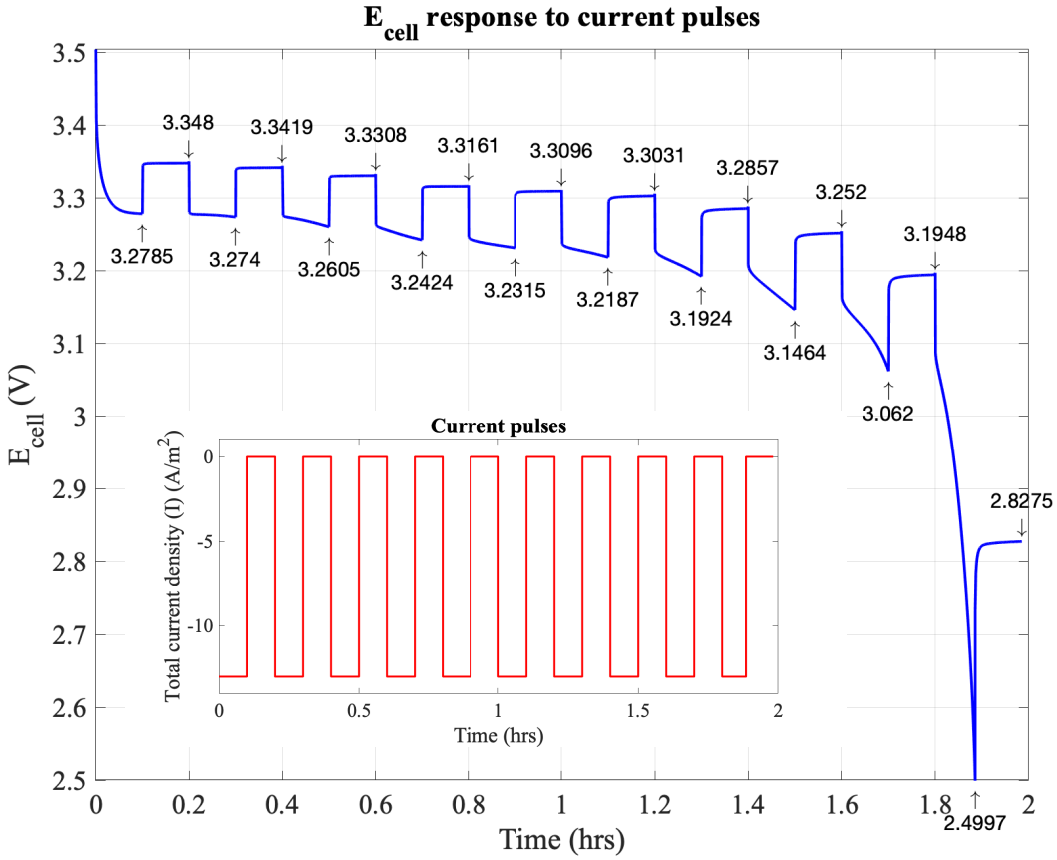

Figure 5.14: Battery response to current pulses ($dt = 100\,ms$)

Figure illustrates Battery voltage (E_{cell}) response profile against time due to applied current pulses from fully charge to discharge state. Inset: Applied current pulses to the battery against time.

In figure 5.14 voltage values are annotated to indicate the E_{cell} just before current is removed and just before current is reapplied. Difference between neighboring low voltage point and high voltage point indicate voltage that was used to overcome internal resistance of battery. Clearly, as battery get discharge the voltage gap is increased which implies that internal resistance of the battery get increased at lower SOC. According to simulation results, internal resistance of the discharge battery is 371% higher compared to full charged battery.

In figure 5.14, it is also possible to observe that, after removal of current ($I = 0$), voltage (E_{cell}) recovery is more sharp and quick. However, in latter pulses E_{cell} recovery is more smooth and slow. As the battery get discharged, diffusion inside electrode becomes slow due to low concentration gradient, thus making voltage recovery slow and smooth.

Farkhondeh et al. [1] also conducted a similar experiment and simulation for lithium-ion battery which has a $LiFePO_4$ cathode and graphite anode. The experiment was

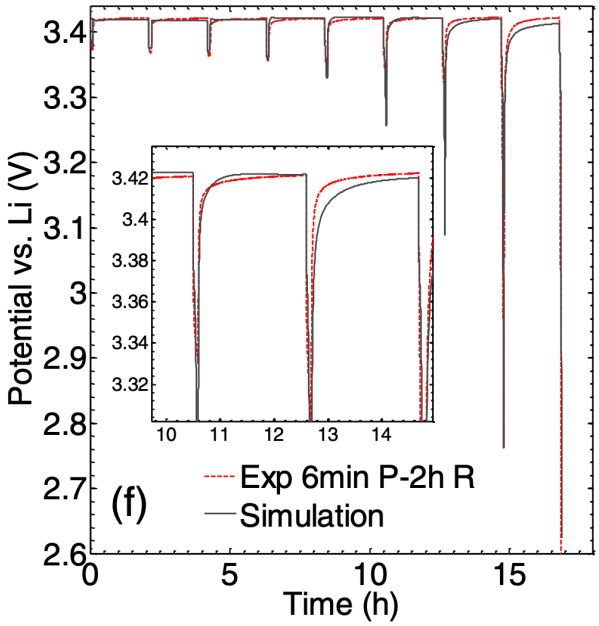

Figure 5.15: Pulse analysis conducted by Farkhondeh et al. [1].

conducted for 6 minute-current-pulses ($I < 0$) with 2 hours relaxation time [1]. Their experiment and simulation results are indicated in figure 5.15 [1]. The comparison of figure 5.14 and figure 5.15 indicate a similar result; the results obtained from the electrochemical model for the increase in internal resistance with time and the characteristics on battery voltage recovery (E_{cell}) are consistent with Farkhondeh et al. [1] results.

Investigation of voltage response due to current pulse in high resolution

Figure 5.16 illustrates the battery voltage behavior (E_{cell}) vs time in seconds. A fully charged battery was discharged at constant current ($I = -13\,A/m^2$) for 100 seconds and the current was completely removed ($I = 0$) for 100 seconds. Then again constant current of $I = -13\,A/m^2$ was applied for 100s. The reaction of E_{cell} due to removal of current occurs in fraction of seconds thus, time resolution of simulation was further reduced until $dt = 0.001s$ to generate figure 5.16.

It is possible to observe that sudden removal of current at 100 seconds (fig. 5.16) results in sharp increase in E_{cell} followed by a gradual increase. This sharp increase in E_{cell} at $t = 100\,s$ represents the Ohmic resistance of battery and subsequent gradual increase in E_{cell} is mainly due to the transport of Li from core towards the surface of spheres (electrode) [2]. According to simulation the ratio between ohmic resistance to diffusion resistance is about 2.14 : 1. However, this ratio varies with SOC and discharge/charge rate [2, 49].

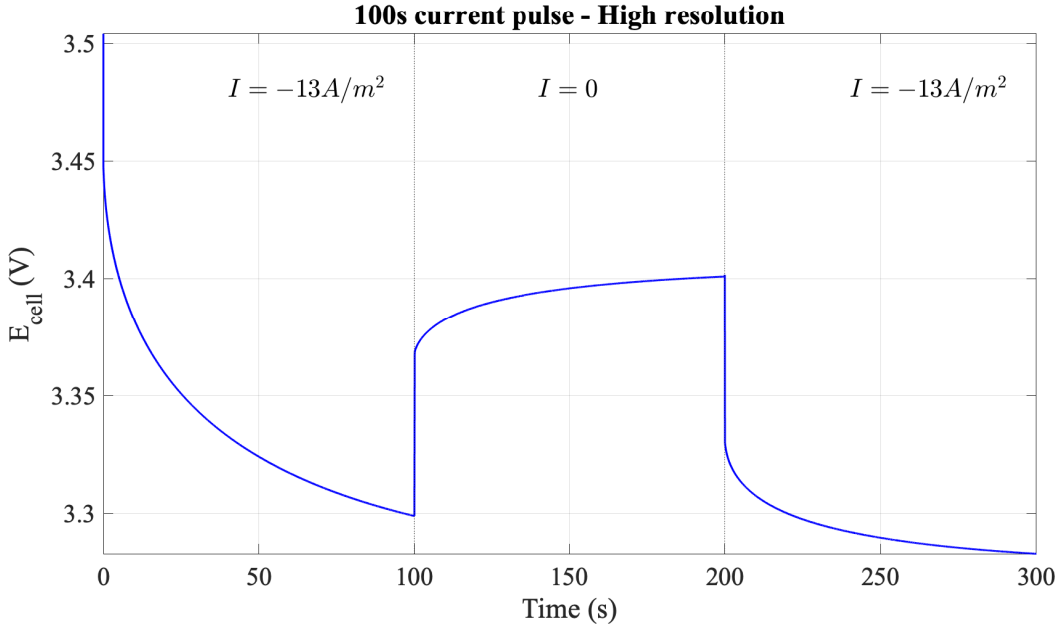

Figure 5.16: Battery response to current pulses ($dt = 1\,ms$)

Figure illustrate battery voltage (E_{cell}) profile against time. Simulation was run with $dt = 0.001\,s$. Graph is divided into 3 sections (at $Time = 100\,s$ and $Time = 200\,s$) which represent regions of applied currents on battery. Current is constant with time for each region and indicated by I.

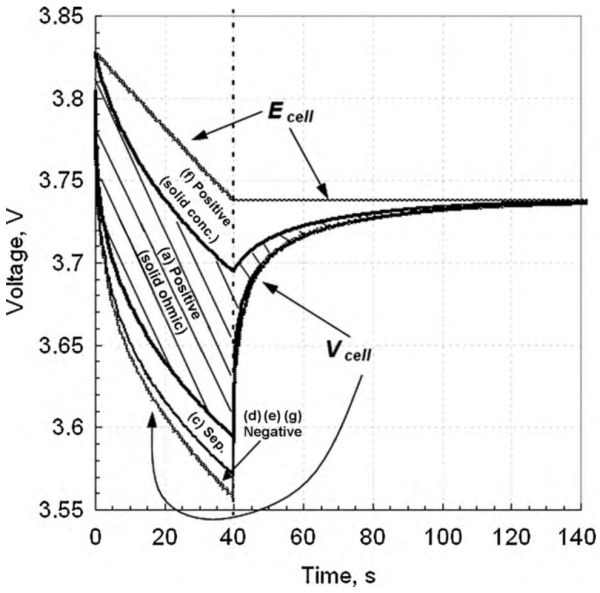

Figure 5.17: Pulse analysis conducted by Bernardi and Go [2].

A pulse analysis conducted by Bernardi and Go [2] is presented in figure 5.17. This study was conducted for a lithium-ion battery which has had a graphite anode and NCA[6] cathode [2]. The figure 5.17 illustrates 40 second-current-pulse with a 100 seconds relaxation period. It is important to note that V_{cell} in figure 5.17 is equivalent to E_{cell} in the electrochemical model. The comparison of figure 5.16 and figure 5.17 indicate that the simulation results obtained from the electrochemical model is consistent with the study conducted by Bernardi and Go [2].

5.2.4 Effect of Capacity Fading

Lithium-ion batteries are prone to have adverse effect on voltage, power delivery and battery operation time due to aging. The effect between battery voltage (E_{cell}) and capacity already demonstrated in section 5.1.2. In this section effects on internal resistance, battery operation time and effect on power delivery are investigated.

Constant current pulse method is an effective strategy to determine internal resistance [49] and to determine effect due to aging. In order to conduct this simulation 16% degraded battery was considered where the initial lithium concentration in anode changed from 26194 mol/m^3 (a new battery) to 21959 mol/m^3 (aged battery). Figure 5.18 demonstrates the constant current pulse simulation conducted on aged battery where $y - axis$ represents battery voltage (E_{cell}) and $x - axis$ represents time in hours. Inset illustrates the square wave current pulses applied on battery; 6 minute discharge at $I = -13\,A/m^2$ and 6 minutes relaxation time ($I = 0$). The battery temperature was set at 25^oC.

The last current pulse (inset of figure 5.18; $Time > 1.6\,hrs$) was shortened because the battery reached its lower current limit ($V_{low} = 2.5V$).

Comparison of figure 5.18 (aged battery) and figure 5.14 (new battery) indicate that effect on E_{cell} is negligible in the initial discharge period. However, E_{cell} becomes significantly affected at second half of discharge period. It is possible to observe that discharge time of the battery has been reduced by approximately 12 minutes for aged battery.

Based on the voltage values presented in the two figures, voltage drop (ΔE_{cell}) due to internal resistance was determined for both aged and new battery. Voltage gap for each pulse was calculated using the difference between voltage just before the current was removed (trough voltage) and voltage just before the current is reapplied (peak voltage). These values are presented in figure 5.19. $x - axis$ of this figure represents the battery operated time.

[6]NCA - This is a lithiated transition-metal oxide compound; also known as $Li_y(Ni\,Co\,Al)O_2$ [2].

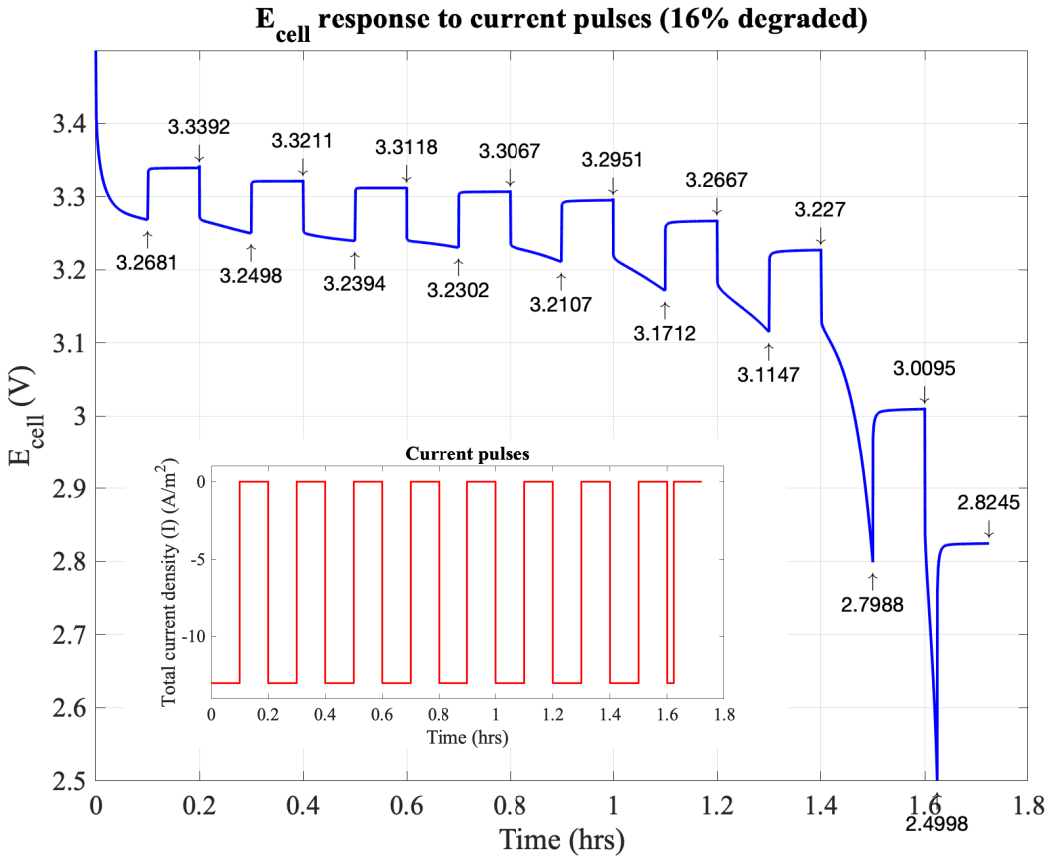

Figure 5.18: Current pulse response on 16% degraded battery

Figure illustrates Battery voltage (E_{cell}) response profile against time due to applied current pulses from fully charge to discharge state for 16% *degraded battery. Inset: Applied current pulses to the battery against time.*

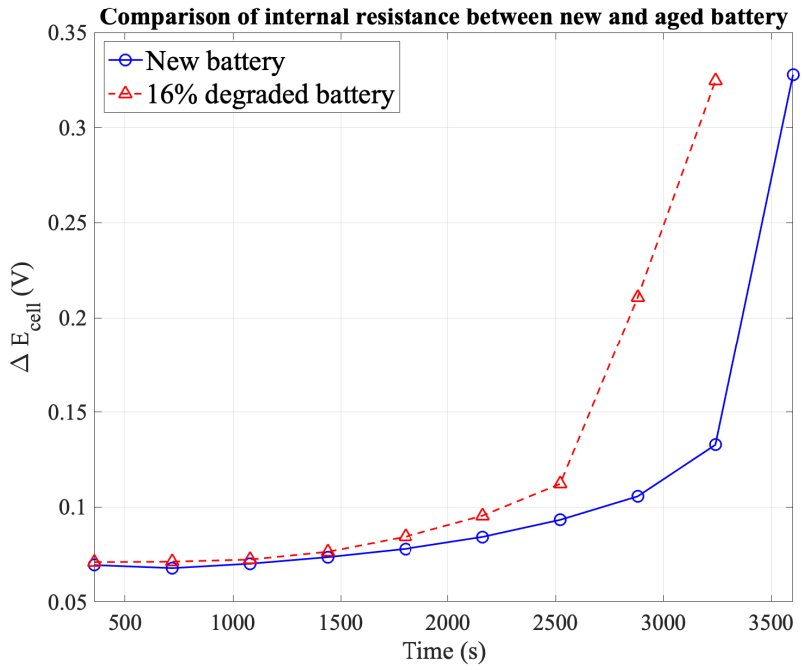

Figure 5.19: Effect of internal resistance due to aging

Figure illustrates increase in ΔE_{cell} against battery discharge time. ΔE_{cell} due to increase in internal resistance of battery. Continuous line represents new battery and dashed line represents 16% degraded battery.

Figure 5.19 demonstrates that with the discharge time internal resistance of the battery increases. At the end of the discharge, the internal resistance increases significantly which the final value becomes 371% higher than fully charged battery. Internal resistance of aged battery is always high. The gap between aged and new battery is small until 1500 s and the gap gradually increases until 2500 s. After 2500 s the gap significantly increases.

Simulation results imply that when battery get aged, operation of battery at low SOC is not a good practice because the performance of the battery becomes inferior. However, Battery Management System (BMS) can be programmed to avoid the utilization of battery at low SOC, as the battery getting aged.

5.3 Simulation Summary

Initially, the electrochemical and capacity fading are validated against experimental data from literature. The simulated results from the electrochemical model indicated a good agreement with experimental data. Simulations were conducted to investigate initial operation of battery, lithium distribution in electrodes, power delivery, voltage response against current pulses and effect of aging.

Investigation of initial operation of battery indicated the rest time given to the battery has an impact on battery performance. Long rest time enables to yield full extent of the energy stored in the battery. However, short rest times can be compensated by operating battery at low discharge/charge rates or operation of battery at elevated temperature than room temperature. The maximum operating temperature of battery is dependent on thermal characteristics and thermal stability of materials that are used to construct the battery.

Investigation of lithium distribution in electrodes indicated that the battery performance is bottlenecked by the properties of cathode ($LiFePO_4$) material. If $LiFePO_4$ is used as a cathode material in a battery, operating the battery at an elevated temperature or operating the battery at a low discharge/charge rate minimize the adverse lithium distribution in electrodes. Graphite as an anode has a constant behavior with lithium distribution according to the model. However, with increasing discharge rate high concentration of lithium is retained in the anode even though the battery is fully discharged.

For high power demanding applications simulation results indicated that it is preferred to use the battery when SOC is above 30%, and it is highly unsuitable to use the battery for high power applications when the battery has less than 10% SOC due to increase in internal resistance which results in increase in power loss due to Joule heating inside the battery.

Constant current pulse analysis facilitates to derive useful information about the battery. This analysis indicate the impact of internal resistance with discharge time. Impact of Ohmic resistance and resistance due to diffusion were apparent in current pulse analysis. A fully charged battery which is discharging at $I = 13\,A/m^2$ at 25^oC has a Ohmic to diffusion resistance of $2.14 : 1$. However, this value depends on discharge rate, SOC and temperature.

Investigation of effects on aging indicated that 16% degraded battery had about 20% lower operating time compared to new battery with same discharge rate ($I = -13\,A/m^2$) and temperature (25^oC). Operation of aged battery at low SOC is unsuitable because

the performance of the battery becomes inferior. The internal resistance of the battery at the end of discharge becomes 371% higher compared to resistance when the battery is fully charged.

Electrochemical model and capacity fading model simulate the behavior of lithium-ion cell which is useful for many applications. Results that are generated in these simulations indicate applications of this model have broad spectrum. This model can be used for applications such as selection of lithium-ion battery for specific applications, optimization of battery parameters in battery development, determination of battery service time, determination of battery replace time and optimization of battery management systems BMS etc.

Chapter 6

Conclusion

Mathematical and numerical modelling of lithium-ion battery provides a convenient platform for development and optimization of batteries. Physical testing of batteries demand long time and expensive equipment. However, a mathematical model can simulate behavior of a battery in a fraction of time compared to time taken for physical testing of batteries. Machine learning and deep learning provide good approximations and require less computational power. However, their 'back box' nature does not provide useful information to understand physical and chemical behavior of batteries. Thus, these models are more useful in battery management systems BMS.

6.1 About the Electrochemical Model

Pseudo Two Dimensional (P2D) model was selected to develop the electrochemical model for lithium-ion battery in this thesis. The model is based on concentrated solution theory and porous electrode theory [13]. Lithium transport in anode and cathode, lithium ions transport in electrolyte, Ohm's law and Butler-Volmer kinetics are utilized in order to simulate the behavior of battery.

Model assumes that electrodes (anode and cathode) are a matrix which consist of homogenous solid spheres. Lithium can intercalate and de-intercalate in and out through the surface of the spheres. The void space between spheres are filled with electrolyte. Separator is an inert solid matrix which void spaces are filled with electrolyte. Separator separates anode and cathode physically and electrically but allow lithium ions to pass through.

The P2D model provide flexibility to change model parameters such as geometrical, trans-

port, kinetic and concentration parameters. This is highly useful for optimization of battery parameters during a development processes, test suitability of new materials for anode, cathode and electrolyte and determine which type of battery is most suitable for a specific application.

The P2D model was numerically constructed using MATLAB. This is an electrochemical model, however, it has flexibility to operate simultaneous with other models such as capacity fading and thermal model. In this thesis both electrochemical and capacity fading are analyzed. Thermal model was developed based on cylindrical geometry and lump heat model, however, the analysis of thermal model is not presented in this thesis.

For simulations, natural graphite was selected as the anode, $LiFePO_4$ was selected as the cathode and $LiPF_6$ in mixture of propylene carbonate, ethylene carbonate, dimethyl carbonate was selected as the electrolyte. Parameters were estimated from the data available in the literature.

The electrochemical model and capacity fading were validated against experimental data from literature. The simulation results and experimental data indicated a good agreement.

6.2 Results

Simulations were conducted to investigate the initial operation of battery, lithium distribution in electrodes, power delivery, constant current pulse analysis and effect of capacity fading. The results indicated that rest time for the battery has an impact on battery performance. However this issue can be overcome by reducing current through battery or increase in temperature. Lithium distribution in electrodes indicated that many limiting parameters exists in the cathode material.

Power delivery of the battery can be improve by increasing the operating temperature of the battery. However, maximum operating temperature of the battery depends on the thermal characteristics and thermal stability of battery material. One of the drawback in electrochemical model is that it is unable to determine thermal stability of material. However, there exists a possibility to develop a supporting model to electrochemical model that determines the thermal stability of battery materials.

Analysis of power delivery indicated that for high power applications, it is suitable to operate the battery above 30% SOC and it is unsuitable to use the battery when SOC is lower than 10%.

Constant current pulse analysis is a key method to determine many battery performance parameters such as Ohmic resistance, electric resistance emerged due to diffusion of lithium in electrodes, relaxation time of the battery at different SOC and temperature etc. This analysis indicated that internal resistance of battery is increased approximately by 371% at lowest SOC compared to fully charged battery ($1C$ discharge at 25^oC).

Analysis of 16% degraded battery indicated that battery operation time is reduced by approximately 20% compared to a new battery. Premature increase in internal resistance due to aging indicated that an aged battery is more suitable to use its upper SOC region.

6.3 Further Improvements

It is possible to further improve and optimize the performance of the electrochemical model which is written in Matlab. At start and end of simulations, the time step (dt) needs to be small because the battery operation process is transient in these regions. This is also applicable for regions with sharp change in total current density ($I(t)$). However, when the simulation reaches a steady state, time step (dt) can be relaxed such that it represents a larger time step. The Matlab code can be improved to optimize the size of time step (dt) by itself with user requirements. Such improvement can reduce the simulation time and computational power needed. Also, readability, simplicity and performance of the Matlab code can be improved by adopting object oriented programing (OOP).

6.4 Applications

The electrochemical model and capacity fading facilitate to simulate many testing cases for lithium-ion batteries. Simulations can be run within few minutes or hours depending on computer performance and resolution required. However, actual battery testing demands days and months. Thus, Mathematical model provide advantage over time and financial resources. The mathematical model is possible to use in applications such as,

- Selection of suitable lithium battery type for a specific application.
- Optimization of battery parameters during the development of a battery.
- Analyze the behavior of new materials that can be used as anode, cathode or electrolyte.

- Determination of battery service frequency.
- Determination of battery replacement frequency.
- Training and optimization of battery management systems (BMS).

In addition to above applications, data generated form the model can be use to train machine learning and deep learning algorithms for lithium-ion batteries which use less computational power than the Pseudo Two Dimensional (P2D) model.

Bibliography

[1] M. Farkhondeh, M. Pritzker, M. Fowler, and C. Delacourt, "Mesoscopic Modeling of a $LiFePO_4$ Electrode: Experimental Validation under Continuous and Intermittent Operating Conditions," *Journal of The Electrochemical Society*, vol. 164, no. 11, pp. E3040–E3053, 2017. [Online]. Available: http://dx.doi.org/10.1149/2.0211706jes

[2] D. M. Bernardi and J.-Y. Go, "Analysis of pulse and relaxation behavior in lithium-ion batteries," *Journal of Power Sources*, vol. 196, no. 1, pp. 412–427, 2011. [Online]. Available: https://doi.org/10.1016/j.jpowsour.2010.06.107

[3] S. A. Qaderi, F. A. Wahedi, A. A. Ashqar, M. B. Kuwair, G. M. Ibrahim, O. Takieddine, F. R. Kamal, R. Paul, and S. K. Mazumdar, "Utilization of Lithium-Ion Batteries in Offshore Platform," in *Abu Dhabi International Petroleum Exhibition & Conference*, vol. Day 1 Mon, November 09, 2020, D012S116R186, Conference Proceedings. [Online]. Available: https://doi.org/10.2118/203333-MS

[4] A. Cordoba-Arenas, S. Onori, Y. Guezennec, and G. Rizzoni, "Capacity and power fade cycle-life model for plug-in hybrid electric vehicle lithium-ion battery cells containing blended spinel and layered-oxide positive electrodes," *Journal of Power Sources*, vol. 278, pp. 473–483, 2015. [Online]. Available: https://doi.org/10.1016/j.jpowsour.2014.12.047

[5] L. Theodorou, S. McGeachie, J. Gill, and K. McKenna, "The Energy Transition, lessons learned from other heavy industries and the opportunities they present for Oil and Gas Operators demonstrated by associated case studies," in *Abu Dhabi International Petroleum Exhibition & Conference*, vol. Day 2 Tue, November 10, 2020, D021S041R003, Conference Proceedings. [Online]. Available: https://doi.org/10.2118/203409-MS

[6] S. O. Settemsdal, "Applying Energy Storage Solutions ESS in Offshore Oil and Gas to Reduce Emissions and Costs," in *SPE Offshore Europe Conference and Exhibition*, vol. Day 2 Wed, September 04, 2019, D021S004R004, Conference Proceedings. [Online]. Available: https://doi.org/10.2118/195777-MS

[7] M. Bilgin, J. Donen, V. Scaini, and M. Snijder, "World's First Hybrid Drilling Rig," in *IADC/SPE International Drilling Conference and Exhibition*, vol. Day 2 Wed, March 04, 2020, D091S008R002, Conference Proceedings. [Online]. Available: https://doi.org/10.2118/199573-MS

[8] H. Yoshida, T. Hyakudome, T. Aoki, N. Fujiya, S. Konno, M. Oomiya, and K. Ozawa, "Improvement of a High Energy Type Lithium-Ion Battery System For Unmanned Underwater Vehicle," in *The Nineteenth International Offshore and Polar Engineering Conference*, vol. All Days, ISOPE-I-09-469, Conference Proceedings.

[9] W. Ayers, "Future Energy Storage for Vessels," in *SNAME Maritime Convention*, vol. Day 3 Fri, November 01, 2019, D033S006R001, Conference Proceedings.

[10] A. Patil, V. Patil, D. Wook Shin, J.-W. Choi, D.-S. Paik, and S.-J. Yoon, "Issue and challenges facing rechargeable thin film lithium batteries," *Materials Research Bulletin*, vol. 43, no. 8, pp. 1913–1942, 2008. [Online]. Available: https://doi.org/10.1016/j.materresbull.2007.08.031

[11] F. Ozanam and M. Rosso, "Silicon as anode material for Li-ion batteries," *Materials Science and Engineering: B*, vol. 213, pp. 2–11, 2016. [Online]. Available: https://doi.org/10.1016/j.mseb.2016.04.016

[12] A. Jokar, B. Rajabloo, M. Désilets, and M. Lacroix, "Review of simplified Pseudo-two-Dimensional models of lithium-ion batteries," *Journal of Power Sources*, vol. 327, pp. 44–55, 2016. [Online]. Available: https://doi.org/10.1016/j.jpowsour.2016.07.036

[13] M. Doyle, T. F. Fuller, and J. Newman, "Modeling of Galvanostatic Charge and Discharge of the Lithium/Polymer/Insertion Cell," *Journal of The Electrochemical Society*, vol. 140, no. 6, pp. 1526–1533, 1993. [Online]. Available: http://dx.doi.org/10.1149/1.2221597

[14] T. F. Fuller, M. Doyle, and J. Newman, "Simulation and Optimization of the Dual Lithium Ion Insertion Cell," *Journal of The Electrochemical Society*, vol. 141, no. 1, pp. 1–10, 1994. [Online]. Available: https://doi.org/10.1149/1.2054684

[15] M. W. Verbrugge and B. J. Koch, "Electrochemical Analysis of Lithiated Graphite Anodes," *Journal of The Electrochemical Society*, vol. 150, no. 3, pp. A374–A384, 2003. [Online]. Available: https://doi.org/10.1149/1.1553788

[16] V. Srinivasan and J. Newman, "Design and Optimization of a Natural Graphite/Iron Phosphate Lithium-Ion Cell," *Journal of The Electrochemical Society*, vol. 151, no. 10, pp. A1530–A1538, 2004. [Online]. Available: https://doi.org/10.1149/1.1785013

[17] R. E. Gerver and J. P. Meyers, "Three-Dimensional Modeling of Electrochemical Performance and Heat Generation of Lithium-Ion Batteries in Tabbed Planar Configurations," *Journal of the Electrochemical Society*, vol. 158, no. 7, pp. A835–A843, 2011. [Online]. Available: https://doi.org/10.1149/1.3591799

[18] M. Safari and C. Delacourt, "Modeling of a Commercial Graphite/$LiFePO_4$ Cell," *Journal of The Electrochemical Society*, vol. 158, no. 5, pp. A562–A571, 2011. [Online]. Available: https://doi.org/10.1149/1.3567007

[19] G. Richardson, G. Denuault, and C. P. Please, "Multiscale modelling and analysis of lithium-ion battery charge and discharge," *Journal of Engineering Mathematics*, vol. 72, no. 1, pp. 41–72, 2012. [Online]. Available: https://doi.org/10.1007/s10665-011-9461-9

[20] Y. Ye, Y. Shi, and A. A. O. Tay, "Electro-thermal cycle life model for lithium iron phosphate battery," *Journal of Power Sources*, vol. 217, pp. 509–518, 2012. [Online]. Available: https://doi.org/10.1016/j.jpowsour.2012.06.055

[21] A. Khandelwal, K. S. Hariharan, V. S. Kumar, P. Gambhire, S. M. Kolake, D. Oh, and S. Doo, "Generalized moving boundary model for charge–discharge of $LiFePO_4$/C cells," *Journal of Power Sources*, vol. 248, pp. 101–114, 2014. [Online]. Available: https://doi.org/10.1016/j.jpowsour.2013.09.066

[22] D. Zhang, B. N. Popov, and R. E. White, "Modeling lithium intercalation of a single spinel particle under potentiodynamic control," *Journal of the Electrochemical Society*, vol. 147, no. 3, pp. 831–838, 2000.

[23] J. Newman and W. Tiedemann, "Porous-electrode theory with battery applications," *AIChE Journal*, vol. 21, no. 1, pp. 25–41, 1975.

[24] G. Ning, R. E. White, and B. N. Popov, "A generalized cycle life model of rechargeable Li-ion batteries," *Electrochimica Acta*, vol. 51, no. 10, pp. 2012–2022, 2006. [Online]. Available: https://doi.org/10.1016/j.electacta.2005.06.033

[25] A. Khandelwal, K. S. Hariharan, P. Gambhire, S. M. Kolake, T. Yeo, and S. Doo, "Thermally coupled moving boundary model for charge–discharge of $LiFePO_4$/C cells," *Journal of Power Sources*, vol. 279, pp. 180–196, 2015. [Online]. Available: https://doi.org/10.1016/j.jpowsour.2015.01.018

[26] B. Sundén, *Electrochemistry and thermodynamics*. Academic Press, 2019, book section 2, pp. 15–36. [Online]. Available: http://www.sciencedirect.com/science/article/pii/B9780128169506000026

[27] J. T. Warner, *Electrochemistry basics.* Elsevier, 2019, book section 2, pp. 17–41. [Online]. Available: http://www.sciencedirect.com/science/article/pii/B9780128147788000028

[28] ——, *Lithium-ion battery operation.* Elsevier, 2019, book section 3, pp. 43–77. [Online]. Available: http://www.sciencedirect.com/science/article/pii/B978012814778800003X

[29] J. Wang, P. Liu, J. Hicks-Garner, E. Sherman, S. Soukiazian, M. Verbrugge, H. Tataria, J. Musser, and P. Finamore, "Cycle-life model for graphite-$LiFePO_4$ cells," *Journal of Power Sources*, vol. 196, no. 8, pp. 3942–3948, 2011. [Online]. Available: https://doi.org/10.1016/j.jpowsour.2010.11.134

[30] J. Christensen, V. Srinivasan, and J. Newman, "Optimization of Lithium Titanate Electrodes for High-Power Cells," *Journal of The Electrochemical Society*, vol. 153, no. 3, pp. A560–A565, 2006. [Online]. Available: https://doi.org/10.1149/1.2172535

[31] S. G. Stewart, V. Srinivasan, and J. Newman, "Modeling the Performance of Lithium-Ion Batteries and Capacitors during Hybrid-Electric-Vehicle Operation," *Journal of The Electrochemical Society*, vol. 155, no. 9, pp. A664–A671, 2008. [Online]. Available: https://doi.org/10.1149/1.2953524

[32] F. Jiang, P. Peng, and Y. Sun, "Thermal analyses of $LiFePO_4$/graphite battery discharge processes," *Journal of Power Sources*, vol. 243, pp. 181–194, 2013. [Online]. Available: https://doi.org/10.1016/j.jpowsour.2013.05.089

[33] S. J. An, J. Li, C. Daniel, D. Mohanty, S. Nagpure, and D. L. Wood, "The state of understanding of the lithium-ion-battery graphite solid electrolyte interphase (SEI) and its relationship to formation cycling," *Carbon*, vol. 105, pp. 52–76, 2016. [Online]. Available: https://doi.org/10.1016/j.carbon.2016.04.008

[34] I. V. Thorat, T. Joshi, K. Zaghib, J. N. Harb, and D. R. Wheeler, "Understanding Rate-Limiting Mechanisms in $LiFePO_4$ Cathodes for Li-Ion Batteries," *Journal of The Electrochemical Society*, vol. 158, no. 11, p. A1185, 2011. [Online]. Available: http://dx.doi.org/10.1149/2.001111jes

[35] L. O. Valøen and J. N. Reimers, "Transport Properties of $LiPF_6$-Based Li-Ion Battery Electrolytes," *Journal of The Electrochemical Society*, vol. 152, no. 5, pp. A882–A891, 2005. [Online]. Available: https://doi.org/10.1149/1.1872737

[36] M. Montanino, S. Passerini, and G. Appetecchi, *Electrolytes for rechargeable lithium batteries.* Cambridge, UNITED KINGDOM: Elsevier Science & Technology, 2015, book section 4, pp. 73–116. [Online]. Available: http://ebookcentral.proquest.com/lib/uisbib/detail.action?docID=2011127

[37] C. F. J. Francis, I. L. Kyratzis, and A. S. Best, "Lithium-Ion Battery Separators for Ionic-Liquid Electrolytes: A Review," *Advanced Materials*, vol. 32, no. 18, p. 1904205, 2020. [Online]. Available: https://doi.org/10.1002/adma.201904205

[38] B. Tjaden, S. J. Cooper, D. J. L. Brett, D. Kramer, and P. R. Shearing, "On the origin and application of the Bruggeman correlation for analysing transport phenomena in electrochemical systems," *Current Opinion in Chemical Engineering*, vol. 12, pp. 44–51, 2016. [Online]. Available: https://doi.org/10.1016/j.coche.2016.02.006

[39] B. Tjaden, D. J. L. Brett, and P. R. Shearing, "Tortuosity in electrochemical devices: a review of calculation approaches," *International Materials Reviews*, vol. 63, no. 2, pp. 47–67, 2018. [Online]. Available: https://doi.org/10.1080/09506608.2016.1249995

[40] K. S. Hariharan, P. Tagade, and S. Ramachandran, *Mathematical Modeling of Lithium Batteries: From Electrochemical Models to State Estimator Algorithms*. Springer, 2017.

[41] C. D. Rahn and C.-Y. Wang, *Lithium-Ion Battery Model*. New York, UNITED KINGDOM: John Wiley & Sons, Incorporated, 2013, book section 6, pp. 132–144. [Online]. Available: http://ebookcentral.proquest.com/lib/uisbib/detail.action?docID=1118513

[42] J. T. Warner, *Lithium-Ion and Other Cell Chemistries*. Elsevier Science & Technology, 2015, book section 7, pp. 81–83. [Online]. Available: http://ebookcentral.proquest.com/lib/uisbib/detail.action?docID=2056916

[43] S. Liu, J. Jiang, W. Shi, Z. Ma, L. Y. Wang, and H. Guo, "Butler–Volmer-Equation-Based Electrical Model for High-Power Lithium Titanate Batteries Used in Electric Vehicles," *IEEE Transactions on Industrial Electronics*, vol. 62, no. 12, pp. 7557–7568, 2015. [Online]. Available: https://doi.org/10.1109/TIE.2015.2449776

[44] B. Sundén, *Transport phenomena in batteries*. Academic Press, 2019, book section 5, pp. 81–91. [Online]. Available: http://www.sciencedirect.com/science/article/pii/B9780128169506000051

[45] Y. F. Reynier, R. Yazami, and B. Fultz, "Thermodynamics of Lithium Intercalation into Graphites and Disordered Carbons," *Journal of The Electrochemical Society*, vol. 151, no. 3, pp. A422–A426, 2004. [Online]. Available: http://dx.doi.org/10.1149/1.1646152

[46] S. Han, Y. Tang, and S. Khaleghi Rahimian, "A numerically efficient method of solving the full-order pseudo-2-dimensional (P2D) Li-ion cell model," *Journal of Power Sources*, vol. 490, p. 229571, 2021. [Online]. Available: https://doi.org/10.1016/j.jpowsour.2021.229571

[47] W. Li, D. Cao, D. Jöst, F. Ringbeck, M. Kuipers, F. Frie, and D. U. Sauer, "Parameter sensitivity analysis of electrochemical model-based battery management systems for lithium-ion batteries," *Applied Energy*, vol. 269, p. 115104, 2020. [Online]. Available: https://doi.org/10.1016/j.apenergy.2020.115104

[48] D. Allart, M. Montaru, and H. Gualous, "Model of Lithium Intercalation into Graphite by Potentiometric Analysis with Equilibrium and Entropy Change Curves of Graphite Electrode," *Journal of The Electrochemical Society*, vol. 165, no. 2, pp. A380–A387, 2018. [Online]. Available: https://dx.doi.org/10.1149/2.1251802jes

[49] H.-G. Schweiger, O. Obeidi, O. Komesker, A. Raschke, M. Schiemann, C. Zehner, M. Gehnen, M. Keller, and P. Birke, "Comparison of Several Methods for Determining the Internal Resistance of Lithium Ion Cells," *Sensors*, vol. 10, no. 6, pp. 5604–5625, 2010. [Online]. Available: https://www.mdpi.com/1424-8220/10/6/5604

[50] L. Rao and J. Newman, "Heat-Generation Rate and General Energy Balance for Insertion Battery Systems," *Journal of The Electrochemical Society*, vol. 144, no. 8, pp. 2697–2704, 1997. [Online]. Available: https://doi.org/10.1149/1.1837884

Appendices

Appendix A

Entropy Values for Open Circuit Voltage (OCV)

This appendix is an extension for section 3.3.2. This appendix presents entropy equations for cathode and anode materials that are used in the battery model ($\frac{dU_n}{dT}$ and $\frac{dU_p}{dT}$). OCV entropy values for negative and positive electrodes ($\frac{dU_n}{dT}$ and $\frac{dU_p}{dT}$) are extracted from experimental data which is published in literature.

A.1 Entropy of Cathode Material

OCV entropy equation for $LiFePO_4$ ($\frac{dU_p}{dT}$) is extracted from Gerver and Meyers [17] and presented in equation (A.1). The equation was developed by Gerver and Meyers [17] based on experimental data. The units of $\frac{dU_p}{dT}$ is V/K.

$$\begin{aligned}\frac{dU_p}{dT} = &- 0.35376\tilde{y}^8 + 1.3902\tilde{y}^7 - 2.2585\tilde{y}^6 + 1.9635\tilde{y}^5 - 0.98716\tilde{y}^4 \\ &+ 0.28857\tilde{y}^3 - 0.046272\tilde{y}^2 + 0.0032158\tilde{y} - 1.9186 \times 10^{-5} ,\end{aligned} \tag{A.1}$$

$$\tilde{y}(x,t) = \frac{c_s(r = r_p, x, t)}{c_{p,max}} , \qquad x \in L_P$$

Figure A.1 illustrates the behavior defined by equation A.1, that represents change of entropy in $LiFePO_4$ with changing Li concentration ratio ($\tilde{y}$).

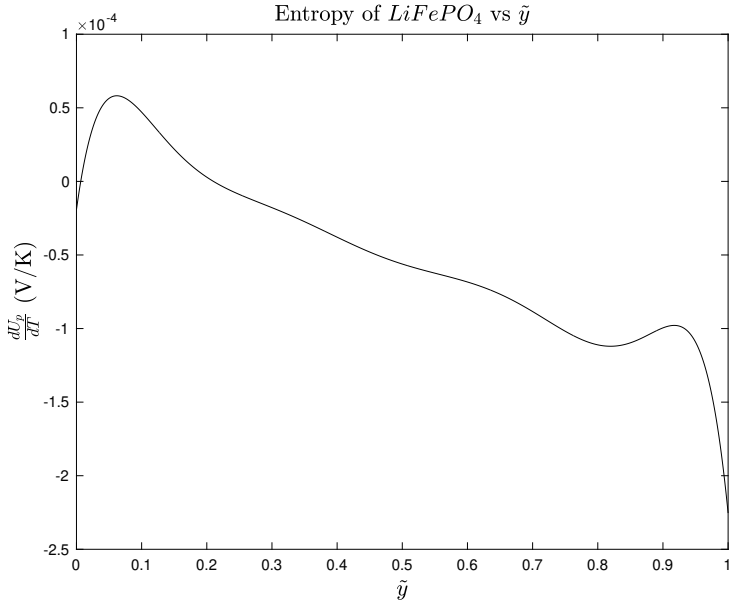

Figure A.1: Change of $LiFePO_4$ entropy against $\tilde{y}$

Figure illustrate the behavior of entropy in $LiFePO_4$ for $\tilde{y} \in [0, 1]$. This is the graphical representation of equation (A.1) *[17].*

A.2 Entropy of Anode Material

Entropy data for for natural graphite ($\frac{dU_n}{dT}$) is taken from Reynier et al. [45], curve fitted and presented in equation (A.2). Coefficients for eq.(A.2) are presented in table A.1. The units of $\frac{dU_n}{dT}$ is V/K.

Comparison of values that are calculated using equation (A.2) and experimental data are presented in figure A.2. Figure illustrates the behavior of entropy with changing Li concentration ratio ($\tilde{x}$) in natural graphite.

$$\begin{aligned}\frac{dU_n}{dT} &= A(\tilde{x}-\beta)^7 + B(\tilde{x}-\beta)^6 + C(\tilde{x}-\beta)^5 + D(\tilde{x}-\beta)^4 + E(\tilde{x}-\beta)^3 \\ &\quad + F(\tilde{x}-\beta)^2 + G(\tilde{x}-\beta) + H \ , \\ \tilde{x}(x,t) &= \frac{c_s(r=r_n,x,t)}{c_{n,max}} \ , \qquad x \in L_N\end{aligned} \tag{A.2}$$

Table A.1: Coefficients for eq.(A.2)

Coefficients	Valid range		
	$0 \leq \tilde{x} < 0.4365$	$0.4365 \leq \tilde{x} < 0.4912$	$0.4912 \leq \tilde{x} \leq 1$
A	10.9	0	-2.351
B	-16.92	0	3.8
C	9.863	0	-2.712
D	-2.474	121	1.064
E	0.135	-8.612	-0.235
F	5.469×10^{-2}	0.1529	2.725×10^{-2}
G	-1.096×10^{-2}	2.072×10^{-4}	-1.503×10^{-3}
H	6.192×10^{-4}	-1.562×10^{-4}	-9.529×10^{-6}
β	0	0.4364	0.4913

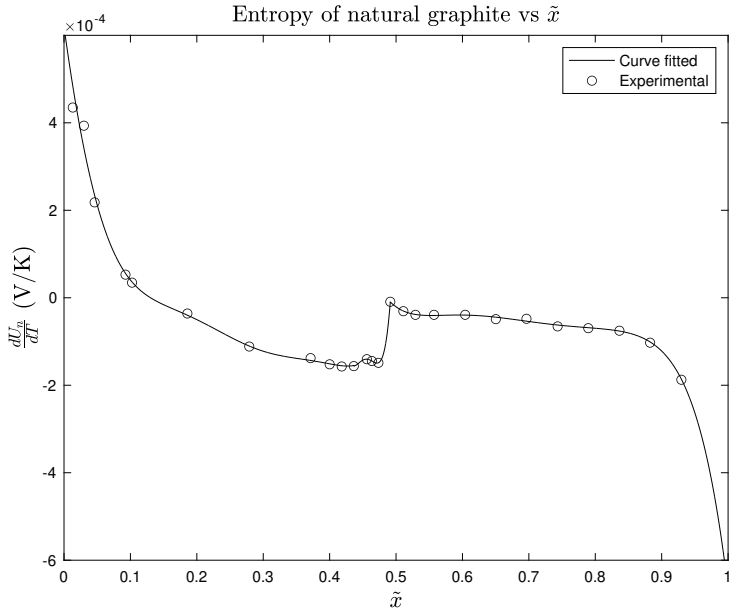

Figure A.2: Change of natural graphite entropy against $\tilde{x}$

The figure illustrates the behavior of entropy in natural graphite for $\tilde{x} \in [0, 1]$. The figure also compares the agreement between experimental data (circles) [45] and values generated with eq.(A.2) *(line).*

Appendix B

Newton-Raphson Method - Derivatives and Matrices

This appendix is an extension to Discretization of Ohms and Butler-Volmer equations at section 4.2.2. Derivatives and organization of $[J]$, $[\Delta\phi]$, $[-f]$ matrices essential to conduct multi-variable Newton-Raphson method are documented in this appendix. Parameters that are used here carries same definitions as section 4.2.2.

Value for $[i_n]_z$ is found using Eq. 4.3, Value for $\frac{\partial[i_n]_z}{\partial[\phi_s]_z}$ is found using Eq. 4.4 and value for $\frac{\partial[i_n]_z}{\partial[\phi_e]_z}$ is found using Eq. 4.5. Functions for electrodes and electrolyte, their derivatives are documented below,

B.1 Functions and Derivatives

B.1.1 Functions and Derivatives for Negative and Positive Electrodes

Center Grid Cells - Both Negative and Positive Electrodes (Eq. 4.8)

$$f_1(z) = \frac{1}{\Delta x^2}\left(\sigma_+[\phi_s]_{z+1} - (\sigma_+ + \sigma_-)[\phi_s]_z + \sigma_-[\phi_s]_{z-1}\right) - a_s[i_n]_z$$

Derivatives

$$\begin{aligned}
\frac{\partial f_1(z)}{\partial [\phi_s]_{z+1}} &= \frac{\sigma_+}{\Delta x^2} \\
\frac{\partial f_1(z)}{\partial [\phi_s]_z} &= -\frac{\sigma_+ + \sigma_-}{\Delta x^2} - a_s \frac{\partial [i_n]_z}{\partial [\phi_s]_z} \\
\frac{\partial f_1(z)}{\partial [\phi_s]_{z-1}} &= \frac{\sigma_-}{\Delta x^2} \\
\frac{\partial f_1(z)}{\partial [\phi_e]_z} &= -a_s \frac{\partial [i_n]_z}{\partial [\phi_e]_z}
\end{aligned}$$

Boundary 1 - Negative Electrode (Eq. 4.9)

$$f_1(1) = \frac{1}{\Delta x}\left(\sigma_+ \frac{[\phi_s]_{z+1} - [\phi_s]_z}{\Delta x} - I\right) - a_s [i_n]_z$$

Derivatives

$$\begin{aligned}
\frac{\partial f_1(1)}{\partial [\phi_s]_{z+1}} &= \frac{\sigma_+}{\Delta x^2} \\
\frac{\partial f_1(1)}{\partial [\phi_s]_z} &= -\frac{\sigma_+}{\Delta x^2} - a_s \frac{\partial [i_n]_z}{\partial [\phi_s]_z} \\
\frac{\partial f_1(1)}{\partial [\phi_e]_z} &= -a_s \frac{\partial [i_n]_z}{\partial [\phi_e]_z}
\end{aligned}$$

Boundary 2 - Negative Electrode (Eq. 4.10)

$$f_1(M_n) = -\sigma_- \left(\frac{[\phi_s]_z - [\phi_s]_{z-1}}{\Delta x^2}\right) - a_s [i_n]_z$$

Derivatives

$$\begin{aligned}
\frac{\partial f_1(M_n)}{\partial [\phi_s]_z} &= -\frac{\sigma_-}{\Delta x^2} - a_s \frac{\partial [i_n]_z}{\partial [\phi_s]_z} \\
\frac{\partial f_1(M_n)}{\partial [\phi_s]_{z-1}} &= \frac{\sigma_-}{\Delta x^2} \\
\frac{\partial f_1(M_n)}{\partial [\phi_e]_z} &= -a_s \frac{\partial [i_n]_z}{\partial [\phi_e]_z}
\end{aligned}$$

Boundary 3 - Positive Electrode (Eq. 4.11)

$$f_1(M_n + M_s + 1) = \sigma_+ \left(\frac{[\phi_s]_{z+1} - [\phi_s]_z}{\Delta x^2}\right) - a_s [i_n]_z$$

Derivatives

$$\begin{aligned}
\frac{\partial f_1(M_n + M_s + 1)}{\partial [\phi_s]_{z+1}} &= \frac{\sigma_+}{\Delta x^2} \\
\frac{\partial f_1(M_n + M_s + 1)}{\partial [\phi_s]_z} &= -\frac{\sigma_+}{\Delta x^2} - a_s \frac{\partial [i_n]_z}{\partial [\phi_s]_z} \\
\frac{\partial f_1(M_n + M_s + 1)}{\partial [\phi_e]_z} &= -a_s \frac{\partial [i_n]_z}{\partial [\phi_e]_z}
\end{aligned}$$

Boundary 4 - Positive Electrode (Eq. 4.12)

$$f_1(M) = \frac{1}{\Delta x}\left(I - \sigma_- \frac{[\phi_s]_z - [\phi_s]_{z-1}}{\Delta x} - I\right) - a_s [i_n]_z$$

Derivatives

$$\begin{aligned}
\frac{\partial f_1(M)}{\partial [\phi_s]_z} &= -\frac{\sigma_+}{\Delta x^2} - a_s \frac{\partial [i_n]_z}{\partial [\phi_s]_z} \\
\frac{\partial f_1(M)}{\partial [\phi_s]_{z-1}} &= \frac{\sigma_{s-}}{\Delta x^2} \\
\frac{\partial f_1(M)}{\partial [\phi_e]_z} &= -a_s \frac{\partial [i_n]_z}{\partial [\phi_e]_z}
\end{aligned}$$

B.1.2 Functions and Derivatives for Electrolyte

$B1$ term is introduced to f_2 function to shortened the equations presented. $B1$ does not depend on ϕ_s or ϕ_e. Expression for $B1$ expressed as follows,

$$B1 = \frac{2R}{F\Delta x}\left(T_+ \kappa_+ \nu_+ \left(\frac{\ln[c_e]_{z+1} - \ln[c_e]_z}{\Delta x}\right) - T_- \kappa_- \nu_- \left(\frac{\ln[c_e]_z - \ln[c_e]_{z-1}}{\Delta x}\right)\right)$$

Center Grid Cells - Electrolyte (Eq. 4.14)

$$f_2(z) = \frac{1}{\Delta x^2}\left(\kappa_+ [\phi_e]_{z+1} - (\kappa_+ + \kappa_-)[\phi_e]_z + \kappa_- [\phi_e]_{z-1}\right) - B1 + a_s [i_n]_z$$

Derivatives

$$\begin{aligned}
\frac{\partial f_2(z)}{\partial [\phi_e]_{z+1}} &= \frac{\kappa_+}{\Delta x^2} \\
\frac{\partial f_2(z)}{\partial [\phi_e]_z} &= -\frac{\kappa_+ + \kappa_-}{\Delta x^2} - a_s \frac{\partial [i_n]_z}{\partial [\phi_e]_z} \\
\frac{\partial f_2(z)}{\partial [\phi_e]_{z-1}} &= \frac{\kappa_-}{\Delta x^2} \\
\frac{\partial f_2(z)}{\partial [\phi_s]_z} &= a_s \frac{\partial [i_n]_z}{\partial [\phi_s]_z}
\end{aligned}$$

Boundary 1 - Electrolyte (Eq. 4.15)

$$f_2(1) = \kappa_+ \left(\frac{[\phi_e]_{z+1} - [\phi_e]_z}{\Delta x^2} \right) - B1 + a_s [i_n]_z$$

Derivatives

$$\begin{aligned}
\frac{\partial f_2(1)}{\partial [\phi_e]_{z+1}} &= \frac{\kappa_+}{\Delta x^2} \\
\frac{\partial f_2(1)}{\partial [\phi_e]_z} &= -\frac{\kappa_+}{\Delta x^2} - a_s \frac{\partial [i_n]_z}{\partial [\phi_e]_z} \\
\frac{\partial f_2(1)}{\partial [\phi_s]_z} &= a_s \frac{\partial [i_n]_z}{\partial [\phi_s]_z}
\end{aligned}$$

Boundary 1 - Electrolyte (Eq. 4.16)

$$f_2(M) = -\kappa_- \left(\frac{[\phi_e]_z - [\phi_e]_{z-1}}{\Delta x^2} \right) - B1 + a_s [i_n]_z$$

Derivatives

$$\begin{aligned}
\frac{\partial f_2(M)}{\partial [\phi_e]_z} &= -\frac{\kappa_-}{\Delta x^2} - a_s \frac{\partial [i_n]_z}{\partial [\phi_e]_z} \\
\frac{\partial f_2(M)}{\partial [\phi_e]_{z-1}} &= \frac{\kappa_-}{\Delta x^2} \\
\frac{\partial f_2(M)}{\partial [\phi_s]_z} &= a_s \frac{\partial [i_n]_z}{\partial [\phi_s]_z}
\end{aligned}$$

B.2 Organization of Matrices

B.2.1 Organization of $[\Delta\phi]$ and $[-f]$ matrices

Discretized variables of ϕ_s and ϕ_e values are organized into $[\Delta\phi]$ is shown below (left). Functions of f_1 and F_2 are organized into $[-f]$ as below (right).

$$[\Delta\phi] = \begin{pmatrix} \Delta\phi_s(1) \\ \Delta\phi_e(1) \\ \Delta\phi_s(2) \\ \Delta\phi_e(2) \\ \vdots \\ \Delta\phi_s(M_n) \\ \Delta\phi_e(M_n) \\ \Delta\phi_e(M_n+1) \\ \Delta\phi_e(M_n+2) \\ \vdots \\ \Delta\phi_e(M_n+M_s) \\ \Delta\phi_s(M_n+M_s+1) \\ \Delta\phi_e(M_n+M_s+1) \\ \vdots \\ \Delta\phi_s(M) \\ \Delta\phi_e(M) \end{pmatrix} \qquad [-f] = - \begin{pmatrix} f_1(1) \\ f_2(1) \\ f_1(2) \\ f_2(2) \\ \vdots \\ f_1(M_n) \\ f_2(M_n) \\ f_2(M_n+1) \\ f_2(M_n+2) \\ \vdots \\ f_2(M_n+M_s) \\ f_1(M_n+M_s+1) \\ f_2(M_n+M_s+1) \\ \vdots \\ f_1(M) \\ f_2(M) \end{pmatrix}$$

B.2.2 Organization of Jacobian $[J]$ matrix

Jacobian matrix is a $(M + M_n + M_s) \times (M + M_n + M_s)$ square matrix. Derivatives are organized in this matrix in accordance with $[\Delta\phi]$ and $[-f]$ matrices. Shown below is the generalized version of organizing the $[J]$ matrix.

$$J = \begin{pmatrix} \frac{\partial f_1(1)}{\partial[\phi_s]_1} & \frac{\partial f_2(1)}{\partial[\phi_e]_1} & \frac{\partial f_1(1)}{\partial[\phi_s]_2} & \cdots & \frac{\partial f_2(1)}{\partial[\phi_e]_{M-1}} & \frac{\partial f_1(1)}{\partial[\phi_s]_M} & \frac{\partial f_2(1)}{\partial[\phi_e]_M} \\ \vdots & \vdots & \vdots & \ddots & \vdots & \vdots & \vdots \\ \frac{\partial f_1(M)}{\partial[\phi_s]_1} & \frac{\partial f_2(M)}{\partial[\phi_e]_1} & \frac{\partial f_1(M)}{\partial[\phi_s]_2} & \cdots & \frac{\partial f_2(M)}{\partial[\phi_e]_{M-1}} & \frac{\partial f_1(M)}{\partial[\phi_s]_M} & \frac{\partial f_2(M)}{\partial[\phi_e]_M} \end{pmatrix}$$

Appendix C

Thermal Model

C.1 Thermal Model

It is considered that compact battery material is organized in a cylindrical geometry shape (Figure C.1). The cylindrical geometry contains only one material (domain) where specific heat capacities, densities and thermal conductivities are volume averaged. The heat generated during the operation of battery add heat (Q_{avg}) to geometry homogeneously at every spacial point. Q_{avg} is volume average heat which includes active heat (Q_{act}), reactive heat (Q_{react}) and ohmic heat (Q_{ohm}) [20]. The ohmic heat generated at current collectors are neglected as conductivity of those materials are considerably high [20]. Cylindrical coordinate system is used since geometry of interest is a cylinder. Figure C.1 demonstrates coordinate system where r_c is radial dimension, θ is angular dimension and z is z dimension. The gradient of divergence for cylindrical coordinate system can be shown as follows,

$$\nabla\left(K\nabla T\right) = \frac{1}{r_c}\frac{\partial}{\partial r_c}\left(r_c K\frac{\partial T}{\partial r_c}\right) + \frac{1}{r_c^2}\frac{\partial}{\partial \theta}\left(K\frac{\partial T}{\partial \theta}\right) + \frac{\partial}{\partial z}\left(K\frac{\partial T}{\partial z}\right)$$

C.1.1 Description of Variables, Parameters and Constants

Table C.1 demonstrates variables and parameters used in thermal model. Ambient Temperature, initial temperature, time and coordinate system variables are independent variables in this model. Initial temperature is same as the initial temperature of electrochemical model. Local temperature (T), heat generation terms ($Q_{act}, Q_{react}, Q_{ohm}, Q_{avg}$) depend on both thermal model and electrochemical model. Transfer current density (i_n),

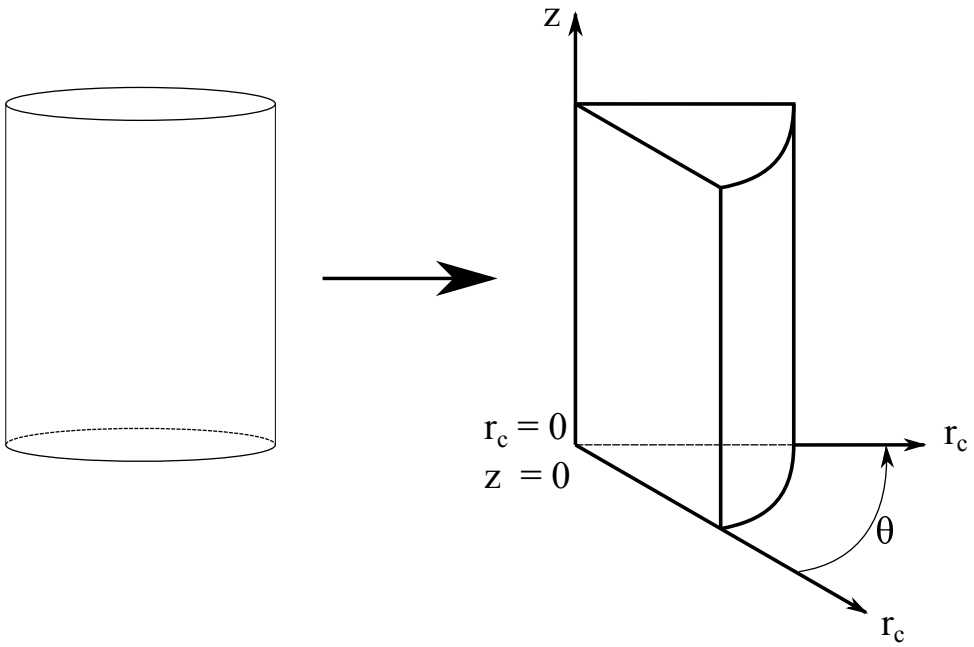

Figure C.1: Schematic diagram of cylindrical battery and coordinate system

electric potentials (ϕ_s, ϕ_e), OCV (U), entropy ($\frac{\partial U}{\partial T}$) and electrolyte concentration (c_e) depend and extract from electrochemical model.

Table C.2 demonstrates constants used in thermal model. Density (ρ), specific heat capacity (C_p) and thermal conductivity (K) are volume averaged values. specific surface area of electrodes (i_n) and electric conductivity at electrodes (σ) are same values as in electrochemical model. Even-though ionic conductivity of electrolyte (κ) considered to be constant inside the thermal model, it is important to note that this is a varying parameter in electrochemical model. Thus, for each time step this values changes. Newton's cooling coefficient (h), emissivity (ε_B) and Stefan-Boltzmann constant (σ_{SB}) are taken from literature sources. λ is considered to be equal to thermal conductivity of material (K) unless otherwise specified.

C.1.2 Governing Equations

Governing equations can be divided into three categories. Heat generation (source) equations, heat transfer equation and boundary conditions. These equations are boxed for ease of identification.

Primary source of heat arises due to charge transfer reaction [25]. This component has reversible and irreversible heat components which occurs at electrode regions [25, 50]. Secondary source arises due to ohmic heat generation [25]. Heat generation due to charge

Table C.1: Variables and parameters - Thermal model

Symbol	Type of Variable	Description
T_{amb}	Independent	Ambient temperature around battery
$T_{initial}$	Independent	Initial temperature of battery
r_c	Independent	Radial axis of battery
z	Independent	z axis of battery
θ	Independent	Angular axis of battery
t	Independent	Time
T	Dependent	Local temperature of battery
i_n	Dependent	Transfer current density
ϕ_s	Dependent	Electric potential at electrodes
ϕ_e	Dependent	Electric potential at electrolyte
U	Dependent	OCV
$\frac{\partial U}{\partial T}$	Dependent	Entropy of cell reaction
c_e	Dependent	Li^+ concentration at electrolyte
Q_{act}	Dependent	Active heat generation
Q_{react}	Dependent	Reactive heat generation
Q_{ohm}	Dependent	Ohmic heat generation
Q_{avg}	Dependent	Average heat generation

Table C.2: Constants - Thermal model

Symbol	Description
a_s	Specific surface area of Electrode material
σ	Electric conductivity of electrode material
κ	Electric conductivity of electrolyte
ρ	Average density of battery material
C_p	Average specific heat capacity of battery material
K	Average thermal conductivity of battery material
h	Newton's cooling coefficient (Convection heat transfer)
ε_B	Emissivity of surface of battery (Blackness)
σ_{SB}	Stefan-Boltzmann constant
λ	Conductivity of heat at surface of battery material

flow in electrolyte has significant heat generation over charge flow through electrodes [50].

Equation C.1 demonstrate active heat generation, also known as irreversible heat component [20, 25]. Magnitude of heat depends on overpotential ($\phi_s - \phi_e - U$) and transfer current density (i_n). This is an exothermic term regardless of charging or discharging since overpotential and transfer current density change signs between the two operations [25].

$$\boxed{Q_{act} = a_s\, i_n\, (\phi_s - \phi_e - U)} \tag{C.1}$$

Equations C.2 expresses reaction heat generation, otherwise known as reversible heat component [20, 25]. Magnitude of this quantity depends on transfer current density (i_n), temperature (T) and entropy ($\frac{\partial U}{\partial T}$). This reaction is endothermic or exothermic which depends on charging or discharging.

Gerver and Meyers [17] mention that, experimental data with curve fitting was used develop equation for entropy change for both negative and positive electrodes. Entropy change for negative and positive electrodes shown in equation C.3 and equation C.4 respectively [17, 20]. At equation C.4, c_s is the Li concentration at surface of electrode material $\big(c_s = c_s(r = r_p, x, t)\big)$.

$$\boxed{Q_{react} = a_s\, i_n\, T\, \frac{\partial U}{\partial T}} \tag{C.2}$$

$$\begin{aligned}\frac{\partial U_n}{\partial T} = {} & 344.1347148\, \frac{\exp(-32.9633287\tilde{x} + 8.316711484)}{1 + 749.0756003\exp(-34.7909964\tilde{x} + 8.887143624)} \\ & - 0.8520278805\tilde{x} + 0.36229929\tilde{x}^2 + 0.2698001697\end{aligned} \tag{C.3}$$

$$\begin{aligned}\frac{\partial U_p}{\partial T} = {} & -0.35376\left(\frac{c_s}{c_{s,max}}\right)^8 + 1.3902\left(\frac{c_s}{c_{s,max}}\right)^7 + 1.9635\left(\frac{c_s}{c_{s,max}}\right)^5 \\ & - 0.98716\left(\frac{c_s}{c_{s,max}}\right)^4 + 0.28857\left(\frac{c_s}{c_{s,max}}\right)^3 - 0.046272\left(\frac{c_s}{c_{s,max}}\right)^2 \\ & + 0.0032158\left(\frac{c_s}{c_{s,max}}\right) - 1.9186 \times 10^{-5}\end{aligned} \tag{C.4}$$

Ohmic heat generation expresses by equation C.5 [20]. The ohmic heat includes heat

generated at electrodes ($\sigma\nabla\phi_s\nabla\phi_s$) and at electrolyte ($\kappa\nabla\phi_e\nabla\phi_e + \kappa\frac{\nabla c_e}{c_e}\nabla\phi_e$). From electrolyte heat generation term, It is apparent that higher Li^+ concentration at electrolyte contribute lower heat generation and vise versa. Ohmic heat is always exothermic regardless of charging or discharging.

$$\boxed{Q_{ohm} = \sigma\nabla\phi_s\nabla\phi_s + \kappa\nabla\phi_s\nabla\phi_s + \kappa\frac{\nabla c_e}{c_e}\nabla\phi_e} \tag{C.5}$$

Average heat generation is the summation of active, reactive and ohmic heats (Equation C.6) [20]. The thermal model assumes that heat is generated homogeneously and equally at each point of geometry, thus, Q_{avg} represents volume average heat generated due to operation of battery.

$$\boxed{Q_{avg} = Q_{act} + Q_{react} + Q_{ohm}} \tag{C.6}$$

Energy balance for cylindrical geometry is expressed in equation C.7 [20]. ρ, C_p and K are volume average properties of battery material.

$$\boxed{\rho C_p\frac{\partial T}{\partial t} + \nabla\left(-K\nabla T\right) = Q_{avg}} \tag{C.7}$$

The thermal model is designed such that, outer boundary of cylindrical geometer; circular area, top and bottom circular areas have similar boundary conditions. This boundary condition is expressed by equation C.8 [20].

$$\boxed{-\lambda\nabla T = -h\left(T_{amb} - T\right) - \varepsilon_B\sigma_{SB}\left(T_{amb}^4 - T^4\right)} \tag{C.8}$$

For better understand boundary condition, let $\bar{r_c}$, $\bar{\theta}$, $\bar{z}$ are dimensionless spacial variables for cylindrical geometry where,

$$0 \leq \bar{r_c}, \bar{\theta}, \bar{z} \leq 1$$

The boundary condition (equation C.8) applies when,

$$\begin{aligned}
\bar{z} = 0,\ 0 \leq \bar{\theta} < 1, \quad 0 \leq \bar{r_c} \leq 1 \\
\bar{z} = 1,\ 0 \leq \bar{\theta} < 1, \quad 0 \leq \bar{r_c} \leq 1 \\
\bar{r_c} = 1,\ 0 \leq \bar{\theta} < 1, \quad 0 \leq \bar{z} \leq 1
\end{aligned}$$

At center of geometry, where,

$$\bar{r_c} = 0, \;\; 0 \leq \bar{\theta} \leq 1, \; 0 < \bar{z} < 1$$

the boundary condition is,

$$-K\nabla T = 0$$

Appendix D

Thermal Model Discretization

D.1 Thermal Model Discretization

D.1.1 Discretization of Source Term

Heat transfer calculations contains mainly three equations; Calculation of source term, Heat transfer at center grid cells and heat transfer at boundaries. Discretization of heat source equation (Eq. C.6) in electrolyte domain is expressed at Eq. D.1.

$$[Q_{avg}]_z = [Q_{act}]_z + [Q_{react}]_z + [Q_{ohm}]_z \tag{D.1}$$

The spacial average heat generation then calculated using Eq. D.2

$$[Q_{avg}]^t = \frac{1}{M}\left(\sum_{z=1}^{M}[Q_{avg}]_z\right) \tag{D.2}$$

Note that z at Eq. D.1 and Eq. D.2 represents index of grid cell at electrolyte domain.

D.1.2 Discretization of Heat Transfer Equation

Cylindrical coordinate system is used for evaluation of heat transfer equation (Eq. C.7). Axes used in thermal model are independent of electrochemical model. Three axes are,

- r_c - Radial axis

- θ - Angular axis
- z - Vertical axis

Eq. C.7 based cylindrical coedinates on above three axes are expressed in Eq D.3. The heat transfer coefficient (K), density (ρ) and specific heat capacity (C_p) of battery material are assumed to be constant with respect to r_c, θ, z and t.

$$\rho C_p \frac{\partial T}{\partial t} - K\left(\frac{1}{r_c}\frac{\partial T}{\partial r_c} + \frac{\partial^2 T}{\partial r_c^2} + \frac{1}{r_c^2}\frac{\partial^2 T}{\partial \theta^2} + \frac{\partial^2 T}{\partial z^2}\right) = Q_{avg} \tag{D.3}$$

However, temperature symmetry long θ axis can be observed as the geometry is a full cylinder and homogeneous heat generation. Thus, $\frac{\partial T}{\partial \theta} = 0$. This results only r_c and z axes to be considered during evaluation. The discretization of Eq. D.3 is expressed at Eq. D.4. Implicit method is used for discretization of equation, but current time step is used to define heat source term ($[Q_{avg}]^t$). Graphical representation of 2 Dimensional grid used for Eq D.4 is presented at Figure D.1.

$$\begin{aligned}\rho C_p\left(\frac{[T]^{t+1}_{(r_c,z)} - [T]^{t}_{(r_c,z)}}{\Delta t}\right) - K\Bigg(\frac{1}{r_c}\Bigg(\frac{[T]^{t+1}_{(r_c+1,z)} - [T]^{t+1}_{(r_c,z)}}{\Delta r_c}\Bigg) \\ + \frac{[T]^{t+1}_{(r_c+1,z)} - 2[T]^{t+1}_{(r_c,z)} + [T]^{t+1}_{(r_c-1,z)}}{\Delta r^2} + \frac{[T]^{t+1}_{(r_c,z+1)} - 2[T]^{t+1}_{(r_c,z)} + [T]^{t+1}_{(r_c,z-1)}}{\Delta z^2}\Bigg) = [Q_{avg}]^t\end{aligned} \tag{D.4}$$

Discretized equation D.4 can be ordered in matrix format for better presentation (Eq. D.5). λ_1, λ_2, λ_3 and $\tilde{Q}$ terms are introduced to present a concise matrix equation. These terms are defined below Eq. D.5

$$\begin{pmatrix}\lambda_2 & \lambda_3 & (1-\lambda_1-2\lambda_2-2\lambda_3) & \lambda_3 & (\lambda_1+\lambda_2)\end{pmatrix}\begin{pmatrix}[T]^{t+1}_{(r_c-1,z)} \\ [T]^{t+1}_{(r_c,z-1)} \\ [T]^{t+1}_{(r_c,z)} \\ [T]^{t+1}_{(r_c,z+1)} \\ [T]^{t+1}_{(r_c+1,z)}\end{pmatrix} = \left(\tilde{Q} + [T]^{t}_{(r_c,z)}\right) \tag{D.5}$$

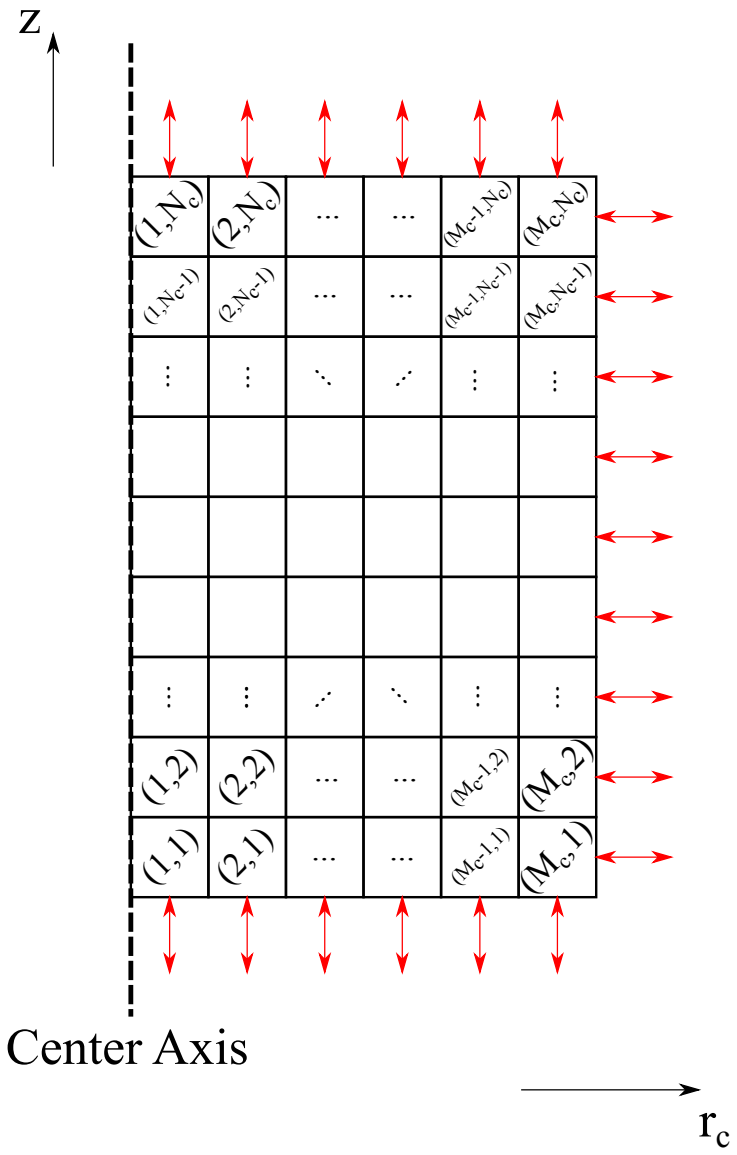

Figure D.1: Grid cells for thermal model

Dashed line indicates axis of cylindrical geometry. Cells are numbered in (r_c, z) coordinate format. M_c, N_c are number of grid cells in r_c and z dimensions respectively. Double headed arrows demonstrate direction of heat loss to/absorb from environment, with each cell at boundary.

where,

$$\lambda_1 = -\frac{K\Delta t}{\rho C_p r_c \Delta r_c} \qquad \lambda_2 = -\frac{K\Delta t}{\rho C_p \Delta r_c^2}$$
$$\lambda_3 = -\frac{K\Delta t}{\rho C_p \Delta z^2} \qquad \tilde{Q} = \frac{[Q_{avg}]^t \Delta t}{\rho C_p}$$

Three surfaces can be identified for heat transfer between boundary and environment. Another boundaries lie at core of the cylinder. These surfaces can be listed and referred with Figure D.1 as follows,

- Top surface of cylinder ($1 \leq r_c \leq M_c, z = N_c$)
- Bottom surface of cylinder ($1 \leq r_c \leq M_c, z = 1$)
- Cylindrical surface of cylinder ($r_c = M_c, 1 \leq z \leq N_c$)
- Cylindrical core ($r_c = 1, 1 < z < N_c$)

Based on above mentioned boundaries, 8 distinct boundary equations can be identified and listed at appendix E. Heat transfer between boundary and environment (Eq. C.8) depends on boundary temperatures. Even though, implicit method is used to solve heat transfer model, quantity of heat transfer to/from environment defined based on boundary temperature at current time step.

The solution is derived using implicit scheme. All subsequent time step temperature values ($[T]_{(r_c,z)}^{(t+1)}$) at grid, organized into a column matrix "x". Based on matrix "x", a square matrix "A" is created which houses all coefficient respect to $[T]_{(r_c,z)}^{(t+1)}$ values. Column matrix "b" is created which contains values at R.H.S of Eq, D.5 and boundary equations presented at appendix E. "x" is then determined using,

$$x = A^{-1}b$$

Values at "x" are volume averaged before new temperature is exported to electrochemical model.

Appendix E

Thermal Model - Equations for Boundaries

Boundary condition equations for thermal model is documented in this appendix. Eight boundary equations exists and they are indexed based on specific region (Fig E.1). Parameters that are used here carries same definitions as in section D.

$$\lambda_1 = -\frac{K\Delta t}{\rho C_p r_c \Delta r_c} \qquad \lambda_2 = -\frac{K\Delta t}{\rho C_p \Delta r_c^2}$$
$$\lambda_3 = -\frac{K\Delta t}{\rho C_p \Delta z^2} \qquad \tilde{Q} = \frac{[Q_{avg}]^t \Delta t}{\rho C_p}$$

L is introduced to represent discretized boundary equation to maintain conciseness of presented equations. The discretization of boundary condition presented in Eq. C.8 as follows,

$$L = \frac{h}{\lambda}\left(T_{amb} - [T]^t_{(r_c,z)}\right) + \frac{\varepsilon_B \sigma_{SB}}{\lambda}\left(\left(T_{amb}\right)^4 - \left([T]^t_{(r_c,z)}\right)^4\right)$$

*λ - *Heat transfer coefficient at boundary, By default* $\lambda = K$

Boundary equations are presented as matrix equations. Thus, temperature values respect

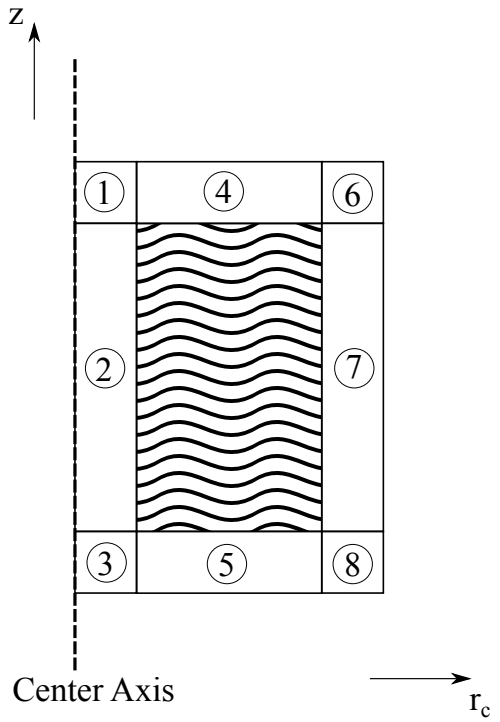

Figure E.1: Boundaries of interest in cylindrical geometry

to subsequent time step are organized as a column matrix, which can be shown as follows,

$$T = \begin{pmatrix} [T]^{t+1}_{(r_c-1,z)} \\ [T]^{t+1}_{(r_c,z-1)} \\ [T]^{t+1}_{(r_c,z)} \\ [T]^{t+1}_{(r_c,z+1)} \\ [T]^{t+1}_{(r_c+1,z)} \end{pmatrix}$$

In figure E.1, vertical dashed line represents axis of cylindrical geometry. Boundary regions are indexed from (1) - (8). Regions (1), (4), (6) are top surface of battery (represents top circular surface of cylinder). Regions (3), (5), (8) are bottom surface of battery (represents bottom circular surface). Regions (6), (7), (8) are the cylindrical surface of battery. The core of battery represented by regions (1), (2), (3). Center grid cells are represented by darkened area of figure E.1. Respective boundary equations are presented below based on the positions (indices) at figure E.1.

$$\textcircled{1} \Rightarrow \begin{bmatrix} 0 & 0 & (1-\lambda_1-\lambda_2-\lambda_3) & \lambda_3 & (\lambda_1+\lambda_2) \end{bmatrix} T = \begin{bmatrix} \tilde{Q} + [T]^t_{(r,z)} - \lambda_3 L\Delta z \end{bmatrix}$$

$$\textcircled{2} \Rightarrow \begin{bmatrix} 0 & \lambda_3 & (1-\lambda_1-\lambda_2-2\lambda_3) & \lambda_3 & (\lambda_1+\lambda_2) \end{bmatrix} T = \begin{bmatrix} \tilde{Q} + [T]^t_{(r,z)} \end{bmatrix}$$

$$\textcircled{3} \Rightarrow \begin{bmatrix} 0 & \lambda_3 & (1-\lambda_1-\lambda_2-\lambda_3) & 0 & (\lambda_1+\lambda_2) \end{bmatrix} T = \begin{bmatrix} \tilde{Q} + [T]^t_{(r,z)} - \lambda_3 L\Delta z \end{bmatrix}$$

$$\textcircled{4} \Rightarrow \begin{bmatrix} \lambda_2 & 0 & (1-\lambda_1-2\lambda_2-\lambda_3) & \lambda_3 & (\lambda_1+\lambda_2) \end{bmatrix} T = \begin{bmatrix} \tilde{Q} + [T]^t_{(r,z)} - \lambda_3 L\Delta z \end{bmatrix}$$

$$\textcircled{5} \Rightarrow \begin{bmatrix} \lambda_2 & \lambda_3 & (1-\lambda_1-2\lambda_2-\lambda_3) & 0 & (\lambda_1+\lambda_2) \end{bmatrix} T = \begin{bmatrix} \tilde{Q} + [T]^t_{(r,z)} - \lambda_3 L\Delta z \end{bmatrix}$$

$$\textcircled{6} \Rightarrow \begin{bmatrix} \lambda_2 & 0 & (1-\lambda_2-\lambda_3) & \lambda_3 & 0 \end{bmatrix} T = \begin{bmatrix} \tilde{Q} + [T]^t_{(r,z)} - \lambda_1 L\Delta r_c - \lambda_2 L\Delta r_c - \lambda_3 L\Delta z \end{bmatrix}$$

$$\textcircled{7} \Rightarrow \begin{bmatrix} \lambda_2 & \lambda_3 & (1-\lambda_2-2\lambda_3) & \lambda_3 & 0 \end{bmatrix} T = \begin{bmatrix} \tilde{Q} + [T]^t_{(r,z)} - \lambda_1 L\Delta r_c - \lambda_2 L\Delta r_c \end{bmatrix}$$

$$\textcircled{8} \Rightarrow \begin{bmatrix} \lambda_2 & \lambda_3 & (1-\lambda_2-\lambda_3) & 0 & 0 \end{bmatrix} T = \begin{bmatrix} \tilde{Q} + [T]^t_{(r,z)} - \lambda_1 L\Delta r_c - \lambda_2 L\Delta r_c - \lambda_3 L\Delta z \end{bmatrix}$$

Appendix F

MATLAB code

This appendix lists the Matlab scrips, functions and input excel file that were used in the electrochemical model. Note that some parts of the code are hidden.

F.1 Input Data

Figure F.1, figure F.2 and figure F.3 demonstrate the sheets of input excel file. Figure F.1 demonstrates the sheet that was used to define battery parameters. Figure F.2 demonstrates constant values and also the input total current density (I). Figure F.3 describes the discretization parameters that were used in the electrochemical model. The parameters presented in these figures (the excel file) can be edited based on the simulation case.

F.2 Matlab Script and Functions

The Matlab script and functions are presented as listings for ease of reference. The list of listings are presented in page 116.

Listing F.1 is the main Matlab script that drives the simulation. This script can be edited based on simulation cases. For example this script can be edited such that the battery can operate many discharge, charge cycles rather than single charge or discharge scenario.

Matlab function presented in listing F.2 organizes the input data into vectors and matrices. This function also defines the initial conditions for the simulation. Matlab function

	A	B	C	D	E	F
1	**Description**	**Symbol**	**Negative**	**Separator**	**Positive**	**Units**
2	Thickness of Electrodes	L_n,L_s,L_p	34	30	70	µm
3	Electrode Porosity	ε	0,55		0,43	
4	Electrolyte Volume Fraction	ε_e	0,33	0,54	0,332	
5	Paricle Radii of Electrodes	r	3,5		0,0365	µm
6	Electric Conductivity (Electrodes)	σ	100		0,5	S/m
7	Anodic Activity Coefficient	α_a	0,5		0,5	
8	Cathodic Activity Coefficient	α_c	0,5		0,5	
9	Maximum Lithium Concentration	C_{max}	31370		22806	mol/m^3
10	Initial Lithium Concentration	C_0	24468,6	1000	684	mol/m^3
11	Reference Diffusivity Coefficient (Electrodes)	D_s	3,90E-14		1,18E-18	m^2/s
12	Activation Energy for Diffuivity (Electrodes)	$E_{D,a}$	35000		35000	J/mol
13	Reference Reaction Coefficient (Electrode-Electrolyte)	k_n , k_p	3E-11		1,4E-12	
14	Activation Energy for Reaction (Electrode-Electrolyte)	$E_{k,a}$	20000		30000	J/mol
15						

Parameters | Constants | Discretization_values | +

Figure F.1: Input excel file - Sheet 'Parameters'

	A	B	C	D
1	**Description**	**Symbol**	**Value**	**Unit**
2	Universal Gas Constant	R	8,3145	J/(K mol)
3	Faraday Constant	F	96487	C/mol
4	Transference Number of Lithium	t^0_+	0,363	
5	Bruggeman Tortuosity Constant (Electrode)	γ	1,5	
6	Bruggeman Tortuosity Constant (Electrolyte)	γ_e	1,5	
7	Reference Temperature	T_{ref}	298,15	K
8	Cell Temperature	T	273,15	K
9	Current Density (-Discharge, + Charge)	I	-6,5	A/m^2
10	Area of battery sheet	A	0,1694	m^2
11				

Parameters | Constants | Discretization_values | +

Figure F.2: Input excel file - Sheet 'Constants'

	A	B	C	D
1	**Description**	**Symbol**	**Value**	**Unit**
2	Battery Running Time	t	9000	s
3	Number of Time Steps	t_n	36000	
4	Grid Size of Electrolyte Domain	M	100	
5	Grid Size of Electrode Domain (Negative)	m_n	50	
6	Grid Size of Electrode Domain (Positive)	m_p	50	

Parameters | Constants | Discretization_values | +

Figure F.3: Input excel file - Sheet 'Discretization_values'

presented in listing F.3 is the main function that runs the simulation. This function houses all necessary sub-functions that are required to run the simulation.

Matlab functions presented in listings F.4, F.6, F.7 and F.8 include the Matlab codes that were derived from the functions in chapter 4. In addition, a new Matlab function was introduced which is listed in listing F.5, in order to calculate the transfer current density (i_n), electrode current density (i_s) and electrolyte current density (i_e).

Matlab function presented in listing F.9 represents the code that is shared by several Matlab functions to calculate the solution using implicit scheme.

Matlab functions for reaction rate coefficients, Li diffusivity in the electrodes, Li^+ diffusion and conductivity in the electrolyte, and Open Circuit Voltage (OCV) are listed in listings F.10, F.11, F.12 and F.13 respectively. These functions can be edited by user based on the battery materials and kinetics.

Since this thesis considers only iso-thermal operation of the battery, Matlab code listed in listing F.14 is used to fill the gap of thermal model. However, Matlab function for the thermal model (cylindrical geometry) is listed in listing F.15 which was discussed in appendices C, D and E.

Listings

Listing F.1: Main.m

```
% BATTERY MODEL FOR LITHIUM ION CELLS (P2D MODEL)
% AUTHOR - YASAS BANDARA
% THESIS - MATHEMATICAL AND NUMERICAL MODELLING OF LITHIUM
   BATTERIES
% SPRING 2021
% DEPARTMENT OF ENERGY AND PETROLEUM ENGINEERING
% UNIVERSITY OF STAVANGER, NORWAY
% SUPERVISORS - STEINAR EVJE, YANGYANG QIAO
% <<<<<<<<<<<<<<<<<<<<<<<<<<<<<<<<<<<
% <<<<<<<<<<<<<<<<<<<<<<<<<<<<<<<<<<<

% <<<<<<<<<< START OF PROGRAM >>>>>>>>>>
clear
clc

% Import valued from the Excel file --->
% Name of the import file
file = 'INPUT';

% Import data to matlab
Sheet1 = readtable(file,'Sheet','Parameters');
Sheet2 = readtable(file,'Sheet','Constants');
Sheet3 = readtable(file,'Sheet','Discretization_values');

% Simulation --->

% Structure the data
[VECTOR, DISCRET, INITIAL, table1, table2, table3]...
    = import_data(Sheet1, Sheet2, Sheet3);

% Start the simulation
[VECTOR, V, Ah, sim, t_val] = main_function(VECTOR, DISCRET,
   INITIAL, table1, table2, table3);


% save data --->
savedata = logical(true); % save data - YES, NO
if savedata
```

```
    if not(isfolder('Results')) % if Resutls folder does not
       exits
        mkdir('Results')        % Create a new folder
    end
    % Get the path and results folder
    out_path = [pwd '/Results'];
    % save name -> C-rate, temperature. 'results'.mat
    filename = strcat(strrep(num2str(table2(8,1)),'.','_')...
        ,'Amp',strrep(num2str(table2(7,1)),'.','_'),'Temp-
           results.mat');
    % Save path and file name
    filename = fullfile(out_path, filename);
    % save the file
    save(filename,'V','Ah','sim','t_val') % Parameters that
       are saved
end

% <<<<<<<<<< END OF PROGRAM >>>>>>>>>>
```

Listing F.2: import_data.m

```
function [VECTOR, DISCRET, INITIAL, table1, table2, table3] =
    import_data(sheet1, sheet2, sheet3)
% Import and structure the input data
% Three cell arrays are created <<INITIAL>>,<<DISCRET>>,<<
   VECTOR>>

% Convert Table to arrays
% Parameters
table1 = table2array(sheet1(:,[3,4,5]));
table1 = [table1(:,1), table1(:,3), table1(:,2)]; %
   reordering table: Anode, Cathode, Separator
% Constants
table2 = table2array(sheet2(:,3));
% Discretization values
table3 = table2array(sheet3(:,3));

% -------------------------
% import Initial values -->
% Define values and order
% 1   delta          % Electrode thickness (micro m)
% 2   epsilon;       % Electrode Porosity
% 3   epsilon_e;     % Electrolyte Volume Fraction
% 4   rp;            % Average Particle Radius (micro m)
% 5   sigma_s;       % Matrix Phase conductivity (S m^(-1))
% 6   c_max;         % Maximum concentration (mol m^(-3))
% 7   c_0;           % Initial concentration (mol m^(-3))
% 8   density;       % density (kg m^(-3))
% 9   C_heat;        % Heat Capacity (J kg^(-1) K^(-1))
% 10  T_cond;        % thermal conductivity (W m^(-1) K^(-1))
% 11  eps_b;         % Bruggeman constant for diffusion and
   conductivity
% 12  alpha_a_neg;   % activity coefficient - anodic -
   negative elec
% 13  alpha_c_neg;   % activity coefficient - cathodic -
   negative elec
% 14  alpha_a_pos;   % activity coefficient - anodic -
   positive elec
% 15  alpha_c_pos;   % activity coefficient - cathodic -
```

```
   positive elec
% 16  R;             % Universal gas constant
% 17  T_ref;         % reference temperature
% 18  T              % initial Temperature
% 19  F              % faraday constant
% 20  trans          % transference number for Lithium

% Assign the input variables
delta          = table1(1,:);   % Electrode thickness (micro m
   )
epsilon        = table1(2,1:2); % Electrode Porosity
epsilon_e      = table1(3,:);   % Electrolyte Volume Fraction
rp             = table1(4,1:2); % Average Particle Radius (
   micro m)
sigma_s        = table1(5,1:2); % Matrix Phase conductivity (S
    m^(-1))
c_max          = table1(8,1:2); % Maximum concentration (mol m
   ^(-3))
c_0            = table1(9,:);   % Initial concentration (mol m
   ^(-3))

% Dummy variables ->
density        = [   0   0  0]; % density (kg m^(-3))
C_heat         = [   0   0  0]; % Heat Capacity (J kg^(-1) K
   ^(-1))
T_cond         = [   0   0  0]; % thermal conductivity (W m
   ^(-1) K^(-1))
rp = rp*10^(-6); % Particle radius is in (micro m) --> (m)
delta = delta*10^(-6);
eps_b_s        = table2(4,1); % Bruggeman exponent for
   electrode
eps_b_e        = table2(5,1); % Bruggeman exponent for
   electrolyte
eps_b          = eps_b_e; %Bruggeman exponent
alpha_a_neg    = table1(6,1); %activity coefficient - anodic -
    negative elec
alpha_c_neg    = table1(7,1); %activity coefficient - cathodic
    - negative elec
alpha_a_pos    = table1(6,2); %activity coefficient - anodic -
```

```
    positive elec
alpha_c_pos    = table1(7,2); %activity coefficient - cathodic
    - positive elec
R              = table2(1,1); % Universal gas constant
T_ref          = table2(6,1); % reference temperature
T              = table2(7,1);  %initial Temperature
F              = table2(2,1); %faraday constant
trans          = table2(3,1); % transference number for Li

% Create a cell array <<INITIAL>>
INITIAL = {delta, epsilon, epsilon_e, rp, sigma_s, c_max, c_0
   , density, ...
    C_heat, T_cond, eps_b, alpha_a_neg, alpha_c_neg,
       alpha_a_pos, ...
    alpha_c_pos, R, T_ref, T, F, trans};
% --------------------------------

% --------------------------------
% Discretizaion Values -->
% Define values and variable order
% 1  - t          % Time length of simulation
% 2  - t_n        % Number of Time steps
% 3  - dt
% 4  - L_n        %negative thickness
% 5  - L_s        %seperator thickness
% 6  - L_p        %positive tickness
% 7  - L          %Length of Battery
% 8  - M_n        % Number of Grid cells - negative
% 9  - M_s        % Number of Grid cells - seperator
% 10 - M_p        % Number of Grid cells - positive
% 11 - M          %total grid cells updated
% 12 - r_n        % particle radius Negative
% 13 - m_n        % Number of Grid cells Negative
% 14 - dr_n       % dr of negative electrode
% 15 - r_p        % particle radius Positive
% 16 - m_p        % Number of Grid cells Positive
% 17 - dr_p       % dr of postive electrode

% Assign values ->
```

```
% Time length of simulation
t       = table3(1,1);
% Number of Time steps
t_n     = table3(2,1);
%Time Grid Size
dt      = t/t_n;  %
% Grid cells
M       = table3(3,1);
L_n     = delta(1); %negative thickness
L_s     = delta(3); %separator thickness
L_p     = delta(2); %positive thickness
L       = L_n+L_s+L_p; %Length of Battery
% Calculation for number of grid cells (neg, sep, pos)
% Number of Grid cells - negative
M_n     = round(M*delta(1)/(delta(1)+delta(2)+delta(3)));
% Number of Grid cells - separator
M_s     = round(M*delta(3)/(delta(1)+delta(2)+delta(3)));
% Number of Grid cells - positive
M_p     = round(M*delta(2)/(delta(1)+delta(2)+delta(3)));
%total grid cells updated
M       = M_n+M_s+M_p;
%Number of Grid cells - negative electrode
m_n     = table3(4,1);
r_n     = rp(1);     % particle radius
dr_n    = r_n/m_n;   % dr of negative electrode
% Number of Grid cells - Positive
m_p     = table3(5,1);        % <---- Variable
r_p     = rp(2);     %particle radius
dr_p    = r_p/m_p;   % dr of postive electrode

% create a cell array <<DISCRET>>
DISCRET = [t, t_n, dt, L_n, L_s, L_p, L, M_n, M_s, M_p, M,
   ...
    r_n, m_n, dr_n, r_p, m_p, dr_p];
% ----------------------------------

% ----------------------------------
% Create a vector with initial conditions
```

```
% ----------------------------------------
               CODE IS HIDDEN
% ----------------------------------------

% Create a cell array <<VECTOR>>
VECTOR = {c_s_n, c_s_p, D_n, D_p, phi_s, phi_e, c_e, c_s_s,
   i_n, i_s, ...
    i_e, U, T, D_e, k_e, sigma_s, epsilon_e0, a_s, k_0_val};

end
```

Listing F.3: main_function.m

```
function [VECTOR, V, Ah, sim, t_val] = main_function(VECTOR,
   DISCRET, INITIAL, table1, table2, table3)
% This function is the main iteration in the program which
   call for required sub-functions for calculations and
   output the final result

% Current Density
I = table2(8,1);
% Upper and lower voltage limits to break at end of charge or
    discharge
if I <= 0
    up_lim = 5.0; % Upper limit
    low_lim = 2.5; % Lower limit
elseif I > 0
    up_lim = 3.6; % Upper limit
    low_lim = 2.0; % Lower limit
end
t_n = table3(2,1);          % Number of iterations
U = VECTOR{1,12};           % Temporary variable to extract
   data
V = zeros(1,t_n);           % Define a voltage vector
V(1,1) = U(DISCRET(11))-U(1); % Voltage change with time step
clear U;                    % intermediate variable U clear
   out
Ah = zeros(1,t_n);          % Energy change with time step
Time_elapsed = zeros(1,t_n); % Actual discharge time
sim = VECTOR;               % working cell variable (vector)

for t = 1:t_n
     % Update input parameters
     sim = UPDATE_VALUES(1,INITIAL, DISCRET, sim, table1);
     % Calculate potential distribution
     sim = OHM_BV_NEWTON(1, I, INITIAL, DISCRET, sim);
     % Calculate transfer current distribution
     sim = BV(1, INITIAL, DISCRET, sim);
     % Calculate electrolyte li concentration distribution
     sim = ELECTROLYTE_MASS(1, INITIAL, DISCRET, sim);
     % calculate electrode li concentration distribution
```

```
        sim = SOLID_MASS(1, INITIAL, DISCRET, sim);
        % Call for thermal model
        sim = THERMAL(1, I, INITIAL, DISCRET, sim);
        % Voltage and energy capacity calculation
        [V,Ah,Time_elapsed]    = V_Ah(t, I, DISCRET, sim, V, Ah,
            Time_elapsed); %
        % save data
        VECTOR(t+1,:) = sim(2,:);
        % update 'sim' working vector
        sim(1,:) = sim(2,:);
        sim(2,:) = [];
        % break the loop if voltage fall below or above limits
        if V(1,t) < low_lim || V(1,t) > up_lim
            break
        end
end

% Plot graph
figure(1)
subplot(1,2,1) % Voltage vs capacity
plot(Ah(1,1:t)*table2(9,1),V(1,1:t))
xlabel('Battery capacity (Ah)')
ylabel('Battery Voltage (V)')
subplot(1,2,2) % Voltage vs time
plot(Time_elapsed(1,1:t),V(1,1:t))
xlabel('Battery operation time (hrs)')
ylabel('Battery Voltage (V)')

% Export values
Ah = Ah(1,1:t)*table2(9,1); % Battery capacity
V = V(1,1:t); % Battery Voltage
t_val = Time_elapsed(1,1:t); % Battery running time

end
```

Listing F.4: OHM_BV_NEWTON.m

```
function VECTOR = OHM_BV_NEWTON(t, I, INITIAL, DISCRET,
   VECTOR)
% This function calculates the solution for the Ohm's law and
    Butler-Volmer equations (Calculate \phi_e and \phi_s)

% Variable Definitions
% i_n - Local Current Density
% i_0 - Exchange Current Density
% c_s_neg --> solid surface concentration negative electrode
% c_s_pos --> solid surface concentration positive electrode
% time - Since Matlab indexing is from 1
t = t + 1;

% Unpacking variables
alpha_a_neg = INITIAL{12};   % Activity coefficients
alpha_c_neg = INITIAL{13};
alpha_a_pos = INITIAL{14};
alpha_c_pos = INITIAL{15};
T           = VECTOR{t-1,13};% Temperature of the cell
F           = INITIAL{19};   % Faraday constant
c_max       = INITIAL{6};    % maximum lithium concentration
   @ electrodes
c_max_neg   = c_max(1);
c_max_pos   = c_max(2);
c_e         = VECTOR{t-1,7}; % lithium concentration at
   electrolyte
M_n         = DISCRET(8);    % Discretization values
M_s         = DISCRET(9);
M_p         = DISCRET(10);
M           = DISCRET(11);
L_n         = DISCRET(4);    % negative thickness
L_s         = DISCRET(5);    % separator thickness
L_p         = DISCRET(6);    % positive thickness
R           = INITIAL{16};   % Universal gas constant
c_s_s       = VECTOR{t-1,8}; % surface lithium concentration
c_s_neg     = c_s_s(1:M_n);
c_s_pos     = c_s_s(M_n+M_s+1:M);
phi_s       = VECTOR{t-1,5}; % Electrode potentials
```

```
phi_e        = VECTOR{t-1,6}; % Electrolyte potentials
U            = VECTOR{t,12};  % Open circuit voltages
sigma_s      = VECTOR{t,16};  % Electrode conductivities
k_e          = VECTOR{t,15};  % Electrolyte conductivity
a_s          = VECTOR{t,18};  % Electrode specific surface
   area
k_0          = VECTOR{t,19};  % Reaction coefficients
i_n          = VECTOR{t-1,9};
%reaction rate constant anode (carbon)
k_0_neg = k_0(1:M_n);
%reaction rate constant anode (LFP)
k_0_pos = k_0(M_n+M_s+1:M);

%Exchange current-->
%negative
dcn = c_max_neg-c_s_neg;
i_0_1 = F*k_0_neg.*c_s_neg.^alpha_c_neg.*...
    (dcn).^(alpha_a_neg).*c_e(1:M_n).^(alpha_a_neg);
%Seperator
i_0_2 = zeros(1,M_s);
%Positive
dcp = c_max_pos-c_s_pos;
i_0_3 = F*k_0_pos.*c_s_pos.^alpha_c_pos.*...
    (dcp).^(alpha_a_pos).*c_e(M_n+M_s+1:M).^(alpha_a_pos);
i_0 = [i_0_1, i_0_2, i_0_3]; %creates one vector

% Averaging electrode conductivities for discretization
sigma_plus = movmean(sigma_s,[0 1]);
sigma_minus= movmean(sigma_s,[1 0]);
k_e_plus = movmean(k_e,[0 1]);
k_e_minus= movmean(k_e,[1 0]);

% Determining Junction coefficient


% ---------------------------------------
              CODE IS HIDDEN
% ---------------------------------------
```

```
% <<<<<<<<<<< NEWTON METHOD >>>>>>>>>>>
% DEFINE NEW VECTORS
dx = [L_n/M_n*ones(1,M_n), L_s/M_s*ones(1,M_s), L_p/M_p*ones
   (1,M_p)];
% \alpha_a
a_a = [alpha_a_neg*ones(1,M_n), zeros(1,M_s), alpha_a_pos*
   ones(1,M_p)];
% \alpha_c
a_c = [alpha_c_neg*ones(1,M_n), zeros(1,M_s), alpha_c_pos*
   ones(1,M_p)];
% DEFINE INITIAL VALUES FOR s (ELECTRODE POTENTIAL) e (
   ELECTROLYTE POTENTIAL)
s = phi_s;
e = phi_e;
% VARIABLE VECTORS
F1      = zeros(1,M);
F2      = zeros(1,M);
% VARIABLE DIFFERENTIAL VECTORS DEFINITIONS
% DS1     = zeors(1,M);
% DS2     = zeors(1,M);
% DS3     = zeors(1,M);
% DSE2    = zeors(1,M);
% DE1     = zeors(1,M);
% DE2     = zeors(1,M);
% DE3     = zeors(1,M);
% DES2    = zeors(1,M);

R_SEI = [0.00*ones(1,M_n), zeros(1,M_s), zeros(1,M_p)]; % SEI
    layer resistance if available
V_SEI = R_SEI.*i_n;
% ITERATIONS STARTS

% ---------------------------------------
              CODE IS HIDDEN
% ---------------------------------------


% <<<<<<<< END OF NEWTON METHOD >>>>>>>>>>>
```

```
% Assign values to output vector
VECTOR{t,5} = s-s(1); % s(1) is deducted because negative
   terminal is grounded
VECTOR{t,6} = e-s(1);
end
```

Listing F.5: BV.m

```
function VECTOR = BV(t_step, INITIAL, DISCRET, VECTOR)
% Function calculates the exchange current density and local
   current density

% Variables
% i_n - Local Current Density
% i_0 - Exchange Current Density
t_step = t_step+1;
% c_s_neg --> solid surface concentration negative electrode
% c_s_pos --> solid surface concentration positive electrode
% Unpacking packages
alpha_a_neg = INITIAL{12}; % Activity coefficients
alpha_c_neg = INITIAL{13};
alpha_a_pos = INITIAL{14};
alpha_c_pos = INITIAL{15};
T           = VECTOR{t_step,13}; % Temperature
T_ref       = INITIAL{17}; % Reference temperature
F           = INITIAL{19}; % Faraday constant
c_max       = INITIAL{6}; % Maximum lithium concentrations
c_max_neg   = c_max(1);
c_max_pos   = c_max(2);
if t_step ==1 % Initial time step
    c_e         = VECTOR{t_step,7};
else
    c_e         = VECTOR{t_step-1,7};
end
M_n         = DISCRET(8); % Discretization values
M_s         = DISCRET(9);
M_p         = DISCRET(10);
M           = DISCRET(11);
R           = INITIAL{16};
if t_step == 1 % For initial time step
    c_s_s       = VECTOR{t_step,8};
else
    c_s_s       = VECTOR{t_step-1,8};
end
c_s_neg     = c_s_s(1:M_n); % Surface concentrations
c_s_pos     = c_s_s(M_n+M_s+1:M);
```

```
phi_s        = VECTOR{t_step,5}; % Electric potentials
phi_e        = VECTOR{t_step,6};
U            = VECTOR{t_step,12}; % OCV
k_0            = VECTOR{t_step,19}; % Reactivity coefficients
% reaction rate constant anode (carbon)
k_0_neg = k_0(1:M_n);
% reaction rate constant anode (LFP)
k_0_pos = k_0(M_n+M_s+1:M);
% Exchange current-->
% negative
dcn = c_max_neg-c_s_neg;
dcn_condition = dcn>=0;
dcn = dcn.*dcn_condition;
% c_n_condition = c_s_neg>0;
% c_s_neg = c_s_neg.*c_n_condition;
i_0_1 = F*k_0_neg.*c_s_neg.^alpha_c_neg.*(dcn).^(alpha_a_neg)
   .*(c_e(1:M_n)).^(alpha_a_neg);
% Seperator
i_0_2 = zeros(1,M_s);
% Positive
dcp = c_max_pos-c_s_pos;
dcp_condition = dcp>=0;
dcp = dcp.*dcp_condition;
i_0_3 = F*k_0_pos.*c_s_pos.^alpha_c_pos.*(dcp).^(alpha_a_pos)
   .*(c_e(M_n+M_s+1:M)).^(alpha_a_pos);
i_0 = [i_0_1, i_0_2, i_0_3]; %creates one vector
i_0 = abs(i_0);

% Butler Volmer Section -->

% ---------------------------------------
              CODE IS HIDDEN
% ---------------------------------------


VECTOR{t_step,10} = i_s;
end
```

Listing F.6: ELECTROLYTE_MASS.m

```
function VECTOR = ELECTROLYTE_MASS(t, INITIAL, DISCRET,
   VECTOR)
% Function calculates the Li+ concentration in electrolyte
   for the new time step

% Variables Unpacking
t = t + 1; % MATLAB indexing starts from 1
trans = INITIAL{20}; % transference number of li+
F     = INITIAL{19}; % Faraday constant
c_old = VECTOR{t-1,7}; % define previous step concentrations
i_n   = VECTOR{t,9}; % define previous step local current
   density
D_e   = VECTOR{t,14};% Electrolyte diffusivity
eps   = VECTOR{t,17};% Electrolyte Volume Fraction
a_s   = VECTOR{t,18};% Specific volume of particles
M_n = DISCRET(8); % number of negative electrode steps
M_s = DISCRET(9); % number of separator steps
M_p = DISCRET(10); % Number of positive electrode steps
M   = DISCRET(11); % total grid cells
dt  = DISCRET(3); % time step size
L_n = DISCRET(4); % negative thickness
L_s = DISCRET(5); % seperator thickness
L_p = DISCRET(6); % positive thickness
A1    = movmean(D_e,[0 1]); % [D_e^{eff}]_{z+0.5}
A2    = movmean(D_e,[1 0]); % [D_e^{eff}]_{z-0.5}
dx_n  = L_n/M_n; % dx at negative electrode
dx_s  = L_s/M_s; % dx at separator region
dx_p  = L_p/M_p; % dx at positive electrode
% lam -> lambda
lam   = [dt./(eps(1:M_n)*dx_n^2), dt./(eps(M_n+1:M_n+M_s)*
   dx_s^2), ...
    dt./(eps(M_n+M_s+1:M)*dx_p^2)];
gamma = (dt./eps)*((1-trans)/F).*a_s;

% ---------------------------------------
               CODE IS HIDDEN
% ---------------------------------------
```

```
% Add new values to VECTOR
VECTOR{t,7} = c_new;
end
```

Listing F.7: SOLID_MASS.m

```
function VECTOR = SOLID_MASS(t, INITIAL, DISCRET, VECTOR)
% This function calculates the mass balance for negative and
   positive electrodes

% variabels
t = t + 1 ; % MATLAB indexing start from 1
M_n = DISCRET(8); % number of negative electrode steps
M_s = DISCRET(9); % number of separator steps
M_p = DISCRET(10); % Number of positive electrode steps
dt  = DISCRET(3);  % time step size
i_n = VECTOR{t,9}; % local current density
F   = INITIAL{19}; % Faraday constant

% NEGATIVE ELECTRODE -->

% ---------------------------------------
              CODE IS HIDDEN
% ---------------------------------------


% Surface concentrations
c_s_s       = [c_s_n_new(:,m_n)', zeros(1,M_s), c_s_p_new(:,
   m_p)'];
% Save new values to VECTOR
VECTOR{t,2} = c_s_p_new;
VECTOR{t,8} = c_s_s;
end
```

Listing F.8: V_Ah.m

```
function [V, Ah, Time_elapsed] = V_Ah(t, I, DISCRET, VECTOR,
   V, Ah,Time_elapsed)
% This function calculates battery voltage, battery capacity
   and battery operation time
% Variables
t = t+1;
phi_s = VECTOR{2,5}; % Electrode potentials
M             = DISCRET(11); % Grid size
dt            = DISCRET(3);  % time step size
% CALCULATIONS -->
v = phi_s(M)-phi_s(1); % voltage for time step
ah = -I*dt/3600; % instant energy output(+) in Ah
V(1,t) = v; % save voltage value
Ah(1,t) = Ah(1,t-1) + abs(ah); % save Ah value
Time_elapsed(1,t) = dt*t/3600; % time elapse of battery
   charge /discharge
end
```

Listing F.9: implicit.m

```
function y = implicit(a,b,c,f)
%  This function solves y=A^(-1)f matrix equation
%                         A                          y        f
% [a(1) c(1)                                      ][ y(1) ] [ f(1) ]
% [b(2) a(2) c(2)                                 ][ y(2) ] [ f(2) ]
% [     b(3) a(3) c(3)                            ][      ] [      ]
% [          ...  ...  ...                        ][ ...  ]=[ ...  ]
% [               ...  ...   ...                  ][      ] [      ]
% [                    b(n-1) a(n-1) c(n-1)      ][y(n-1)] [f(n-1)]
% [                           b(n)  a(n)         ][ y(n) ] [ f(n) ]

m = length(f);
A = zeros(m,m);
for i = 1:m;
    A(i,i) = a(i);
end

% ---------------------------------------
              CODE IS HIDDEN
% ---------------------------------------


y = A\f;
end
```

Listing F.10: k_0.m

```
function [k] = k_0(t_step, INITIAL, DISCRET, VECTOR, table1)
% Calculation of Reaction rate constant for negative and
   positive

t_step = t_step + 1;
R = INITIAL{16};
T = VECTOR{t_step,13};
M_n = DISCRET(8);  % number of negative electrode steps
M_s = DISCRET(9);  % number of seprature steps
%M_p = DISCRET(10); % Number of positive electrode steps
M   = DISCRET(11); %total grid cells
% Import paramters
k0_n = table1(12,1); % Pre exponent coefficient of negative
   electrode
k0_p = table1(12,2); % Pre exponent coefficient of positive
   electride
Ea_n = table1(13,1); % Activation energy of negative
   electrode
Ea_p = table1(13,2); % Activation energy of positive
   electrode
t_ref = INITIAL{1,17}; % reference temperature
% Negative Electrode Reaction constant
% Eqn from ref: Ye, 2012
k_n = k0_n * exp((Ea_n/R)*(1/t_ref-1./T(1:M_n)));
% Positive Electrode Reaction constant
% Eqn from ref: Ye, 2012
k_p = k0_p .* exp((Ea_p/R)*(1/t_ref-1./T(M_n+M_s+1:M)));
% Create final vector
k = [k_n, zeros(1,M_s), k_p];
end
```

Listing F.11: Dn_Dp.m

```
function [D_n,D_p] = Dn_Dp(R, T, M_n, M_s, M, table1, INITIAL
    )
% Calculation of diffusivity of negative and positive
    electrodes

% Variables
% D_n - Solid negative electrode diffusivity
% D_p - Solid positive electrode diffusivity
% R   - Universal Gas Constant
% T   - Absolute temperature (vector)
% M_n = DISCRET(8);  % number of negative electrode steps
% M_s = DISCRET(9);  % number of seprature steps
% M_p = DISCRET(10); % Number of positive electrode steps
% M   = DISCRET(11); %total grid cells
% import parameters
B_n = table1(10,1); % Pre-exponent coefficient of negative
    electrode
B_p = table1(10,2); % Pre-exponent coefficient of positive
    electrode
Ea_n = table1(11,1); % Activation enegy for negative
    electrode
Ea_p = table1(11,2); % Activation enegy for positive
    electrode
t_ref = INITIAL{1,17};

% Negative Electrode - eqn from ref:Ye, 2012
D_n = B_n * exp((Ea_n/R)*(1/t_ref-1./T(1:M_n)));
% Positive Electrode - eqn from ref: Ye, 2012
D_p = B_p * exp((Ea_p/R)*(1/t_ref-1./T(M_n+M_s+1:M)));
end
```

Listing F.12: De_ke.m

```
function [D_e, k_e] = De_ke(t_step, INITIAL, DISCRET, VECTOR)
% Calculation of electrolyte diffusivity and conductivity

%Variables
% D_e - Diffusivity
% k_e - Conductivity
% c   - concentration Li+
% T   - Absolute temperature
t_step = t_step+1;
c = VECTOR{t_step,7};
T = VECTOR{t_step,13};

% ---------------------------------------
              CODE IS HIDDEN
% ---------------------------------------

% Calculation of Effective values -->
eps = VECTOR{t_step,17}; % Electrolyte vol frac, (vector)
b     = INITIAL{11}; %Bruggeman constant
eps_b = eps.^b;
D_e = D_e.*eps_b;%eps_b;
k_e = k_e.*eps_b;
% End of calculating effective values

end
```

Listing F.13: U_eq.m

```
function [U] = U_eq(t_step, INITIAL, DISCRET, VECTOR)
% This function calculates teh OCV of electrodes and their
   entropies

t_step = t_step+1;
T = VECTOR{t_step,13};     % temperature
T_ref = INITIAL{1,17};     % Reference temperature
c_s_s = VECTOR{t_step,8}; %solid surface concentration
c_max = INITIAL{6}; %Maximum concentration
M_n = DISCRET(8);  % number of negative electrode steps
M_s = DISCRET(9);  % number of seprature steps
M_p = DISCRET(10); % Number of positive electrode steps
M   = DISCRET(11); %total grid cells

% Surface SOC in negative electrode
x = c_s_s(1:M_n)./c_max(1);
% Sureface SOC in positve electrode
c =c_s_s(M_n+M_s+1:M);
c_max =c_max(2);
y = c/c_max;

% OCV model used in Ye 2012 Data used from Safari 2011 and
   Gerver
% Calculation of entropy - For negative electrode
dundt = zeros(1,length(x));

% ---------------------------------------
              CODE IS HIDDEN
% ---------------------------------------

% Calculate the U_n value
U_n = U_n_ref + (T(1:M_n)-T_ref).* du_n_dt;

% LiFePO4 electrode

% ---------------------------------------
              CODE IS HIDDEN
% ---------------------------------------
```

```
% Calculate the U_p values
U_p = U_p_ref + (T(M_n+M_s+1:M)-T_ref).*du_p_dt;

% Pack the values
U = [U_n, zeros(1,M_s), U_p];
end
```

Listing F.14: THERMAL.m

```
function VECTOR = THERMAL(t, I, INITIAL, DISCRET, VECTOR)
% This function helps to run the electrochemical model
   without a thermal model (Iso-thermally). If thermal model
   is needed to be included in the simulation, function for
   the thermal model can be included in main_function.m
t = t+1; % Matlab index starts from 1
T = VECTOR{t-1,13};
VECTOR{t,13} = T;
end
```

Listing F.15: THERMAL_MODEL.m

```
 function [T_new, T_avg, t_core, t_surf] =
    THERMAL_MODEL_CYLINDER(T_old, VECTOR_SIM, DISCRET,
    INITIAL, t)
% Thermal model - Calculate temperature distribution in
   cylindrical geometry
% This model was not used in this thesis

% Battery schematic diagram
%
%                    ___
%      ^         ___|   |___
%      |        |      1 4  6|
%      |        |            |
%      |        |            |
%      |        |            |
%      z        |            |
%      |        |      2     7|
%      |        |            |
%      |        |            |
%      |        |            |
%      |        |            |
%      v        |_____3_5__8|
%                     ------>r
%

% Temperature grid indices
%
```

```
% [1,1]     [1,2]    [1,3]    [1,4]   ... [1,M-1]    [1,M]
% [2,1]     [2,2]    [2,3]    [2,4]   ... [2,M-1]    [2,M]
% [3,1]     [3,2]    [3,3]    [3,4]   ... [3,M-1]    [3,M]
%  :          :        :        :      ...     :         :
% [N-1,1] [N-1,2] [N-1,3] [N-1,4] ... [N-1,M-1] [N-1,M]
% [N,1]    [N,2]    [N,3]    [N,4]   ... [N,M-1]    [N,M]

% Assumption
%   * No temperature change w.r.t to \theeta

% Parameters define here
% Ambient Temperature
T_amb = 298.15;
% Newtons cooling coefficient
h = 45; % Ye12
% stefan coefficient
e = 0.5;
% Radius of Battery
r = 0.013;
% hight of Battery
z = 0.065;
% Stefan Boltzmann constant
SB = 5.67037 * 10^(-8);
% Thermal conductivity
%K = INITIAL{1,10} * INITIAL{1,1}';
K = 1.04;
% Density of battery
%rho = INITIAL{1,8} * INITIAL{1,1}';
rho = 1130;
% Specific Heat Capacity of Battery
%C_p = INITIAL{1,9} * INITIAL{1,1}';
C_p = 800;
% Tuning parameter heat dissipation
lam = K;

% Parameters from electrochemical model
% time increment
dt = DISCRET(1,3);
% Specific surface area of electrodes
```

```
a_s = VECTOR_SIM{t,18};
% Transfer Current Density
i_n = VECTOR_SIM{t,9};
i_s = VECTOR_SIM{t,10};
i_e = VECTOR_SIM{t,11};
% Solid phase voltage
phi_s = VECTOR_SIM{t,5};
% Electrolyte voltage
phi_e = VECTOR_SIM{t,6};
% OCV
U = VECTOR_SIM{t,12};
% solid phase conductivity
sigma = VECTOR_SIM{t,16};
% electrolyte conductivity
kappa = VECTOR_SIM{t,15};
% Li+ concentration in electrolyte
c_e = VECTOR_SIM{t,7};
% surface concentration of solid matrix
c_s_s = VECTOR_SIM{t,8};
% Maximum concentration of solid phase
c_max = INITIAL{1,6};
% negative electrode spacial steps
M_n = DISCRET(1,8);
% separator spacial steps
M_s = DISCRET(1,9);
% positive electrode spacial steps
M_p = DISCRET(1,10);
% Battery lengths
L = DISCRET(1,7);
L_n = DISCRET(1,4);
L_s = DISCRET(1,5);
L_p =  DISCRET(1,6);
% Temperature
T = VECTOR_SIM{t,13};

% Calculation of average heat generation

% ---------------------------------------
              CODE IS HIDDEN
```

```
% ---------------------------------------

% total heat generation
Q_avg = abs(Q_act) + Q_rec + abs(Q_ohm);
% average heat generation
dx = [repmat(L_n/M_n,1,M_n),repmat(L_s/M_s,1,M_s), repmat(L_p
   /M_p,1,M_p)];
Q_avg = (Q_avg*dx')/L;

% number of grid cells in r dimension
M = 20;
% number of grid cells in z dimension
N = 10;
% Spacial Step increments
dr = r/M;
dz = z/N;

% Solved using Ax=b
% define A matrix and b matrix
A = zeros(M*N,M*N);
b = zeros(M*N,1);
% Define Temperature matrix (Substitute values)
if length(T_old) == 1
    T_old = INITIAL{1,18}* ones(N,M);
end

% ---------------------------------------
              CODE IS HIDDEN
% ---------------------------------------


% Solve
y = A\b;
T_new = reshape(y,[N, M]);
%T_old = T_new;
T_avg = mean(T_new,'all')*ones(1,DISCRET(1,11)); % M - number
    of grid cells

figure(3)
```

```
contour(T_new,'ShowText','on')

t_core = T_new(N/2,1);
t_surf = T_new(N/2,M);

end
```